

DISSERTATION

**Characterization of a novel cond*Zfyve26*–Null mouse model:
A prerequisite for defining the therapeutic potential of somatic
gene repair in Hereditary Spastic Paraplegia Type SPG15**

**Charakterisierung des cond*Zfyve26*–Null Mausmodells
als Tool für die Bestimmung des therapeutischen Potenzials
somatischer Genreparatur bei HSP Typ SPG15**

zur Erlangung des akademischen Grades
Doctor rerum medicinalium (Dr. rer. medic.)

vorgelegt der Medizinischen Fakultät
Charité – Universitätsmedizin Berlin

von

Thanh Tuyen, Pham

Erstbetreuer*in: Priv.-Doz. Dr. med. Dr. med. univ., Amir, Jahić

Datum der Promotion: **23.03.2024**

Contents

List of Figures	IV
Abbreviations	VI
Abstract	1
Zusammenfassung	2
1 Introduction	4
1.1 Hereditary Spastic Paraplegia (HSP)	4
1.1.1 Clinical characteristics	4
1.1.2 Genetic characteristics	4
1.1.3 Molecular mechanisms	5
1.1.4 Therapy	6
1.1.5 Disease models	8
1.2 <i>Zfyve26</i> associated HSP Type SPG15	9
1.2.1 Clinical characteristics	9
1.2.2 Genetic characteristics	10
1.2.3 Molecular mechanisms	10
1.2.4 Therapy	11
1.2.5 Disease models	12
1.3 Description of research aims	13
2 Materials and Methods	15
2.1 Generation of cond <i>Zfyve26</i> -Null mice	15
2.2 Animals	17
2.3 Genotyping	17

2.4	Sequencing	18
2.5	Gene expression analyses	18
2.6	Immunoblotting analyses	19
2.7	Phenotyping	19
2.8	Tissue processing	21
2.9	Histology and immunohistochemistry	22
2.10	Cell Culture	22
2.11	Immunofluorescence staining of primary cells	23
2.12	Antibodies	24
2.13	Data and image analysis	24
2.14	<i>Zfyve26</i> knock-in gene targeting vector	26
3	Results	27
3.1	Genotyping and sequencing confirmed correct insertion of the stop-cassette into the murine <i>Zfyve26</i> gene.	27
3.2	Mutant animals were viable and fertile.	28
3.3	<i>Zfyve26</i> transcripts were reduced upon stop-cassette insertion.	29
3.4	Body weight between experimental cohorts was inconsistent.	30
3.5	Gait analysis revealed trend towards poorer performance in homozygous cond <i>Zfyve26</i> - Null 1C5 mice.	33
3.5.1	Foot base angle	33
3.5.2	Ladder climbing and grip strength	33
3.5.3	Rotarod	35
3.5.4	Indirect calorimetry.	36
3.6	Disruption of <i>Zfyve26</i> gene caused neuronal loss.	43
3.7	Reduction of <i>Zfyve26</i> gene levels led to altered cell homeostasis.	44
4	Discussion and Outlook	46
5	Conclusion	56
	Bibliography	57
	Appendix	73

Statutory Declaration	77
Curriculum Vitae	79
Publication list	81
Acknowledgments	82

List of Figures

1	Functional fields of HSP proteins	6
2	Targeted disruption of the murine <i>Zfyve26</i> gene	15
3	PCR screening of targeted embryonic stem cell clones	16
4	Tests used to assess motor phenotype in mice	21
5	<i>Zfyve26</i> knock-in gene targeting vector after Neo-deletion provided by Cyagen US Inc.	26
6	Targeted disruption of murine <i>Zfyve26</i> gene	28
7	Reproductive ability of cond <i>Zfyve26</i> -Null animals	29
8	Reduction of <i>Zfyve26</i> gene expression levels in homozygous cond <i>Zfyve26</i> -Null mice	30
9	Body weight of cond <i>Zfyve26</i> -Null 1C5 mice might be litter specific	32
10	Testing of motor performance in cond <i>Zfyve26</i> -Null 1C5 line: Foot base angle	33
11	Testing of motor performance in cond <i>Zfyve26</i> -Null 1C5 line: Ladder climbing and grip strength	34
12	Testing of motor performance in cond <i>Zfyve26</i> -Null 1C5 line: Rotarod	35
13	Indirect calorimetry: Energy expenditure	37
14	Indirect calorimetry: Respiratory Exchange Ratio	38
15	Indirect calorimetry: Food consumption	39
16	Indirect calorimetry: Water consumption	40
17	Indirect calorimetry: Locomotion activity	41
18	Indirect calorimetry: Ambulation activity	42
19	Quantification of neurons in the cortex	43
20	Quantification of Purkinje cells in the cerebellum	44

21	Characterization of relevant <i>Zfyve26</i> gene/Spastizin protein associated cell compartments in MAF	45
22	A novel cond <i>Zfyve26</i> -Null mouse model	55

Abbreviations

ALR	Autophagic lysosome reformation
AP4	Adaptor Protein complex 4
AP5	Adaptor Protein complex 5
ARL6IP1	ADP Ribosylation Factor Like GTPase 6 Interacting Protein 1
ATP13A2	ATPase Cation Transporting 13A2
bp	Base pair
C12orf65	Chromosome 12 Open Reading Frame 65
Cas9	CRISPR-associated protein 9
cDNA	Complementary DNA
CNS	Central nervous system
CNS	central nervous system
CO₂	Carbon dioxide
CPT1C	Carnitine Palmitoyltransferase 1C
Cre	causes recombination
CRISPR	Clustered regularly interspaced short palindromic repeats
Ctip2	Chicken ovalbumin upstream promoter transcription factor-interacting protein 2
Ct	Threshold cycle

CX47	Connexin 47
Cy3	Cyanine dye 3
Cy5	Cyanine dye 5
CYP2U1	Cytochrome P450 Family 2 Subfamily U Member 1
CYP7B1	25-hydroxycholesterol 7-alpha-hydroxylase
CYP7B1	Cytochrome P450 Family 7 Subfamily B Member 1
DAPI	4,6-diamidino-2-phenylindole
DDHD1	DDHD Domain Containing 1
DDHD2	DDHD Domain Containing 2
DMEM	Dulbecco's modified Eagle Medium
DNA	Deoxyribonucleic acid
dNTP	Deoxynucleoside triphosphate
DTT	Diethiothreitol
EDTA	Ethylenediaminetetraacetic acid
EEA1	Early endosome antigen 1
ERLIN2	ER Lipid Raft Associated 2
ERLLIN1	ER Lipid Raft Associated 1
ER	Endoplasmic reticulum
ESC	Embryonic stem cell
ex	Exon
FA2H	Fatty Acid 2-Hydroxylase
FARS2	Phenylalanyl-TRNA Synthetase 2, Mitochondrial
GABA_B	gamma-aminobutyric acid B

GABA	gamma-aminobutyric acid
GAPDH	Glyceraldehyde 3-phosphate dehydrogenase
GBA2	Glucosylceramidase Beta 2
g	g-force
H&E	Hematoxylin and Eosin
HCl	Hydrochloric acid
hiPSC	Human induced pluripotent stem cell
HRP	Horseradish peroxidase
HSP60	Heatshock Protein 60
HSP	Hereditary Spastic Paraplegia
IBA57	Iron-Sulfur Cluster Assembly Factor IBA57
kD	Kilodalton
KIF1A	Kinesin Family Member 1A
KIF1C	Kinesin Family Member 1C
KIF5A	Kinesin Family Member 5A
KO	Knockout
L-Dopa	Levodopa
Lamp1	Lysosome-associated membrane protein 1
LC3	Microtubule-associated protein light chain 3
loxP	locus of crossing (x) over, P1
M-MLV	Moloney murine leukemia virus
MAF	Mouse adult fibroblast
MAG	Myelin Associated Glycoprotein

MEF	Mouse embryonic fibroblast
mRNA	Messenger ribonucleic acid
N.A.	Not available
NaOH	Sodium hydroxide
NIPA1	Non Imprinted In Prader-Willi/Angelman Syndrome 1
O₂	Oxygen dioxide
ON	Overnight
PBSB	Phosphate-buffered saline-Brij
PBS	Phosphate-buffered saline
PCR	Polymerase chain reaction
pH	Potential of hydrogen
PLP	Proteolipid Protein
PtdIns(3)P	Phosphatidylinositol 3-phosphate
qPCR	Quantitative PCR
RAB3GAP2	RAB3 GTPase Activating Non-Catalytic Protein Subunit 2
REEP1	Receptor Accessory Protein 1
REEP2	Receptor Accessory Protein 2
RER	Respiratory exchange ratio
RNase	Ribonuclease
RNasin	Ribonuclease inhibitor
RNA	Ribonucleic acid
ROI	Region of interest
rpm	Revolution per minute

RT	Room temperature
SDS	Sodium dodecyl sulfate
SLC33A1	Solute Carrier Family 33 Member 1
Slc33a1	Solute carrier family 33 acetyl-CoA transporter member 1
SPG	Spastic Paraplegia
T_m	Melting temperature
TECPR2	Tectonin Beta-Propeller Repeat Containing 2
Trk-fused gene	Trafficking From ER To Golgi Regulator
USP8	Ubiquitin Specific Peptidase 8
VPS37A	Vacuolar Protein Sorting-Associated Protein 37A
Vps37a	Vacuolar protein sorting 37A
V	Volume
WDR48	WD Repeat Domain 48
WT	wild-type
Zfyve26	Zinc finger FYVE domain-containing protein 26

Abstract

Hereditary Spastic Paraplegia (HSP) is caused by a length-dependent axonopathy of the corticospinal motor neurons, which results in progressive weakness and spasticity of the legs. There are more than 80 identified HSP gene loci and over 60 HSP gene products. Bi-allelic mutations in the *Zfyve26* gene are associated with HSP type SPG15 and result in the functional loss of spastizin protein, causing defects in cellular homeostasis followed by neurodegeneration. Currently, there is no causative therapy for HSP available.

This study aimed at the functional characterization and validation of a novel *condZfyve26*-Null mouse model as a prerequisite for testing and defining the therapeutic potential of somatic gene repair in HSP. *Zfyve26* gene function was inactivated in mice using a floxed stop-cassette, resulting in animals resembling a classical knockout. *General characterization:* Genome modification of *condZfyve26*-Null mice did not have any off-target effects on animal viability and fertility. Higher body weight of a female homozygous *condZfyve26*-Null cohort compared to wild-type (WT) could hint at a hitherto undescribed sexual dimorphism in HSP. *Molecular characterization:* Genotyping and sequencing analyses confirmed the correct insertion of the stop-cassette into intron 2 of the murine *Zfyve26* gene. *Zfyve26* mRNA levels were reduced by up to >90% in brain lysates of homozygous *condZfyve26*-Null animals suggesting a sufficient inactivation of *Zfyve26* gene function. *Characterization of motor function:* Overall trend towards a worse performance in gait tests were observed in homozygous *condZfyve26*-Null mice compared to WT littermates. *Histological characterization:* In homozygous *condZfyve26*-Null mice, number of cortical neurons were reduced to 36% of WT level. Loss of Purkinje cells in the cerebellum of homozygous *condZfyve26*-Null mice by 24% compared to WT were observed upon *Zfyve26* disruption. *Cell biological characterization:* Depletion of free lysosomes and increased autophagosome levels in homozygous *condZfyve26*-Null mouse adult fibroblasts hinted at defects in autophagic lysosome reformation, a pathway crucial to maintain cell homeostasis.

The data support previous findings and confirm defects in the autophagic as well as lysosomal system as the underlying pathomechanism of *Zfyve26* associated HSP type SPG15. Taken together the novel *condZfyve26*-Null mouse line can be used as a sophisticated tool to control *Zfyve26* gene expression temporally and spatially, thereby providing a valid experimental approach for testing the therapeutic potential of somatic gene repair in HSP.

Zusammenfassung

Hereditäre Spastische Paraplegie (HSP) wird durch eine längenabhängige Axonopathie der kortikospinalen Motoneuronen verursacht, die zu einer fortschreitenden Schwäche und Spastik der Beine führt. Es gibt mehr als 80 identifizierte HSP-Genloci und über 60 HSP-Genprodukte. Bi-allelische Mutationen im *Zfyve26*-Gen sind mit dem HSP-Typ SPG15 assoziiert und führen zu einem Funktionsverlust des Spastizin-Proteins, was Defekte in der zellulären Homöostase und Neurodegeneration verursacht. Derzeit gibt es keine ursächliche Therapie für HSP.

Ziel dieser Studie war die funktionelle Charakterisierung und Validierung eines neuartigen *condZfyve26*-Null-Mausmodells als Voraussetzung für die Prüfung und Definition des therapeutischen Potenzials der somatischen Genreparatur bei HSP. Die *Zfyve26* Genfunktion wurde in Mäusen mittels einer geflochtenen Stopp-Kassette inaktiviert. Dies sollte zur Generierung von Mäusen führen, die einem klassischen Knockout ähnelten. *Allgemeine Charakterisierung:* Die Genomveränderung der *condZfyve26*-Null-Mäuse hatte keine Auswirkungen auf die Lebensfähigkeit und Fruchtbarkeit der Tiere. Das höhere Körpergewicht einer weiblichen homozygoten *condZfyve26*-Null-Kohorte im Vergleich zum Wildtyp (WT) könnte auf einen bisher unbeschriebenen Geschlechtsdimorphismus bei HSP hindeuten. *Molekulare Charakterisierung:* Genotypisierungs- und Sequenzierungsanalysen bestätigten die korrekte Einfügung der Stopp-Kassette in Intron 2 des murinen *Zfyve26*-Gens. *Zfyve26* mRNA-Level waren in Hirnlysaten von homozygoten *condZfyve26*-Null-Tieren um bis zu >90% reduziert, was auf eine ausreichende Inaktivierung der *Zfyve26*-Genfunktion schließen ließ. *Charakterisierung der motorischen Funktion:* Bei homozygoten *condZfyve26*-Null-Mäusen wurde im Vergleich zum WT ein allgemeiner Trend zu einer schlechteren Leistung in Bewegungstests beobachtet. *Histologische Charakterisierung:* Bei homozygoten *condZfyve26*-Null-Mäusen war die Anzahl der kortikalen Neuronen auf 36% des WT-Niveaus reduziert und ein Verlust von 24% der Purkinje-Zellen im Kleinhirn wurde nach der *Zfyve26*-Disruption beobachtet. *Zellbiologische Charakterisierung:* Die Abnahme freier Lysosomen und der erhöhte Autophagosomenspiegel in homozygoten *condZfyve26*-Null-Mausfibroblasten deuteten auf Defekte bei der autophagischen Lysosomenreformation hin, ein für die Aufrechterhaltung der Zellhomöostase entscheidender Mechanismus.

Die Daten unterstützen frühere Befunde und bestätigen Defekte im autophagischen und lysosomalen System als zugrundeliegenden Pathomechanismus der *Zfyve26*-assoziierten HSP

Typ SPG15. Zusammenfassend kann die neuartige *condZfyve26*-Null-Mauslinie als hochentwickeltes Werkzeug zur zeitlichen und räumlichen Kontrolle der *Zfyve26*-Genexpression verwendet werden und bietet damit einen validen experimentellen Ansatz zur Prüfung des therapeutischen Potenzials der somatischen Genreparatur bei HSP.

Chapter 1

Introduction

1.1 Hereditary Spastic Paraplegia (HSP)

1.1.1 Clinical characteristics

Hereditary Spastic Paraplegia (HSP) is the general term for a genetically and clinically heterogeneous group of neurodegenerative diseases that affect movement. The clinical characteristics is a progressive weakness and spasticity of the lower extremities which are caused by a length-dependent degeneration of the axons of the corticospinal motor neurons [1–9]. HSP is classified as pure (lower limb spasticity and weakness) or complicated when additional clinical symptoms are present, e.g., cognitive impairment, learning disability, loss of control of balance and coordination, vision impairment, epilepsy or degeneration of peripheral nerves [1, 10, 11]. Age of onset is highly heterogeneous [3, 11]. The estimated prevalence is 3.6 per 100,000 people for all HSP forms [12], which classifies HSP as a rare disease. Due to the low prevalence and overlapping symptoms with other neurological diseases, e.g., amyotrophic lateral sclerosis (ALS) or multiple sclerosis (MS), HSP is often misdiagnosed [13].

1.1.2 Genetic characteristics

Both mode of inheritance and genetic background with multiple affected gene loci in one HSP gene are highly heterogeneous [3]. There are more than 80 identified HSP gene loci (SPG1-80, plus other) and over 60 HSP gene products [14, 15]. The majority of HSP genes are expressed ubiquitously throughout the human organism, but the clinical picture is and remains primarily and almost exclusively characterized by neurological symptoms of

the lower extremities [6]. HSP can be autosomal recessively (e.g., SPG11, SPG15, SPG48), autosomal dominantly (e.g., SPG4, SPG6, SPG8) or in fewer cases X-linked recessively (e.g., SPG1, SPG2, SPG22) inherited [1, 13, 14]. The spectrum of mutations underlying HSP include missense, nonsense, splice, truncating, exon deletion, small insertions and deletions (indels), which either lead to loss of protein function (e.g., SPG1, SPG4, SPG11, SPG15) or gain of protein function (e.g., SPG3A, again SPG4) [13, 14, 16–18]. The latter can result in the generation and accumulation of neurotoxic mutants as reported for the M1 isoform of the Spastin protein (SPG4), for NIPA1 mutants (SPG6) and as proposed for Strumpellin mutants (SPG8) [17, 19–22]. SPG4 is suggested to be associated with both loss of spastin protein function (caused by spastin protein haploinsufficiency) and spastin gain of protein function (caused by mutant spastin protein) [18].

1.1.3 Molecular mechanisms

The high genetic heterogeneity of HSPs is accompanied by a heterogeneity of the cellular processes that are disturbed upon altered HSP protein function [2, 15]. Studies suggest that HSP proteins are crucial within several cellular processes that can be functionally clustered as (i) membrane traffic, organelle shaping and biogenesis (in Figure 1: Mitochondria, ER-to-Golgi vesicle transport, Golgi-to-ER transport, anterograde transport, microtubules, tubular ER, lysosomes/ endosomes/ autophagosomes), (ii) mitochondrial regulation (mitochondria); (iii) myelination and lipid/sterol modification (lipid/ sterol metabolism, myelin/ oligodendrocytes); (iv) axon pathfinding; (v) nucleotide metabolism and (vi) other/unknown [1, 3–5, 7, 14, 23]. It remains unclear how these subcellular abnormalities result in neurodegeneration and whether the processes interact at the molecular level.

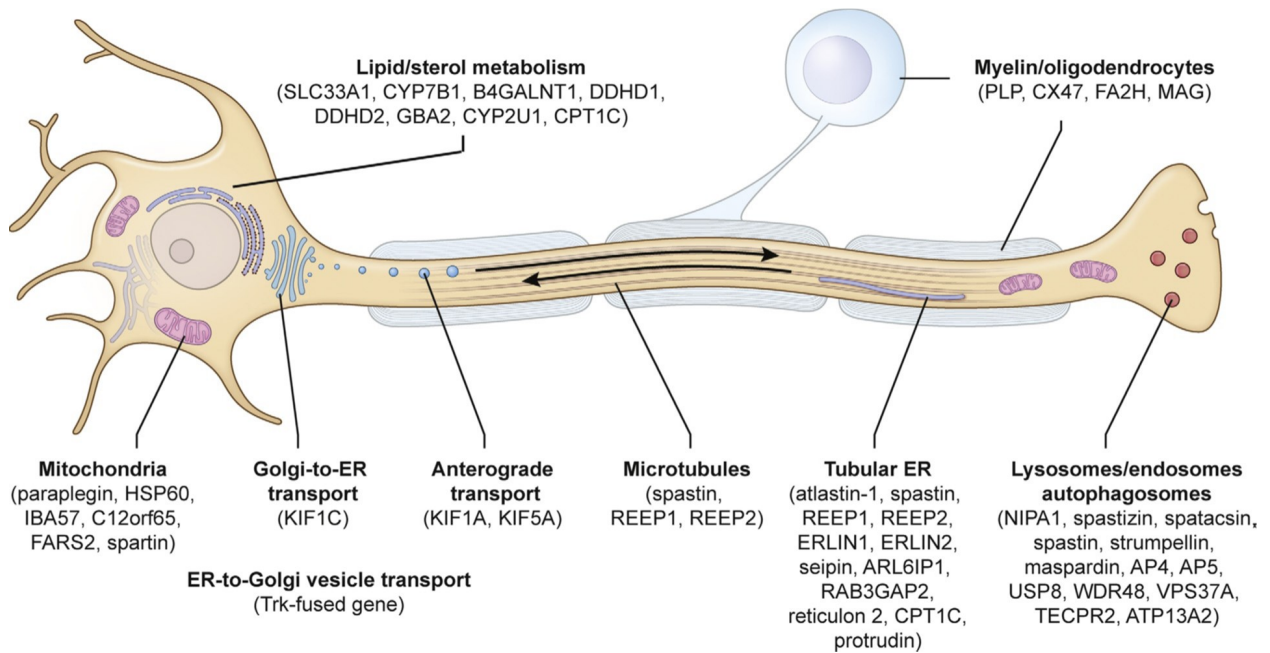


Figure 1. Functional fields of HSP proteins. Schematic depiction of an upper motor neuron displaying different proposed functional fields of selected HSP gene products. ER: endoplasmic reticulum. A more detailed list with all HSP gene products and their proposed functions can be found in Blackstone, 2018 (Table 41.2) [14]. Image taken from [14]

1.1.4 Therapy

To date there is no causal therapy available to slow disease progression, prevent or reverse HSP [23]. The therapeutic spectrum of HSP is limited to purely symptomatic measures to reduce muscle spasticity and to treat other common symptoms [11, 23–25].

Pharmacological treatments. A pharmacological approach to therapeutically target HSP is the intramuscular injection of botulinum toxin type-A (BoNTA), which was shown to improve gait velocity and to reduce muscle tone in HSP patients [11, 25–28]. The antiepileptic and antinociceptive drug, gabapentin, reduces "neurotransmitter release and attenuation of postsynaptic excitability" [29]. However, a study with SPG4 patients reported no statistically significant clinical difference between gabapentin and placebo treatments [25, 30]. Another drug is progabide, which is a GABA receptor agonist and significantly reduced spasticity in 87% of the patients [25, 31]. The dopamine amino acid precursor and Parkinson's disease drug, levodopa (L-Dopa), is considered to treat HSP patients with parkinsonian symptoms, as SPG11 and SPG8 patients were shown to be L-Dopa responsive [32–34]. Studies suggest the administration of cholesterol lowering drugs like simvastatin and ezetimibe [35], or atorvastatin [36] to treat SPG5 patients.

Physical therapy. Treatment of an HSP patient with electrical stimulation was reported to

improve motor function with a 27% increase in velocity [37]. Furthermore, robotic-aided gait training in uncomplicated HSP patients had positive long term effects on balance, walking speed and life quality [38, 39]. Physical therapy is applied to build up and preserve muscle strength [40]. HSP patients exhibited improved functional abilities after eight weeks of intensive physiotherapy interventions [41]. However, despite its broad application, there are no clear guidelines on "appropriate types and timing of physical therapy in HSP" [25].

Interventional and surgical therapies. These include the muscle relaxant and antispastic agent, baclofen, which is a GABA_B receptor agonist [11, 23, 25]. Intrathecal baclofen therapy led to reduced lower limb's spasticity, decreased muscle tone and improved walking ability in HSP patients with severe spasticity [42–44]. A neurosurgical intervention is selective dorsal rhizotomy (SDR), a procedure, in which problematic nerve roots in the spinal cord are selectively resected and is hence considered as treatment of spinal-related spasticity in pure HSP [25, 45]. Uncomplicated HSP patients, who underwent SDR exhibited reduced muscular spasm, improved walking ability over a long period. However, SDR is not recommended for the treatment of complicated HSP forms as the surgery may be riskier and its effect less foreseeable [46].

Gene therapy. Gene therapy in HSP is compared to other neurological diseases, such as in spinal muscular atrophy [47], Huntington's, Parkinson's and Alzheimer's disease [48, 49], relatively slowly progressing due to its high genetic heterogeneity and variety of pathogenic mechanisms [40, 49]. Hence, until now there are no gene specific therapies available to treat HSP [50]. However, in the last years various molecular tools and methods for an effective application of gene therapy have been developed and improved, e.g., specific drug delivery using nanocarriers [48, 51, 52] and targeted gene manipulation using the CRISPR/Cas9 system [18, 48, 53]. The latter is already tested as tool for targeting neurodegenerative diseases like amyotrophic lateral sclerosis (ALS) [54]. Moreover, gene therapy is suggested to treat both gain- and loss of function mechanisms underlying SPG4 pathology [18]. Therefore, gene therapy is now considered as a promising option to treat hereditary neurodegenerative diseases, such as HSP [18, 40, 55–57].

1.1.5 Disease models

Danio rerio. The zebrafish is a vertebrate model broadly used to study developmental biology and human disease, due to similarities to human biology [58]. Simple genetic manipulation and a high reproduction rate allow large-scale experimental analysis and phenotype based screening [58, 59]. However, drawbacks are the absence of organs like lungs and breasts, or temperature limitations of the host organism as its optimal maintenance temperature is 28 °C, which could pose a problem when working with drugs or human tumor cells (optimum is 37 °C) [60]. Regarding the use of this model organism in HSP research, in an SPG11 zebrafish model, neurodegeneration was prevented and motor phenotype was rescued by the administration of miglustat to decrease ganglioside levels, which accumulates upon loss of Spatacsin protein [61]. Based on these results miglustat is currently undergoing phase 2 of a pharmacological trial with SPG11 patients to evaluate its safety [62]. Knockdown of Slc33a1 (SPG42) in zebrafish embryos revealed a critical role of acetyl-CoA transporter in motorneuron development and function [63]. Vps37a (SPG53) knockdown in zebrafish larvae resulted in the loss of motility [64].

Drosophila melanogaster. Thanks to its high reproduction rate, short generation time, easy and cheap maintenance, fully sequenced genome and the wide variety of fast and inexpensive gene manipulation tools, drosophila is a widely used model organism [65, 66]. There are drosophila models of neurodegenerative diseases like epilepsy, CNS injury, Alzheimer's and Parkinson's disease, or HSP [67]. For example, the role of spastin protein and therapeutic approaches have been investigated in an SPG4 drosophila model, in which treatment with vinca alkaloids attenuated disease related phenotypes [68]. Disadvantages of drosophila as a model organism are the less complex immune system as in vertebrates and the difference in brain anatomy [69].

Ex vivo models. *Ex vivo* models include cell models like patient-derived fibroblasts, primary cortical neurons and human induced pluripotent stem cells (hiPSCs). hiPSCs hold great potential for patient-specific cell therapies as unwanted immune reactions can be overcome [70, 71]. hiPSCs are generated from human somatic cells (e.g., skin, blood), which were reprogrammed to an "embryonic-like state" [71] and can differentiate into any type of cell. As a human model system hiPSCs are used to study human development and disease [70–72], such as HSP. For example, in an hiPSC model of SPG3A, axon defects were rescued

pharmacologically [73]. A study with hiPSCs derived from SPG4 patients restored neurite function by lentiviral overexpression of single spastin isoforms, highlighting the potential of gene therapy [74]. Nevertheless, the application of hiPSCs and other human cells to model disease can be challenging, as kinetics of disease development and pathology in a laboratory context (cell culture dish) differ from those in a patient [72]. Furthermore, purified cell populations lack interaction with other cell types, failing to mimic the natural environment in the human body [72].

Mus musculus. The mouse is one of the most complex and important organisms in science for modeling human development and disease in vertebrates. Despite the differences between mouse and human (e.g., genome, neuroanatomy, immune system, behavior), the application of mouse models in preclinical trials can elevate the "likelihood of successful drug development" [75] and help prevent "translational failures in human patients" [76]. A mouse model delivers insights into systemic interactions within an organism, not only between cell types but between whole systems [76]. Valid murine disease models represent an ideal tool to dissect disease mechanisms as well as to evaluate novel therapy approaches in neurodegenerative diseases like HSP [77]. An SPG11 and SPG15 knockout mouse model confirmed a role of the respective proteins in the same molecular pathway, *i.e.*, autophagy and autophagic lysosome reformation [78]. Interestingly, experiments with an SPG11 and SPG15 double knockout mouse model did not reveal an aggravated pathology [78]. In an SPG5 knockout mouse model, the mutated CYP7B1 gene was replaced by the intravenous administration of mRNA, highlighting the potential of mRNA as a causal treatment strategy [79]. The intramuscular adeno-associated viral (AAV) delivery of the paraplegin protein was shown to rescue axon degeneration of peripheral neurons in an SPG7 mouse model [80]. These studies demonstrate the importance of mouse models in the development of gene therapies for HSP.

1.2 *Zfyve26* associated HSP Type SPG15

1.2.1 Clinical characteristics

SPG15 is a form of complex HSP with onset typically in mid- to late childhood or adolescence (between 5-18 years of age) [11, 81]. Clinically, SPG15 patients cannot be distinguished from SPG11 patients with certainty as their phenotypes largely overlap, probably because

their associated proteins spastizin (SPG15) and spatacsin (SPG11) share common cellular pathways [11, 82, 83]. Best diagnostic predictor for SPG15 (as well as for SPG11) is the thinning of the corpus callosum (TCC), which can be observed in MRI (magnet resonance imaging) scans of the brain [83]. Analysis of SPG15 is suggested to be restricted to SPG11 negative patients, as SPG11 has a higher prevalence (accounts for ca. 20% of autosomal recessive HSP cases, SPG15 less than 3%) [13, 83]. A study with SPG15 patients observed additional complicated symptoms, such as cognitive impairment in 61% of cases, peripheral neuropathy 44%, cerebellar ataxia 67% and TCC 42% [83].

1.2.2 Genetic characteristics

SPG15 is among the most prevalent autosomal recessive HSPs with a worldwide prevalence of 0.13 per 100,000 [12]. SPG15 is associated with bi-allelic loss of function mutations in the *Zfyve26* gene (NCBI Reference Sequence: NM_015346 [84]), which is located on chromosome 14q24.1 and encodes the Zinc finger FYVE domain-containing protein 26 (also known as Spastizin) [11, 14, 81]. Putative functional domains are: The zinc finger C2H2 (exon 24), the FYVE domain (exon 28-29) and the leucine zipper (exon 36) [81]. Mutations in *Zfyve26* gene result in premature stop codons, which probably lead to RNA degradation by nonsense-mediated mRNA decay [81]. More specifically, studies with SPG15 patients revealed different homozygous truncating spastizin mutations with missense mutations being the most frequent ones: (i) nonsense mutations, (ii) frameshift deletions, (iii) splice mutations, (iv) indel-inversion rearrangements that delete exons [81, 83]. All mutations in *Zfyve26* gene lead to loss of spastizin protein function, which results in HSP type SPG15 [13].

1.2.3 Molecular mechanisms

Functional domains of spastizin protein. The highly conserved FYVE domain of the spastizin protein recruits and mediates the docking of spastizin onto membranes containing phosphatidylinositol 3-phosphate [PtdIns(3)P], such as endosomes [85–87]. Another functional domain of spastizin protein is the zinc finger (ZNF) protein, which belongs to a group of transcriptional activator proteins [88, 89]. As regulator of gene expression the ZNF protein interacts with DNA, RNA and other proteins, hence is involved in physiological processes (e.g., cell proliferation, differentiation, tissue homeostasis, adipogenesis) [88]. Mutations in the ZNF protein can contribute to the development of diseases like cancer and neurodegen-

eration via its transcription factor function [88]. The third functional domain of spastizin protein is the leucine zipper domain, which binds to a specific DNA sequence and acts as an enhancer binding protein [90–92].

Autophagy and the endolysosomal system. Spastizin protein is an interacting partner of Beclin1 protein, which regulates autophagy and endocytosis [93–97]. Loss of Spastizin protein function was shown to result in defects in endolysosomal trafficking [86, 87, 98]. More specifically, loss of spastizin protein was accompanied by impaired autophagic lysosome reformation (ALR), a cellular mechanism that generates new lysosomes, as well as the accumulation of large deposits in lysosomes of neurons [86, 87, 98]. The observed lysosomal pathology upon *Zfyve26* disruption is proposed to be the underlying mechanism of SPG15 associated neurodegeneration [11, 87, 99].

AP-5 protein complex. Spastizin interacts with spatacsin (associated with SPG11) and AP5Z1 (SPG48) in the coat like adaptor protein complex 5 (AP-5), with spastizin and spatacsin forming a scaffold [82, 100, 101]. The AP-5/SPG11/SPG15 localizes to late endosomal and lysosomal compartments and is involved in membrane traffic. While AP5Z1 acts in intracellular protein sorting and cargo trafficking, spastizin mediates the docking of the coat onto membranes via its FYVE domain [82, 98, 100–102].

Lipid metabolism. Recently, a link between loss of spastizin protein function and alteration in cellular lipid metabolism was discovered [99]. The accumulation of lipids within lysosomes hint at defects in cellular lipid homeostasis, which are linked to lysosomal aberrations. This classifies SPG15 as a lysosomal storage disease. Normally, for recycle, storage or functional purposes cholesterol, a crucial component of the cell plasma membrane, is transported from lysosomes to the endoplasmic reticulum and the plasma membrane [103], but is kept in lysosomes upon lysosomal recycling defects in neurons. It is also proposed that spastizin itself plays a role in lipid transport [99].

1.2.4 Therapy

Treatment of SPG15 aims at "reducing symptoms and preventing secondary complications" [11]. A detailed description of HSP treatments can be found under 1.1.4. Spasticity and weakness of lower limbs in SPG15 patients are treated with physical therapy, pharmaceuticals, botulinum toxin injections or surgery. Cerebellar dysfunction can be supported by

assessing home safety and fall risk of patients. To treat Parkinsonism administration of L-Dopa is considered. Besides the consultation with a social worker, cognitive impairment, developmental delay and intellectual disability are treated with physical and occupational therapy. Speech therapy assists with speech delay and defects. Further symptoms are bladder and eye problems, which are treated with anticholinergic drugs for urinary urgency, referral to an urologist and an ophthalmologist, respectively [11].

The drug dalfampridine (4-Aminopyridine) elevates the conduction of action potentials in demyelinated axons by blocking voltage-gated potassium channels [104–106] and is used to treat multiple sclerosis and spinal cord injuries [25, 107]. Studies demonstrated that oral administration of 10 mg of dalfampridine twice a day over 15 d led to improved walking ability, spasticity as well as hand dexterity in SPG15 and other HSP patients [104, 108]. No serious adverse effects of dalfampridine treatment, such as seizures, dizziness, nausea, balance disorder [107] were reported. These results support the use of dalfampridine as a "safe alternative treatment" [108] for SPG15 patients.

1.2.5 Disease models

Danio rerio. Knock-down of *Zfyve26* gene in zebrafish generated a neuronal phenotype similar to the defects observed in SPG15 patients [109]. Here, loss of spastizin protein function caused motor defects and abnormal branching of spinal cord motor neurons. Furthermore, this study hints at a functional relationship between the proteins spastizin and spatacsin (associated with SPG11) that may act in a common pathway, *i.e.*, intracellular trafficking.

Ex vivo models. Cellular disease models to study SPG15 include fibroblasts, primary cortical neurons as well as human induced pluripotent stem cells (hiPSCs) derived from SPG15 patients [110]. The analysis of mitochondrial morphology in hiPSCs-derived neurons revealed impaired mitochondrial dynamics as the underlying pathology of axonal defects in SPG15, demonstrating a "potential therapeutic target for SPG15" [110].

Mus musculus. In an SPG15 mouse model, exon 15 of the murine *Zfyve26* gene was deleted resulting in *Zfyve26* knockout (KO) mice, that exhibited a similar clinical and histological phenotype to SPG15 patients [87]. The murine *Zfyve26* gene is located on mouse chromosome 12 and consists of 42 exons with a start codon in exon 2 and the a stop codon in exon 42. Mutations in *Zfyve26* gene resulted in a premature stop codon, which probably

led to nonsense mediated mRNA degradation of truncated spastizin protein [81]. SPG15 KO mice developed spastic paraplegia accompanied by loss of brain structures (cortex, cerebellum) and axons of corticospinal motor neurons. Loss of spastizin protein led to the accumulation of large deposits in lysosomes hinting at endolysosomal dysfunction, which in turn may have caused neurodegeneration. In summary, this study proposed defects in endolysosomal membrane trafficking as the underlying pathology of SPG15. Based on these results, murine models pose a suitable tool for modeling SPG15 disease progression and, as a next step, for developing a targeted/causative therapy.

1.3 Description of research aims

Subject of this doctoral thesis is the functional characterization and validation of a novel *condZfyve26*-Null mouse model as a prerequisite for defining the therapeutic potential of somatic gene repair in HSP type SPG15. In this mouse model the ubiquitous *Zfyve26* gene expression was conditionally inactivated by the insertion of a stop-cassette (flanked by loxP sequences) into intron 2 of the murine *Zfyve26* gene (in the following named *condZfyve26*-Null) generating a mouse line, which resembles a classical knockout model. The Cre-loxP system is considered a sophisticated tool to modify and control the genome *in vivo* both temporally and spatially [111–113]. In the first place the applied Cre-loxP gene targeting strategy aims at reproducing the human *Zfyve26* functional loss in murine tissue. To examine the effects of the gene targeting strategy and to validate the novel *condZfyve26*-Null mouse line as an SPG15 disease model, the newly generated mouse line needed to be characterized on different functional levels. Therefore, the goals of this dissertation work were defined as follows:

1. Validation of the gene targeting strategy: Genotyping of *condZfyve26*-Null offspring, *Zfyve26* gene expression analysis and Spastizin protein expression analysis.
2. Assessment of general parameters of the *condZfyve26*-Null mouse line: Viability, fertility, mortality, body weight and metabolism.
3. HSP-specific locomotor studies of *condZfyve26*-Null mice: Foot base angle, rotarod analysis, ladder test and grip strength.
4. Histological characterization of the central nervous system in *condZfyve26*-Null mice and detection of HSP-specific pathologies.

5. Cell biological analysis of selected subcellular structures and functional fields in mouse tissues of cond*Zfyve26*-Null line.

Once characterization and validation are completed the novel cond*Zfyve26*-Null mouse model can be used as a sophisticated tool to control *Zfyve26* gene expression *in vivo* temporally and spatially. Importantly, the novel cond*Zfyve26*-Null mouse model provides the experimental basis for testing and defining the therapeutic potential of somatic gene repair in HSP.

Chapter 2

Materials and Methods

2.1 Generation of cond*Zfyve26*-Null mice

Customized generation of a mouse *Zfyve26* conditional knockin model in C57BL/6 mice was carried out by Cyagen US Inc. For that purpose a floxed stop-cassette was inserted into intron 2 of the *Zfyve26* targeting vector (Figure 2 and 5), which consists of an endogenous splice acceptor (SA) of intron 2, an internal ribosome entry site (IRES) with mCherry and a poly(A) signal (pA). The neomycin resistance cassette (Neo) is used for positive selection and is flanked by self-deletion sequences (SDA: self-deletion-anchor).

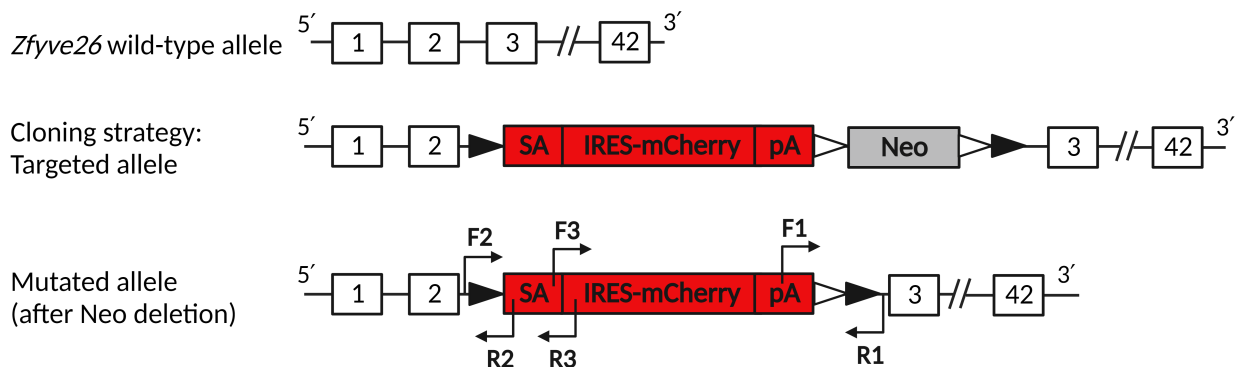


Figure 2. Targeted disruption of the murine *Zfyve26* gene. Schematic depiction of the cloning strategy. The murine *Zfyve26* gene consists of 42 exons (boxes with 1–42). The floxed (loxP sites as black triangles) stop-cassette (red) was inserted into intron 2 and consists of an endogenous splice acceptor (SA) of intron 2, an internal ribosome entry site (IRES) with mCherry and a poly(A) signal (pA). The neomycin resistance cassette (Neo, grey) is used for positive selection and is flanked by self-deletion sequences (SDA: self-deletion-anchor; white triangles). The mutated allele resembles a classical knockout, in which murine *Zfyve26* transcription is inhibited. Black arrows: Primer pairs used for genotyping (Forward 1 vs. Reverse 1; Forward 2 vs. Reverse 2; Forward 3 vs. Reverse 3).

Next, the linearized targeting vector was transfected into embryonic stem cells (ESCs) with a C57BL/6N genetic background, subsequently screened for three specific regions of the stop-cassette (Neo, 5' loxP site, IRES-mCherry) and finally re-implanted into pseudo-pregnant females. For specific primer pairs used see 2.3. Germline transmission of founder animals was confirmed by breeding with wild-type females and subsequent genotyping of the offspring. Heterozygous targeted mice were generated from ESC clone 1C5 and 2D3 (red asterisk in Figure 3). For this study, both heterozygous targeted animals were used for breeding purposes to generate wild-type, heterozygous and homozygous targeted animals. Respective ESC clone used is denoted within each result and its respective figure (in the following referred to as *condZfyve26*-Null 1C5 and 2D3 mouse line, respectively).

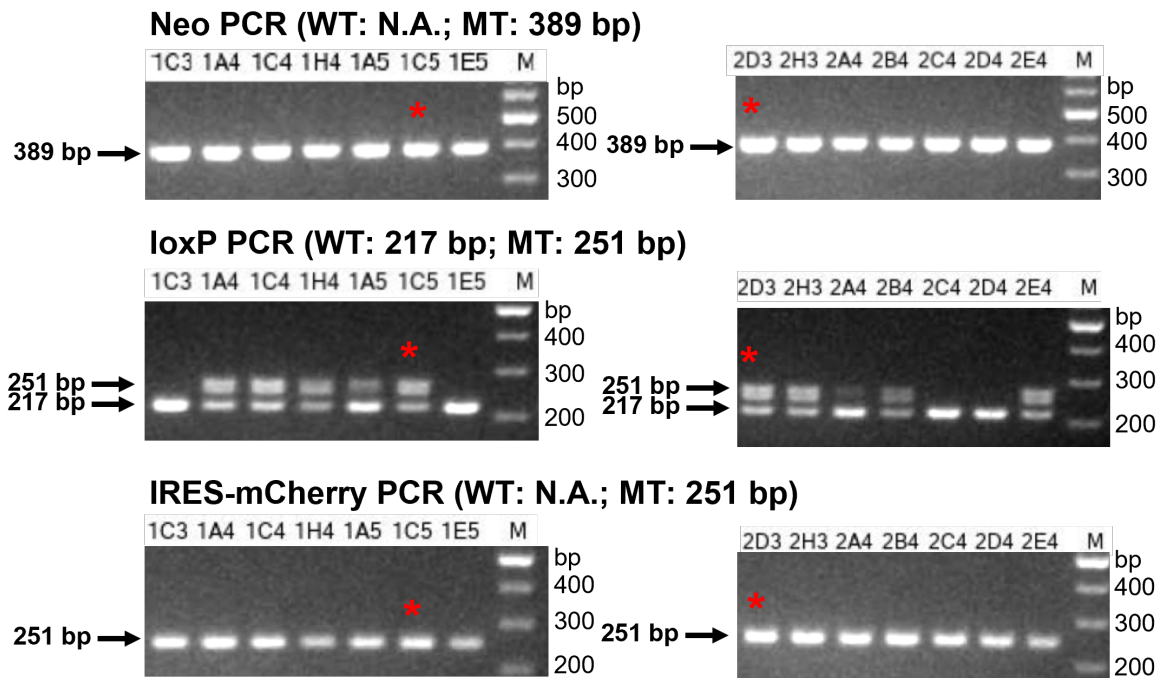


Figure 3. PCR screening of targeted embryonic stem cell (ESC) clones. PCR based genotyping confirmed correctly targeted clones. Expected bands for wild-type (WT) and mutant (MT) allele are indicated in respective PCR results. Screening was for three specific regions of the stop-cassette with top row: Neo (neomycin resistance cassette) deletion; middle row: loxP (5' loxP site); bottom row: IRES-mCherry (internal ribosome entry site with mCherry). *Left*: 1C5 ESC clone and *right*: 2D3 ESC clone are marked with red asterisks. N.A.: not available, M: marker, bp: base pair. Results generated by Cyagen US Inc.

2.2 Animals

All animal experiments were approved by the Landesamt für Gesundheit und Soziales (LaGeSo) in Berlin, Germany (approval number and date: G0126/20, 31.08.2020). Studies were performed with mice on a C57BL/6N background. Animals were kept at 22 °C in groups of 2–5 in a 12 h light/dark cycle and fed on a regular diet *ad libidum*.

2.3 Genotyping

Genomic DNA was extracted from mouse ear or tail biopsies using the Hot Sodium Hydroxide and Tris (HotSHOT) method. Tissue lysis (30 min, 95 °C and 5 min cooling on ice) was with alkaline lysis reagent (25 mM NaOH, 0.2 mM EDTA, pH 12) followed by inactivation with 1 × V of neutralizing reagent (40 mM Tris-HCl, pH 5).

Genotyping PCR was with 5 ng/μl of genomic DNA, 0.5 μM of the respective primer, 200 μM dNTP (Thermo Scientific, R0181), 0.04 U/μl Taq DNA Polymerase (Genecraft, GC-002-5000) and 1 × V Taq Reaction Buffer (Genecraft, GC-002-006). The following PCR program was applied: Initial denaturation (5 min, 94 °C), Denaturation (30 s, 94 °C, 35 cycles), Annealing (30 s, T_m of respective primer pair, 35 cycles), Extension (45 s, 72 °C, 35 cycles), Final extension (10 min, 72 °C), Hold (4 °C). The following *Zfyve26* primer sequences were used as pairs in a PCR mix:

F1 (Neo-delete PCR) 5'-CAAAGGTTGGCTATAAAGAGGTCAT-3'

R1 (Neo-delete PCR) 5'-CACTGTTTTGAGATAGGGTTTCACA-3'

F2 (loxP PCR) 5'-AAGTACACTTAGGAGCTGAGTATGG-3'

R2 (loxP PCR) 5'-CTCCCCACACCTGACTTAGTTTTATT-3'

F3 (IRES-mCherry PCR) 5'-TTCTCACTAGGACTTACCAGTTCAG-3'

R3 (IRES-mCherry PCR) 5'-CCTCACATTGCCAAAAGACGG-3'

Agarose gel electrophoresis (40 min, 100 V) was with a 2% agarose gel containing 1 × SYBR Safe DNA Gel Stain (Invitrogen, S33102) and with 1 × TriTrack DNA loading buffer (Thermo Scientific, R1161). The primer pair F1/R1 amplified a 408 bp mutant allele; the primer pair F2/R2 a 217 bp wild-type and/ or a 251 bp mutant allele; the F3/R3 a 251 bp mutant allele.

2.4 Sequencing

Gel DNA was extracted using the ZymoClean Gel DNA Recovery Kit (Zymo Research, D4008) following the manufacturer's protocol. Sequencing was with 2 ng/ μ l of DNA and 5 μ M of the respective primer and carried out by Eurofins Genomics. Software used for sequence analysis were Reverse Complement by Bioinformatics.org and FinchTV.

2.5 Gene expression analyses

For gene expression analyses, total RNA was isolated from brain samples (30 mg of cerebral cortex) using the RNeasy Mini Kit (Qiagen, 74104) following the manual instructions. Reverse transcription was carried out with 1 μ g of RNA. Primer annealing to the single-stranded template (5 min, 70 °C and 5 min on ice) was with 10 μ g/ml of random primers (Promega, C1181). For DNA polymerization (1 h, 37 °C), 0.5 mM dNTP (Thermo Scientific, R0181), 2 U/ μ l RNase sin (Promega, N2515), 1 \times M-MLV RT Buffer (Promega, M5313) and 1.6 U/ μ l M-MLV reverse transcriptase (Promega, M3682) were added to the reaction mix. Enzyme deactivation was for 15 min at 70 °C.

Quantitative real-time PCR (qPCR) was performed with cDNA (equivalent to 10 ng of reverse transcribed RNA), primers (75 nM) and the GoTaq qPCR Master Mix (Promega, A6001). Experiments were performed for three biological replicates in triplicates using an MX3000P qPCR System (Stratagene). Sample *Ct* values were normalized to GAPDH and fold change was calculated using the delta delta *Ct* method ($2^{-\Delta\Delta Ct}$)[114].

The following primer sequences were used as pairs in a PCR mix:

GAPDH-F 5'-GTCAAGGCCGAGAATGGGAA-3'

GAPDH-R 5'-CTCGTGGTTCACACCCATCA-3'

Zfyve26 (ex2)-F1 5'-AGACTGGGAGTTGGCACAAG-3'

Zfyve26 (ex3)-R1 5'-GCCAGAGCCAGGCTAATCTC-3'

Zfyve26 (ex21)-F2 5'-TGGGCAAGACTTGGATGACC-3'

Zfyve26 (ex22)-R2 5'-CGCAGCTCCATTAGCTTCCT-3'

Zfyve26 (ex39)-F3 5'-GAATTGCATTCCGTGTTCTGC-3'

Zfyve26 (ex40)-R3 5'-CAGGCAGTTGAGGAGGATGG-3'

2.6 Immunoblotting analyses

Tissue was homogenized using a prechilled Dounce homogenizer containing cold PBS and 1 × complete protease inhibitor (Roche, 11697498001). After centrifugation (5 min, 4 °C, 1200 × g) to remove insoluble cell debris, 60–100 µg protein in the supernatant was denatured (5 min, 95 °C) with 1 × Laemmli reducing buffer (0.2 M Tris-HCl, 0.4 M DTT, 8% SDS, 6 mM bromphenol blue, 4.3 M glycerol).

Protein was separated (45 min, 100 V) in a 7.5% SDS-polyacrylamide gel electrophoresis and transferred (60 min, 200 mA with constant A) onto a nitrocellulose membrane (Whatman, NBA083C001EA). After Ponceau S staining membrane was blocked (15 min, RT, rocking) with 2% BSA (Carl Roth, T844.2) in PBSB (PBS with 0.2% (w/v) Brij 58, pH 7.4) (Merck, 8.14727).

Primary antibody was incubated (ON, 4 °C, rocking) and detected (1 h, RT, rocking) with a horseradish peroxidase-conjugated secondary antibody. Membrane was washed (3 × 5 min, RT, rocking) with PBSB in between all incubation steps. Development of membrane was with an ultra-sensitive enhanced chemoluminescence (ECL) substrate (Thermo Scientific, 32106) and imaged using a VersaDoc 4000 MP Imaging System (Biorad).

2.7 Phenotyping

Body weight. Mouse body weight was measured on a weekly basis throughout the study by the same experimenter. Animals of an experimental cohort were weighed in the same order using the same scale. Weighing of mice was carried out prior to moving them into new cages.

Foot base angle. Prior to the experimental phase mice were trained to walk on a horizontal beam (width: 6 cm, length: 100 cm, height: 20 cm, material: polyoxymethylene) towards their home cages. Walking was video-recorded and single frames were acquired to measure the foot-base-angle at toe-off positions of the hind-paws using ImageJ.

Ladder climbing test. During the initial learning phase mice were trained to climb up a 55° angled ladder (width: 6 cm, length: 97 cm, distance between rungs: 2 cm, number of rungs: 44). Climbing was video recorded for quantification of correct and incorrect placement of the hind-paws onto the rungs. For quantification the first and last ten rungs of the ladder were not considered resulting in a total number of 12 rungs per hind-paw. Steps of the hindpaws

(24 steps in total) were categorized as follows: Mistakes were defined as slip (hindpaw slipped from the rung), skip (mouse skipped at least one rung) and correction (mouse readjusted its placement of the hindpaw on the rung), while consecutive steps with the midportion of the limb placed on the rung while none of the named mistakes occurred were counted as correct ones.

Grip strength test. Mice were placed on a grid connected to a sensor (Bioseb, BIO-GS3). The grasping applied by all four limbs was measured to assess the maximal muscle strength. Obtained grams force from the grip tests were normalized against mouse body weight in grams resulting in a gf/g ratio.

Rotarod test. Testing was with a rotarod Model LE8205 (Bioseb, BX-ROD). Animals were trained to walk on a beam that was rotating at an accelerating speed (4–40 rpm within 300 s). Measurement of maximal latency until falling off the beam (3 runs/animal/time point).

Indirect calorimetry. Animals were singly housed in 8 metabolic cages of the PhenoMaster system (TSE LabMaster Systems, Bad Homburg, Germany). The chamber was set to 22 °C with a 12 h:12 h light–dark cycle (light at 06:00 hr and dark at 18:00 hr). Following the adaptation phase (24 h) data collection was carried out for 24 h to assess locomotion activity, VO_2 , VCO_2 , food intake and respiratory exchange ratio ($RER = VCO_2/VO_2$). Metabolic parameters were measured every 27 min.

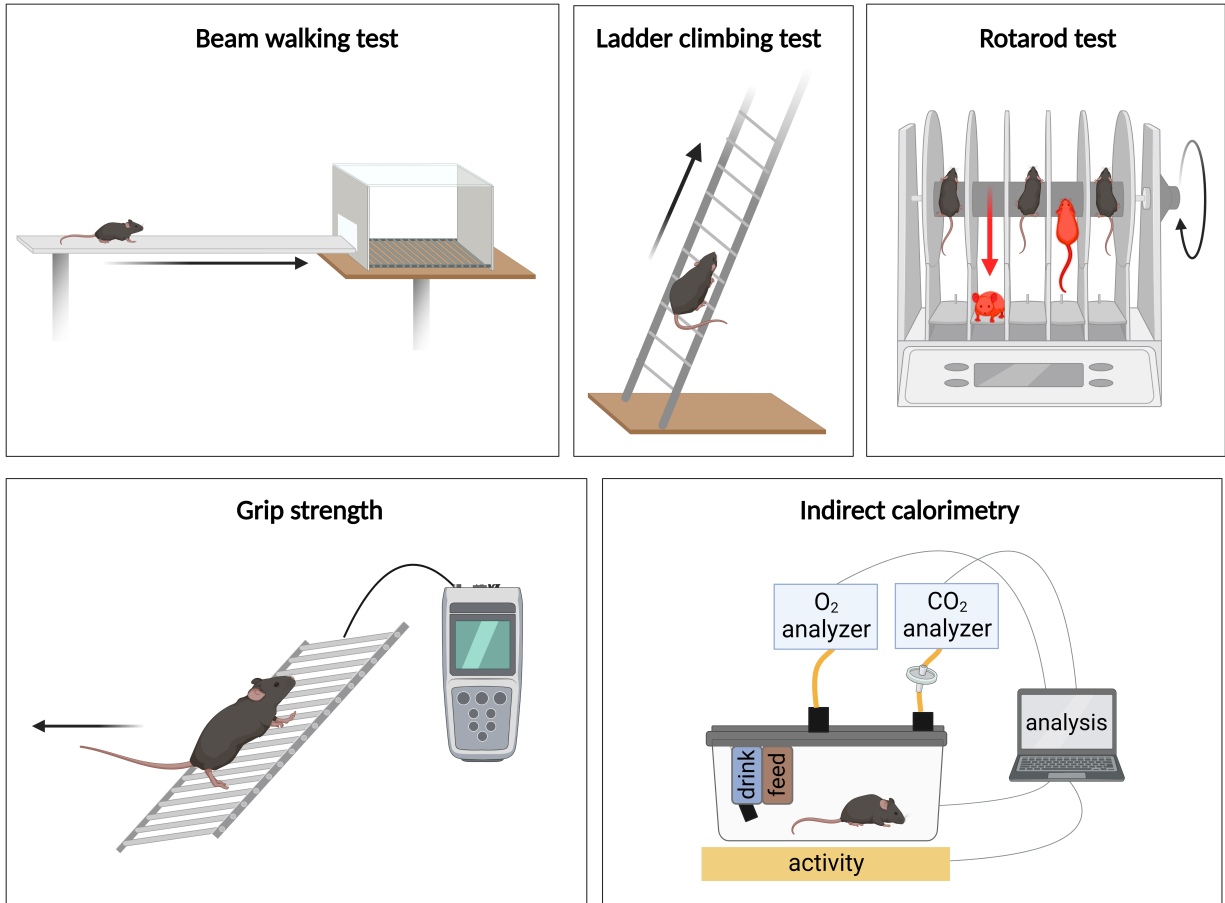


Figure 4. Tests used to assess motor phenotype in mice. *Beam walking test over time:* Mouse is trained to walk across a horizontal beam towards its home cage. Measurement of foot-base-angle as indicator of spasticity of hindlegs. *Ladder climbing test over time:* Assessment of motor function and coordination. Quantification of pre-defined mistakes (e. g. slips, jumps, skips). *Rotarod test over time:* Mouse is placed on a rotating beam. Time until fall provides measurement of motor coordination and motility. *Grip strength test:* Grasping applied by four limbs is measured to assess maximal muscle strength and neuromuscular function. *Indirect calorimetry over time:* Assessment of energy expenditure, locomotion activity, VO_2 , VCO_2 , food and water intake, respiratory exchange ratio ($RER = VCO_2/VO_2$). Parameters provide insights into metabolism.

2.8 Tissue processing

Mice were anesthetized with injection anesthesia (intraperitoneal) with ketamine/xylazine (100 mg/10 mg/kg body weight) and subsequent inhalation anesthesia with 2% isoflurane in 100% oxygen. After cardiac puncture and perfusion with 50 mL of cold PBS (-/-) (Gibco, 14190094), organs (brain, heart, kidneys, liver, lungs, left and right femoral muscles, spinal cord) were immediately removed, washed with cold PBS and either snap-frozen in liquid nitrogen or fixed in 3.7% formaldehyde (FA, Carl Roth, 7398.1). Optional after PBS perfusion, organs were perfused with 20 mL of 3.7% FA for pre-fixation.

For histology, organs were fixed for 2 h at RT, washed (3×15 min, RT, rocking) with

PBS (-/-) and incubated (1 h, RT, rocking) in freshly prepared 30% sucrose in PBS. Organs were kept at 4 °C in new sucrose solution until they sank to the bottom of the vial, embedded in Tissue-TEK OCT-Compound (Sakura Finetech, 4583) and stored at -80 °C.

2.9 Histology and immunohistochemistry

Brain sections were technically acquired using a cryostat (Leica, CM1900), stained and thesis published by Master's student Yick Chi Fung. Semithin sections of collected and fixed spinal cords could not be acquired and hence analysed due to technical constraints of the cryostat used.

10 μ m thick brain sections were stained with Hematoxylin and Eosin (H&E) following the manufacturer's protocol (Carl Roth, 9194.1), mounted on microscope slides embedded in mounting medium (Thermo Scientific, 9990402) and immediately imaged with a light microscope (Zeiss Axio Observer).

Immunohistochemical staining was performed with free floating sections of brain (40 μ m) and spinal cord (20 to 40 μ m). Washing (10 min, RT, rocking) was first in PBS (-/-), then in 0.25% (v/v) Triton/PBS and subsequently 2 \times in PBS. Blocking (1 h, RT, rocking) of tissue was with 5% (v/v) normal goat serum (Abcam, ab7481) in PBS. After primary antibody (in 5% NGS/PBS) incubation (ON, 4 °C, rocking, in the dark), sections were washed 3 \times in PBS as in previous steps, followed by secondary antibody (in PBS) incubation (1 h, RT, rocking, in the dark). Samples were washed 3 \times with PBS as in previous steps. Nucleic acid staining was with 0.02 μ g/ml DAPI (Sigma-Aldrich, D9542) in PBS for 10 min at RT in the dark with rocking, followed by washing steps (1 \times with PBS, 1 \times with 0.25% (v/v) Triton/PBS). Tissues were mounted on microscope slides embedded in mounting medium (Thermo Scientific, 9990402). Objects were dried and stored ON prior to imaging with a fluorescence microscope (Zeiss Axio Observer and Nikon Scanning Confocal A1Rsi+ provided by the Advanced Medical BioImaging Core Facility at the Charité).

2.10 Cell Culture

Isolation of primary mouse fibroblast cultures. Mouse adult fibroblasts (MAF) were isolated from several 1 mm mouse ear or tail tissues and pooled to establish primary cell cultures for

ex vivo experiments. After disinfection with 70% ethanol biopsies were washed with PBS (-/-) and then transferred into a 60 mm petri dish under a laminar flow hood. Tissue was minced in PBS containing 0.2% (w/v) collagenase A (Sigma Aldrich, C0130) and 2 U/ml dispase I (Sigma Aldrich, D4818) using a sterile scalpel and needle. Incubation was for 90 min at 37 °C and 400 rpm. After centrifugation (5 min, RT, 1000 × g) pellet was resuspended in warm culture medium DMEM high glucose, GlutaMax (Gibco, 10566016) supplemented with 10% (v/v) fetal bovine serum (Gibco, 10082147), 1% (v/v) penicillin/streptomycin 10 000 U/10 000 g/ml (Biochrom, A2212) and 1% (v/v) MEM non-essential amino acids solution (Gibco, 11140050). Cells were seeded on a 60 mm culture dish and incubated at 37 °C and 5% CO₂. Prior to the experiments cells were splitted once.

Cell culture maintenance. Cells were grown in a 100 mm petri dish in maintenance medium DMEM (Gibco, 11965092) supplemented with 10% (v/v) fetal bovine serum (Gibco, 10082147) and 1% (v/v) penicillin/streptomycin 10 000 U/10 000 mg/ml (Biochrom, A2212) at 37 °C in a 5% CO₂ incubator. Cells were allowed to grow until a confluence of 100% was reached. For passaging, cells were washed with 0.1% PBS/EDTA and treated (5 min, 37 °C) with 0.25% Trypsin/EDTA (Gibco, 25200056). After Trypsin inactivation with warm culture media and centrifugation (5 min, 1200 rcf) cell pellet was resuspended and transferred to new culture dishes with fresh media.

2.11 Immunofluorescence staining of primary cells

Primary mouse adult fibroblasts (MAF, not older than three passages) were plated on coverslips in a 6-well plate and grown until a confluency of 50% was reached. After washing with cold PBS, cells were fixed (15 min, RT) in 3.7% Formaldehyde. For LC3 stainings, fixation (10 min, 4 °C) was with ice-cold methanol. Washing (3 × 5 min, RT, rocking) was with cold PBS. Cells were incubated (2 h, RT, rocking, in the dark, in wet chamber) with 10% (v/v) normal goat serum and 0.1% (v/v) Tween20 (Serva, 37470) in PBS. After primary antibody incubation (ON, 4 °C, rocking, in the dark, in wet chamber), cells were washed as in previous steps with PBST (PBS with 0.1% (v/v) Tween20) and incubated (2 h, RT, rocking, in the dark, in wet chamber) with secondary antibody. Samples were washed with PBST as in previous steps. Nucleic acid staining was with 0.02 µg/ml DAPI for 10 min at RT in the dark with rocking, followed by washing steps. Cells were mounted on microscope slides

embedded in Shandon Immu-Mount mounting medium (Thermo Scientific, 9990402). Imaging was with a fluorescence microscope (Zeiss Axio Observer and Nikon Scanning Confocal A1Rsi+ provided by the Advanced Medical BioImaging Core Facility at the Charité).

2.12 Antibodies

Anti-Spastizin antisera were generated by immunization of rabbits against either the N-terminal epitope TSSELSTSTSEGSLSA of mouse Spastizin (residues 782-797) or the C-terminal epitope ENELVRSEFYEQAPS of mouse Spastizin (residues 1908-1923) by Kaneka Eurogentec S.A. (Belgium). Purification of sera was with affinity chromatography with the respective peptide bound to a matrix. For immunoblotting, both anti-Spastizin antibodies were used at a dilution of 1:100 in PBS.

The following antibodies were obtained commercially and used for immunoblotting and immunofluorescence.

Primary antibodies: mouse anti- β -Actin, 1:3000 (Sigma Aldrich, A1978); rabbit anti-Calbindin d28-K, 1:500 (Swant, CB38); rabbit anti-EEA1, 1:500 (Abcam UK, ab2900); mouse anti-GFAP, 1:1000 (Millipore, MAB360); mouse anti-NeuN, 1:500 (Millipore, MAB377); rabbit anti-Lamp1, 1:500 (Abcam UK, ab24170); rabbit anti-LC3B, 1:400 (Cell Signaling, 2775S); rabbit anti-Strumpellin (C-14), 1:200 (Santa Cruz, Sc-87442).

Secondary antibodies: goat anti-rabbit Horseradish Peroxidase, 1:5000 (Dako, P0448); rabbit anti-mouse Horseradish Peroxidase, 1:5000 (Dako, P0260); goat anti-rabbit coupled with Cy5, 1:1000 (Jackson ImmunoResearch Laboratories USA, 111-175-144); goat anti-rabbit coupled with Cy3, 1:1000 (Jackson ImmunoResearch Laboratories USA, 111-165-003); donkey anti-rat coupled with Alexa 488, 1:1000 (Invitrogen, A-21208).

2.13 Data and image analysis

Figure preparation and statistical tests. All image measurements were obtained from the raw data. The data was plotted and statistically analyzed using a Student's two-tailed, parametric t-test with Welch's correction using GraphPad Prism9 (GraphPad Software, San Diego, CA). All significant values and statistical tests are denoted within each figure and in their respective legends. All p -values are to be considered exploratory and do not adjust for

multiple testing.

Indirect calorimetry. Data analysis of indirect calorimetry (TSE LabMaster analysis) was carried out with *CalR*: A Web-based Analysis Tool for Indirect Calorimetry Experiments (<https://CalRapp.org/>) [115]. Uncorrected values for VCO_2 , VO_2 and energy expenditure were included in the analysis, *i.e.*, plots were not normalized or adjusted to the body weight. The experimental period integrated into the analysis was shortened to a total time frame of 24 h (12 h light, 12 h dark period), excluding the light photoperiods of the initial acclimation and the experimental phase.

Quantification of immunofluorescence image. Cellular vesicles were quantified using ImageJ. Images were converted to 8-bit and processed (Binary - convert to mask, watershed). Threshold was adjusted according to the individual imaging exposure time (minimum threshold value: 50 per 1000 ms exposure time, maximal threshold value: 255). Then 60 regions of interest (100 μ m) were analyzed per animal.

Quantification of Western blotting. Bands were quantified by densitometry using ImageJ. First, all values were normalized to their respective GAPDH values. Treatments (condZfyve26-Null) were then normalized relative to the control sample (wild-type) and expressed as a fold difference above control.

Images. Schemes and images were created with BioRender.com (extended version) or with Microsoft PowerPoint.

Chapter 3

Results

According to the recommendation of the biostatistics consultation by the Charité Institute of Biometry and Clinical Epidemiology from 10.02.2023 (see biostatistics certificate in appendix), no statistical tests were performed due to small sample sizes in experiments. Therefore, this work focuses on the descriptive analysis of the data.

3.1 Genotyping and sequencing confirmed correct insertion of the stop-cassette into the murine *Zfyve26* gene.

For genotyping of pups, various regions of the stop-cassette (*i.e.*, Neomycin cassette (Neo) deletion, 5' loxP site, IRES-mCherry) were screened using three specific primer pairs in a PCR (Figure 2) with F 1/R 1: wild-type not available (N.A.) and mutant 408 bp; F 2/R 2: wild-type 217 bp and mutant 251 bp; F 3/R 3: wild-type N.A. and mutant 251 bp (Figure 6, left). Desired pups were selected based on PCR screening results.

Subsequent sequencing analyses of the Neo deletion site (32 bases), loxP site (34 bases) and mCherry (1299 bases) approved correct gene manipulation (Figure 6, right). As reference, the *Zfyve26* knock-in gene targeting vector after Neo-deletion provided by Cyagen US Inc. was used (Figure 5).

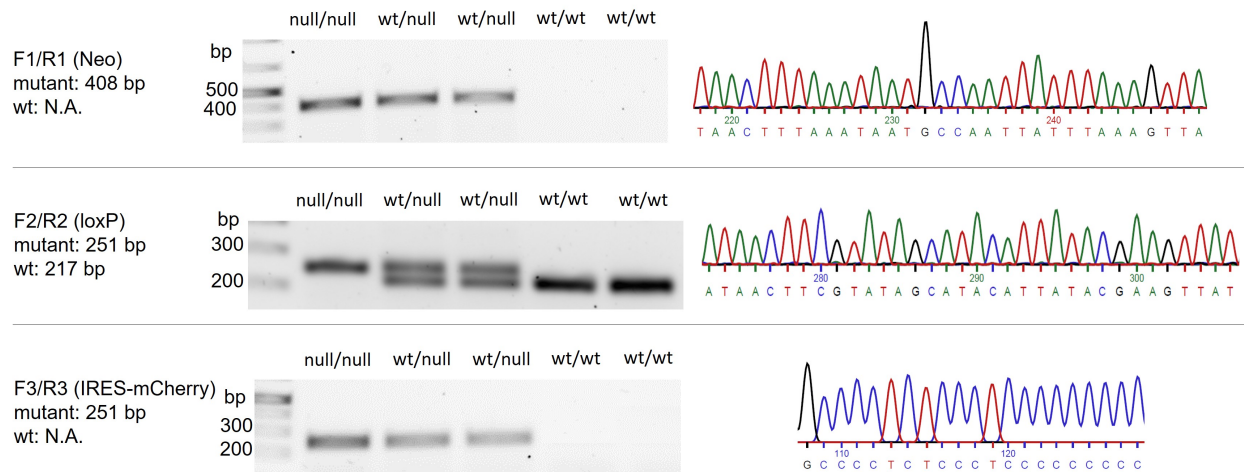


Figure 6. Targeted disruption of murine *Zfyve26* gene. *Left:* Expected PCR products with homozygous (null/null), heterozygous (wt/null) and wild-type (wt/wt) animals. *Right:* Exemplary results of sequencing analyses of relevant PCR products: Neo PCR (32 bases), loxP PCR (34 bases) and IRES-mCherry PCR (1299 bases, here shown excerpt only). Wt: wild-type, bp: base pair, N.A.: not available.

3.2 Mutant animals were viable and fertile.

The HSP type SPG15 is inherited autosomal recessively [81]. This means that in theory animals heterozygous for the mutated *Zfyve26* variant are asymptomatic carriers, while animals carrying two mutated *Zfyve26* alleles (homozygous) are affected. According to Mendelian inheritance, this means that the expected ratio between wild-type (wt/wt), heterozygous (wt/null) and homozygous (null/null) offspring of a 1:1 heterozygous breeding is 0.25, 0.5 and 0.25 (Figure 7 A). Taken together the reproduction results of 16 generations of cond*Zfyve26*-Null animals delivered the same number of homozygous (33/147) and wild-type (32/147) animals with a ratio of 0.22 each and the expected nearly two-fold number (82/147) of heterozygous pups (ratio: 0.56) (Figure 7 B,C). Offspring derived from 1C5 embryonic stem cell (ESC) clone (in the following referred to as cond*Zfyve26*-Null 1C5 mouse line) and 2D3 ESC clone (in the following referred to as cond*Zfyve26*-Null 2D3 mouse line) were pooled together as there were no differences in the ratio between both clones. The data thus indicated that in mutants germline transmission was correct and the stop-cassette was stably inherited to the next generations.

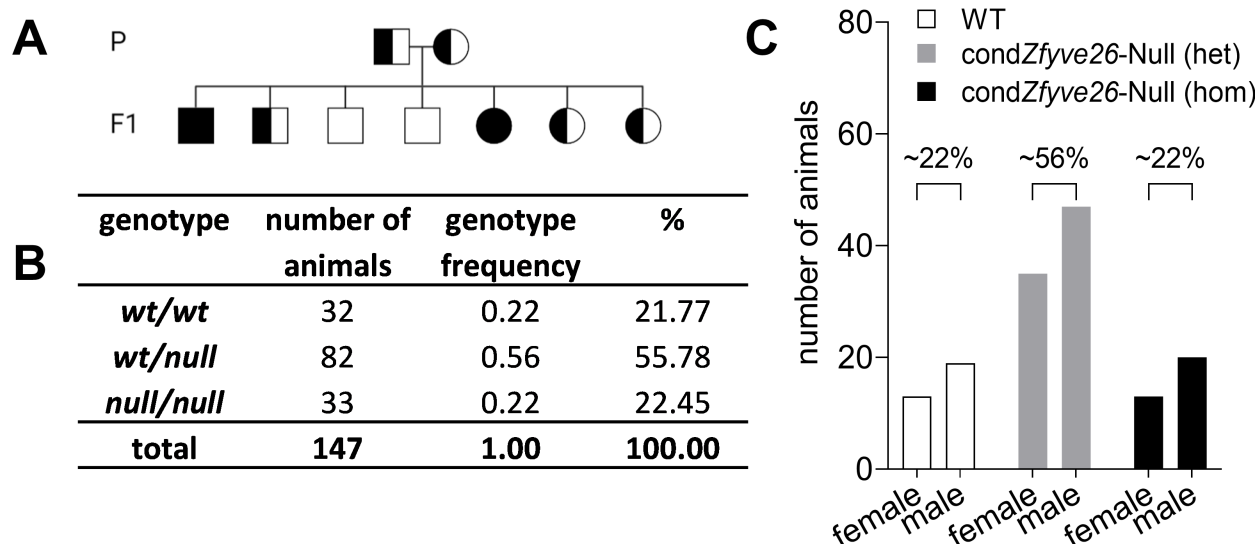


Figure 7. Reproductive ability of *condZfyve26*-Null animals. (A) Pedigree of an exemplary litter produced by 1:1 mating of heterozygous animals. Circles depict females and squares depict males. The Mendelian ratio predicts a genotype distribution of 50% heterozygous (black and white fill), 25% homozygous (black fill) and 25% wild-type (white fill) *condZfyve26*-Null offspring. P: parental generation; F1: first filial generation. (B) Number of 16 generations of wild-type (*wt/wt*), heterozygous (*wt/null*) and homozygous (*null/null*) *condZfyve26*-Null pups generated by 1:1 mating of heterozygous animals and respective genotype frequency. Mice generated from embryonic stem cell clone 1C5 and 2D3 were pooled together as there was no difference in ratio. (C) Graphical presentation of total number of animals splitted into female and male pups. Genotype frequencies from (B) are presented in percentage above the respective bars. het: heterozygous *condZfyve26*-Null; hom: homozygous *condZfyve26*-Null.

3.3 *Zfyve26* transcripts were reduced upon stop-cassette insertion.

In order to analyze the effect of stop-cassette insertion into intron 2 of the *Zfyve26* gene, *Zfyve26* expression levels of homozygous *condZfyve26*-Null animals were compared with those of wild-type littermates using quantitative PCR (qPCR) (Figure 8). The insertion is predicted to cause a disruption in *Zfyve26* gene expression. Three primer pairs were used targeting the 5' end (exon 2/exon 3), a middle section (exon 21/exon 22) and the 3' end (exon 39/exon 40) of the *Zfyve26* transcript. In homozygous *condZfyve26*-Null 1C5 mice, *Zfyve26* gene expression was reduced to 20.8% of wild-type level for ex2/ex3, to 55.2% for ex21/ex22 and to 42.3% for ex39/ex40 (Figure 8 A, left). In homozygous *condZfyve26*-Null 2D3 the fold change was more prominent with reductions in *Zfyve26* transcripts by more than 90% compared to wild-type levels (primer pair ex2/ex3: mean fold change = 0.7%; ex21/ex22: mean fold change = 2%; ex39/ex40: mean fold change = 9.6%) (Figure 8 A, right). Taken together, the data confirmed a sufficient inhibition of *Zfyve26* in homozygous *condZfyve26*-Null mice on the transcript level.

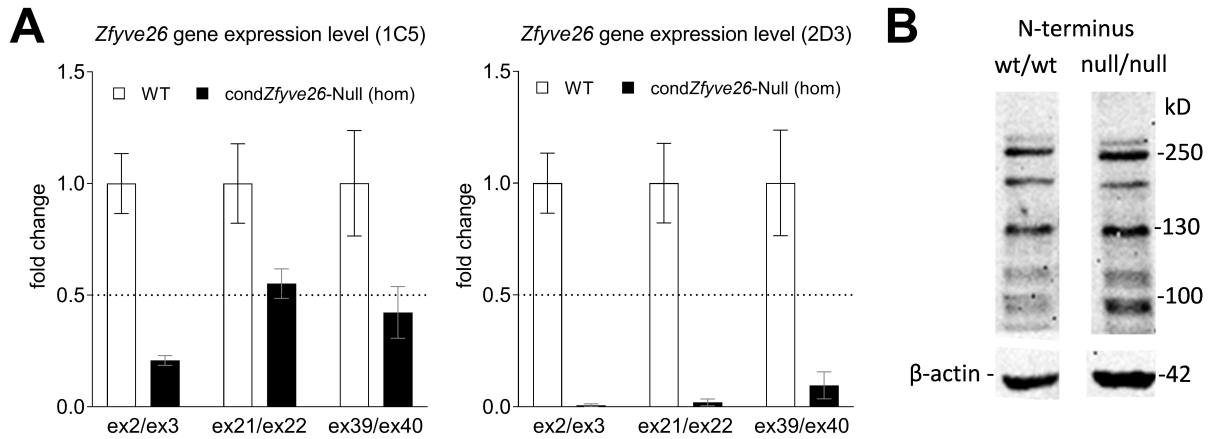


Figure 8. Reduction of *Zfyve26* gene expression levels in homozygous cond*Zfyve26*-Null mice. Quantitative PCR (qPCR) was performed on brain-derived cDNA to analyze gene expression of *Zfyve26* in homozygous (hom) cond*Zfyve26*-Null mice. Specific primer pairs used are indicated as exon forward vs. exon reverse. Normalized expression levels of cond*Zfyve26*-Null (hom) are shown as relative fold change of the gene expression level in wild-type (WT) littermates. **(A) Left:** 1C5 cohort: Reduction in *Zfyve26* gene expression across all gene regions in homozygous cond*Zfyve26*-Null mice (N=5 animals, n=10 data points) by >45% compared to WT (N=6 animals, n=11 data points). **Right:** 2D3 cohort: Reduction in *Zfyve26* gene expression across all gene regions in homozygous cond*Zfyve26*-Null mice (N=3 animals, n=6 data points) by >90% compared to WT (samples as in 1C5: N=6 animals, n=11 data points). Diagram depicts normalized (GAPDH) geometrical means; error bars represent SEM. Age of mice: 18–77 weeks (no age dependency observed). **(B)** Western blot analysis using an affinity purified antibody against the N-terminus of spastizin protein (285 kD) detected several unspecific bands in brain lysates from wild-type (wt/wt) and homozygous cond*Zfyve26*-Null (null/null) mice. Beta-actin (42 kD) served as a loading control. kD: kilodalton

Next, the gene expression data should be validated on the protein expression level using western blotting. Spastizin protein levels in homozygous cond*Zfyve26*-Null animals were expected to be absent upon *Zfyve26* gene disruption. However, immunoblotting with affinity purified antibodies against either the N- or C-terminus of spastizin detected a variety of unspecific bands in brain lysates from wild-type and homozygous cond*Zfyve26*-Null 1C5 and 2D3 mice (Figure 8 B, representative result of an immunoblot using the N-terminal anti-spastizin antibody). Thus, the targeted detection of a spastizin specific band at its predicted molecular mass of 285 kD was not possible with the antibodies and protein ladder used.

3.4 Body weight between experimental cohorts was inconsistent.

Body weight was assessed over time throughout the entire study for two different experimental cohorts of the cond*Zfyve26*-Null 1C5 mouse line: Cohort 1 with N=26 (13 wild-type with 8 males and 5 females, 13 homozygous cond*Zfyve26*-Null with 8 males and 5 females) and

cohort 2 with N=8 (4 wild-type with 2 males and 2 females, 4 homozygous *condZfyve26*-Null with 2 females and 2 males).

Animals of cohort 1 were weighed from age 18 to 59 weeks. Due to the small number of animals no statistical tests were conducted. However, clear trends were observed. There was no difference in the body weight between the genotypes in the first male cohort (Figure 9 A). The difference between the means (mean body weight of homozygous *condZfyve26*-Null minus mean body weight of wild-type) was $0.21 \text{ g} \pm 1.11 \text{ g}$ (SEM) (Figure 9 A'). Throughout the study the body weight of female homozygous *condZfyve26*-Null animals of cohort 1 was higher compared to their female wild-type littermates (Figure 9 B). The body weight of homozygous *condZfyve26*-Null females increased more steeply resulting in a sharper curve that reached its maximal difference in female body weight (14.40 g) at the end of the study at 59 weeks (wild-type mean body weight at age 59 weeks = 32.60 g and homozygous *condZfyve26*-Null body weight mean at age 59 weeks = 47.00 g) with the homozygous *condZfyve26*-Null group being as heavy as their male littermates (average male body weight at age 59 weeks = 46.00 g). The overall difference between the means of both female groups was $8.89 \text{ g} \pm 1.04 \text{ g}$ (mean body weight of homozygous *condZfyve26*-Null minus mean body weight of wild-type) (Figure 9 B'). This observed body weight of female mice could not be replicated in cohort 2.

Animals of cohort 2 were weighed from age 28 to 59 weeks. In general, males of the second cohort tended to be lighter than animals of the first cohort (Figure 9 C). In contrast to cohort 1, homozygous *condZfyve26*-Null males of cohort 2 were slightly lighter than their wild-type littermates (wild-type mean = 38.65 g; *condZfyve26*-Null (hom) mean = 36.34 g). The difference between the means was $-2.31 \text{ g} \pm 0.74 \text{ g}$ (mean body weight of homozygous *condZfyve26*-Null minus mean body weight of wild-type) (Figure 9 C'). The phenotype observed in the first female cohort could not be replicated in the second cohort, indicating that body weight could be litter specific in *condZfyve26*-Null mice of the 1C5 line. For females, there was no difference in the body weight at any time point (Figure 9 D). The body weight ranged between 25.00 g and 37.50 g. The difference in body weight between the group means was $-1.19 \text{ g} \pm 0.74 \text{ g}$ (mean body weight of homozygous *condZfyve26*-Null minus mean body weight of wild-type) (Figure 9 D').

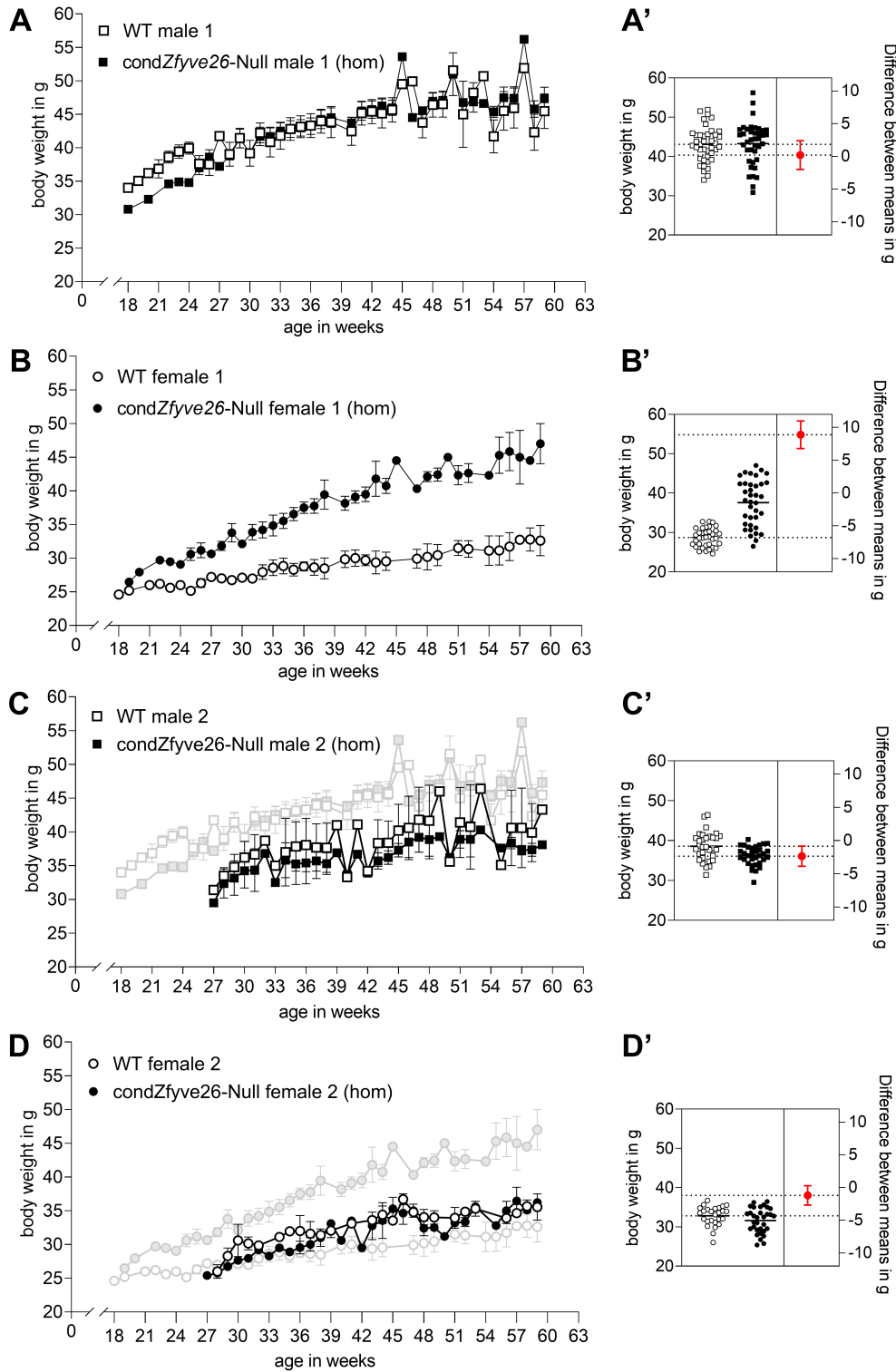


Figure 9. Body weight of *condZfyve26*-Null 1C5 mice might be litter specific. Body weight of wild-type (WT) and homozygous (hom) *condZfyve26*-Null animals in gram (g) over time (left) and respective estimation plots showing the difference between group means (right, in red and in g, *condZfyve26*-Null (hom) minus WT). (**A–B**): Cohort 1 with N=26 animals. (**A,A'**) Body weight of males did not show any differences between both groups. (**B,B'**) Body weight of female *condZfyve26*-Null (hom) animals increased steeper compared to their WT littermates and was higher throughout the study. (**C–D**): Cohort 2 with N=8 animals. For direct comparison, body weight values of cohort 1 are transparently displayed. (**C,C'**) Body weight of *condZfyve26*-Null (hom) males was slightly reduced compared to their WT littermates. (**D,D'**) There was no difference in the body weight between female groups. Data shown as mean \pm SEM.

3.5 Gait analysis revealed trend towards poorer performance in homozygous *condZfyve26*-Null 1C5 mice.

To assess the motor phenotype of wild-type and homozygous *condZfyve26*-Null 1C5 mice quantitatively, standardized movement tests [87, 116] were applied over time.

3.5.1 Foot base angle

The foot base angle (FBA) was measured at toe-off position of both hindpaws (Figure 10 A). Signs of gait disorder and motor deficit are a decrease in angle values. Quantification revealed mean angle values between 58° and 70° for males (Figure 10 B) and values between 66° and 73° for females (Figure 10 C). Temporally, a trend towards a decreasing FBA in homozygous *condZfyve26*-Null mice compared to their wild-type littermates was observed, both in the male and female cohort. At all timepoints all animals were able to traverse the beam without falling off the beam, an indication of existing balance.

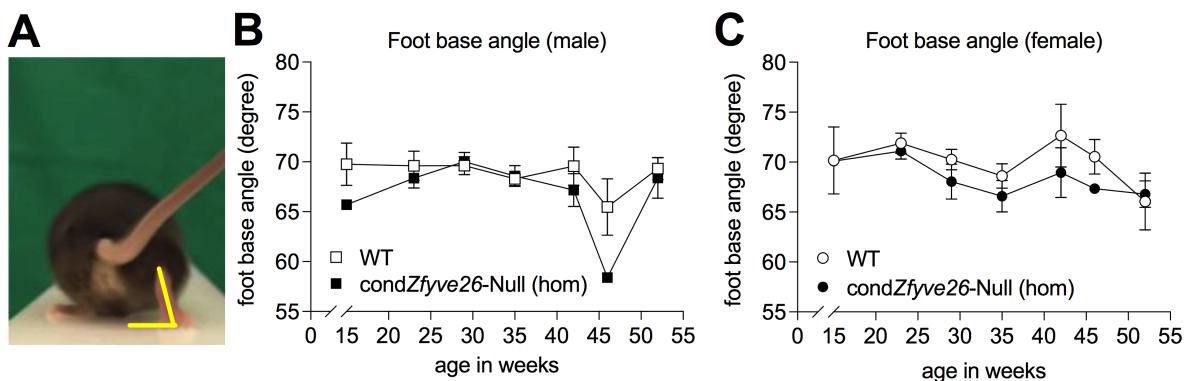


Figure 10. Testing of motor performance in *condZfyve26*-Null 1C5 line: Foot base angle. (A) Measurement of foot base angle at toe-off position (yellow lines) using single video frames of mice walking across a beam. (B, C) Wild-type (WT, N=13 with 8 males and 5 females) and homozygous (hom) *condZfyve26*-Null (N=13 with 8 males and 5 females). All data shown as mean \pm SEM.

3.5.2 Ladder climbing and grip strength

The ladder climbing test was applied to quantify complex motor behavior in mice. For detailed definition and categorization of steps see chapter 2.7. Overall, the most prominent mistakes were skips, followed by slips, while corrections occurred less frequently (Figure 11).

Male wild-type animals scored more correct steps than homozygous *condZfyve26*-Null mice (Figure 11 A). At 16–24 weeks, 82.9% of all steps in wild-type males were correctly placed compared to 78.6% in homozygous *condZfyve26*-Null males. At 44–52 weeks, the share of correct steps in wild-type animals increased to 89.8% while the amount of correct steps placed stayed similar with 80.9% in homozygous *condZfyve26*-Null males, resulting in a bigger difference in performance between the genotypes.

At an age between 16 and 24 weeks wild-type females scored 71.6% correct steps while their homozygous *condZfyve26*-Null female littermates scored 70.8% correct steps (Figure 11 A'). At the latest time point tested (age 44–52 weeks), female wild-type animals reached 76.8% correct steps vs. 81.6% in homozygous *condZfyve26*-Null females. Taken together the data revealed an increase in correct steps over time for both sexes, but overall males scored better than females as they made fewer mistakes.

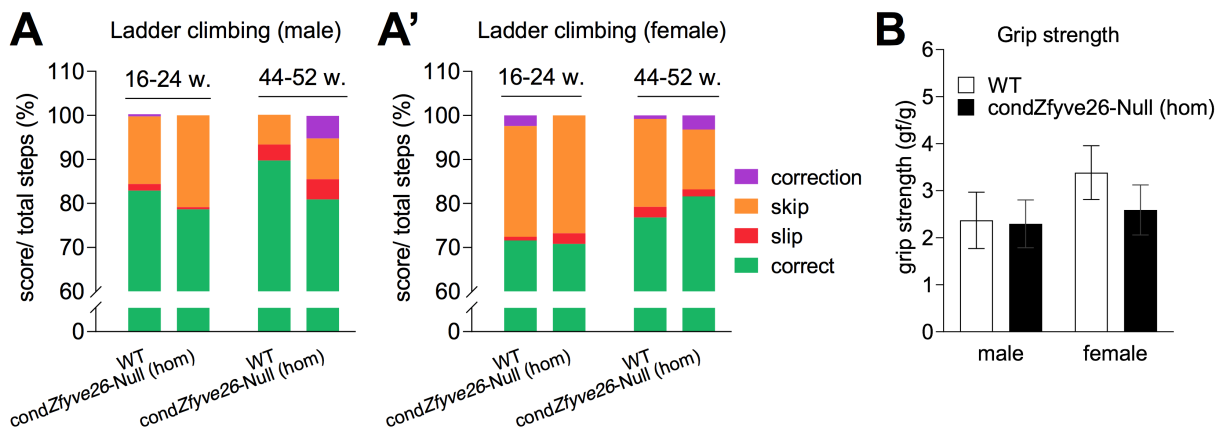


Figure 11. Testing of motor performance in *condZfyve26*-Null 1C5 line: Ladder climbing and grip strength. Wild-type (WT, N=13 with 8 males and 5 females) and homozygous (hom) *condZfyve26*-Null (N=13 with 8 males and 5 females). **(A-A')** Ladder climbing test at 16–24 and 44–52 weeks (w.) of age. The relative score categories are indicated as colored bars, adding up to 100%. Data shown as mean. **(B)** Four-limb grip strength values obtained (duplicate) were normalized against mouse body weight, grams force/gram (gf/g). Average age was 40 weeks. Data shown as mean \pm SD.

Four-limb grip strength values obtained were normalized against mouse body weight (grams force/gram). Testing of grip strength to measure the neuromuscular function did not reveal any differences in the maximal muscle strength between male homozygous *condZfyve26*-Null mice (average grip strength = 2.3 gf/g) and their wild-type littermates (average grip strength = 2.4 gf/g) (Figure 11 B). However, normalized grip strength was reduced in female homozygous *condZfyve26*-Null animals (average grip strength = 2.6 gf/g) by 0.8 gf/g com-

pared to wild-type females (average grip strength = 3.4 gf/g). Interestingly, the normalized grip strength values in females were higher than those obtained in males.

3.5.3 Rotarod

Rotarod test over time was applied to evaluate coordination and balance of mice. Maximal time until fall was quantified (Figure 12 A and B). Latency values were normalized to body weight, resulting in seconds per gram weight (sec/g) (Figure 12 A' and B'). Overall, latency to fall decreased with increasing age for all genotypes and sexes.

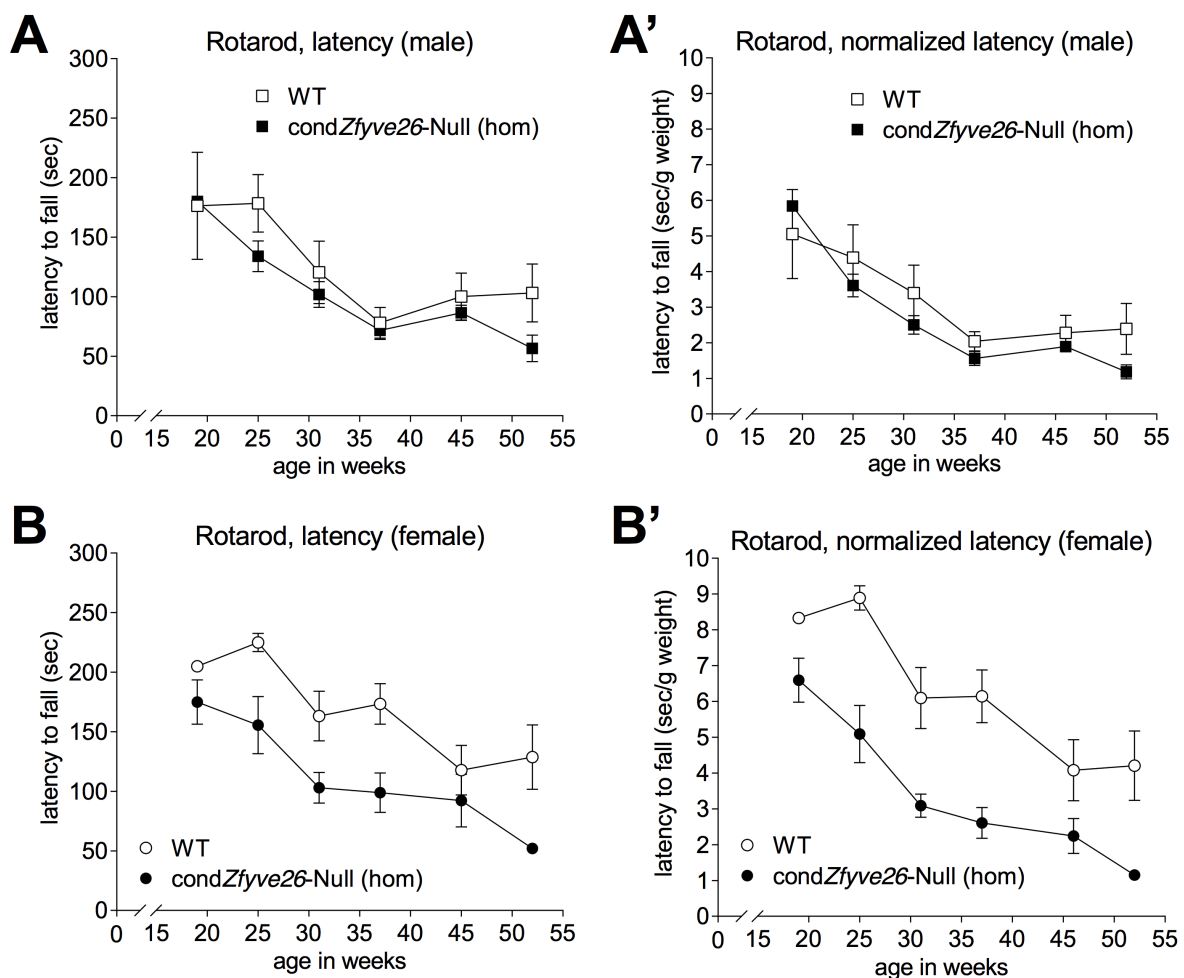


Figure 12. Testing of motor performance in *condZfyve26*-Null 1C5 line: Rotarod. (A and B) Latency to fall in second (sec). (A' and B') Latency to fall in second (sec) was normalized to body weight (g), resulting in sec/g weight. The latency to fall was decreased in both male and female homozygous *condZfyve26*-Null mice compared to their respective wild-type littermates. The difference in performance was bigger in females. Wild-type (WT, N=13 with 8 males and 5 females) and homozygous (hom) *condZfyve26*-Null (N=13 with 8 males and 5 females). All data shown as mean \pm SEM.

A trend towards a poorer performance of male homozygous *condZfyve26*-Null mice was observed: Starting at 25 weeks of age, they tended to fall off the rotating beam earlier than wild-type animals (Figure 12 A and A'). For females, the difference in performance between both genotypes was more distinct. The analysis revealed a strong decrease in latency to fall in homozygous *condZfyve26*-Null animals compared to their wild-type littermates (Figure 12 B and B'). While males did not remain on the beam for longer than 180 s on average (at 19 weeks of age) throughout the study, female wild-type animals reached maximal 225 s on average (at age 25 weeks). As in the grip strength, the data revealed a body weight dependency, which was more prominent in females.

3.5.4 Indirect calorimetry.

The cause underlying the higher body weight observed in the female cohort 1 (see Figure 9) should be further investigated by indirect calorimetry. After the outbreak of a zoonotic pathogen in the animal facility and the subsequent culling of the entire first cohort (see official document in appendix) indirect calorimetry was carried out with a second experimental cohort (cohort 2). Indirect calorimetry was for 24 h (12 h light and 12 h dark period) at three time points (T1–T3): Age 30, 48 and 60 weeks. Mice were single housed. Data are either blotted as four groups with two animals each (left diagrams: wild-type male, homozygous *condZfyve26*-Null male, wild-type female, homozygous *condZfyve26*-Null female), or male and female animals grouped into two groups with four animals each (right diagrams: wild-type vs. homozygous *condZfyve26*-Null). In summary, indirect calorimetry did not hint at differences in metabolic activity between wild-type and homozygous *condZfyve26*-Null animals.

Energy expenditure

Energy expenditure (EE) in kilocalories per hour (kcal/hr) was assessed to analyze the amount of energy used by an animal to maintain its essential body functions, or energy spent on physical activity and thermoregulation (Figure 13). For all animals, EE did not change dramatically over time (T1–T3) as values constantly ranged between 0.4 and 0.7 kcal/hr. In general both individual male animals had higher EE values than females (at T1 the EE values measured in female homozygous *condZfyve26*-Null were clearly lower than those of other groups), hinting at a body weight dependency of EE (Figure 13, left).

When comparing wild-type (WT) with homozygous *condZfyve26*-Null, at 30 weeks (T1) of age EE values of homozygous *condZfyve26*-Null tended to be slightly lower, which is probably due to the low EE values measured in female homozygous *condZfyve26*-Null; however, at later testing points (T2 and T3) the curves of both genotypes were strongly overlapping, ruling out any major differences in EE (Figure 13, right). Independent of genotype and sex, measured EE values were higher during the dark photoperiods, which was expected since mice are nocturnal animals, which are active during the night [117].

Energy expenditure (kcal/hr)

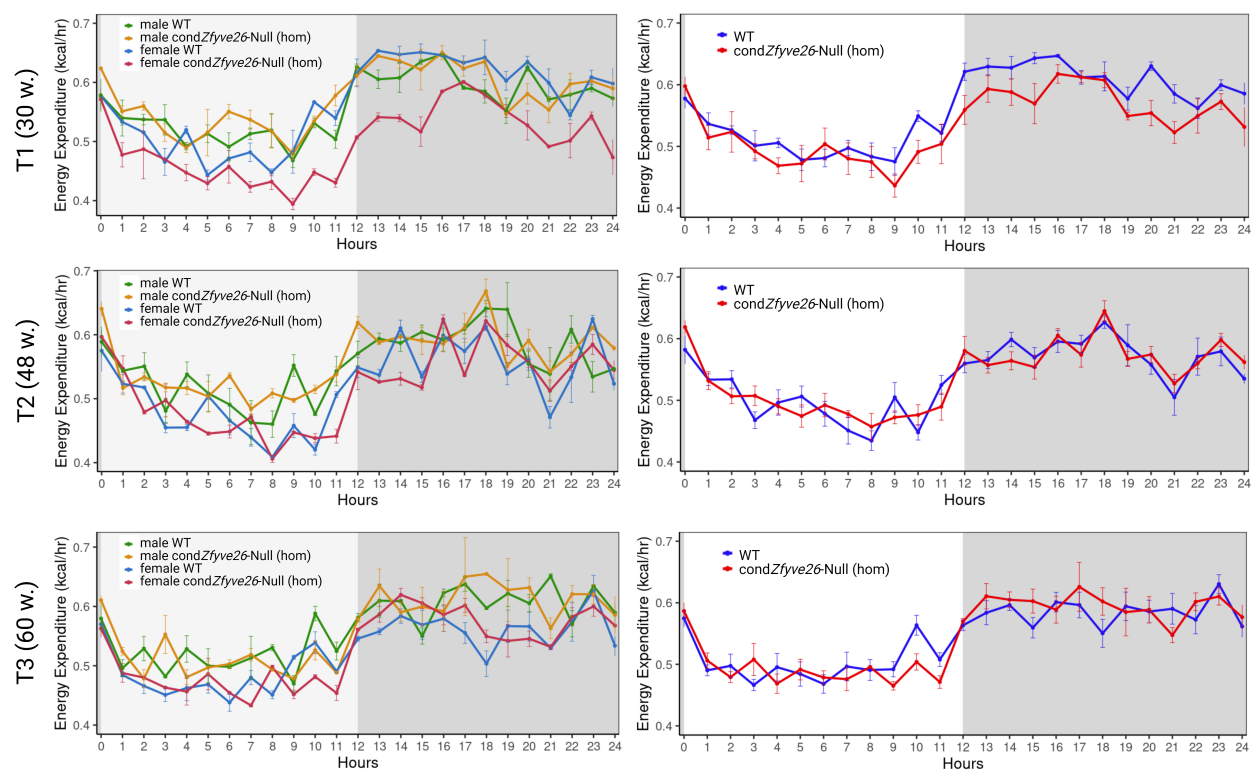


Figure 13. Indirect calorimetry: Energy expenditure. Mice were single housed and tested over time at three time points (T1–T3) at age 30, 48 and 60 weeks (w.). *Left:* Four cohorts with wild-type (WT) male (N=2), homozygous (hom) *condZfyve26*-Null male (N=2), wild-type female (N=2) and homozygous *condZfyve26*-Null female (N=2). *Right:* Males and females grouped as wild-type (N=4) vs. homozygous *condZfyve26*-Null (N=4). Metabolic data versus time. 12 h light and 12 h dark photoperiods are indicated as white and grey backgrounds, respectively. kcal/hr: kilocalories per hour.

Respiratory exchange ratio

The ratio between metabolic CO₂ production and O₂ intake results in the respiratory exchange ratio (RER, Figure 14), which provides information on the type of energy source catabolized in a specific time frame: RER values of 0.71 indicate fat as the primary energy source, RERs of 0.74 are an indicator of protein metabolism with uric acid as metabolic end product, while values of 0.81 indicate protein metabolism with urea as metabolic end product and values of 1.0 indicate carbohydrate metabolism [118]. Independent of genotype and sex, RER levels tended to be higher during dark periods compared to those obtained during light periods. Interestingly, RER levels increased over time for all groups (Figure 14, right): At 30 weeks of age (T1) RER values ranged between 0.7 and 0.8, at 48 weeks (T2) between 0.75 and 0.8 and at 60 weeks (T3) between 0.8 and 0.95, suggesting that the main energy source shifted from fat and proteins to carbohydrates with age.

Respiratory Exchange Ratio (RER)

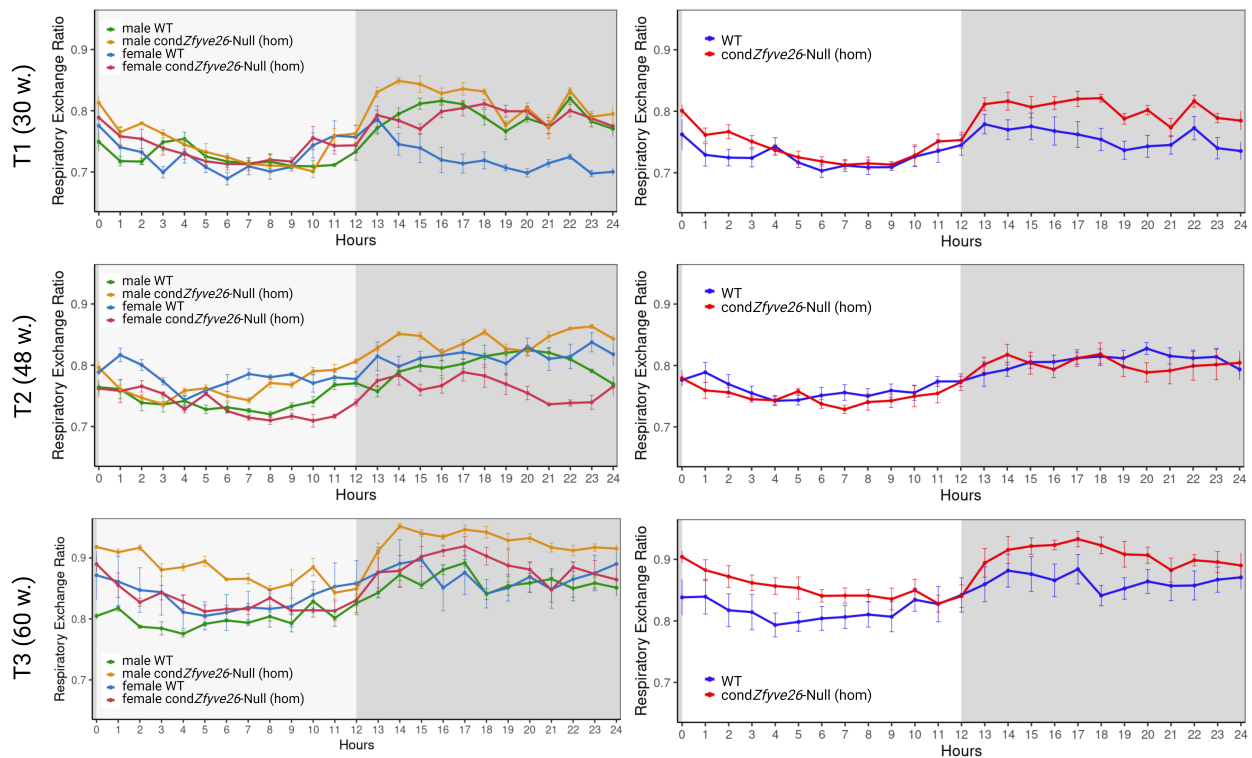


Figure 14. Indirect calorimetry: Respiratory Exchange Ratio (RER). Mice were single housed and tested over time at three time points (T1–T3) at age 30, 48 and 60 weeks (w.). RER = CO₂ intake/O₂ production. RER values indicate the type of metabolism: RER = 0.71 fat metabolism, RER = 0.74 protein metabolism (uric acid), RER = 0.81 protein metabolism (urea), RER = 1.0 carbohydrate metabolism. *Left:* Four cohorts with wild-type (WT) male (N=2), homozygous (hom) *condZfyve26*-Null male (N=2), wild-type female (N=2) and homozygous *condZfyve26*-Null female (N=2). *Right:* Males and females grouped as wild-type (N=4) vs. homozygous *condZfyve26*-Null (N=4). Metabolic data versus time. 12 h light and 12 h dark photoperiods are indicated as white and grey backgrounds, respectively.

Food and water consumption

Overall, hourly food consumed in kilocalories (kcal/hr) and hourly water consumed in millilitre (ml/hr) were higher during dark periods, independently of age, genotype and sex (Figure 15 and 16). Comparison of food consumption between homozygous *condZfyve26*-Null animals and wild-type littermates revealed a weak trend towards a higher food consumption in homozygous *condZfyve26*-Null at 60 weeks of age (Figure 15, right). Furthermore, water consumption tended to be slightly higher in homozygous *condZfyve26*-Null at all time points compared to wild-type (Figure 16, right). Despite the trends, no clear differences between ages, genotypes and sexes were observed.

Food consumed per hour (kcal/hr)

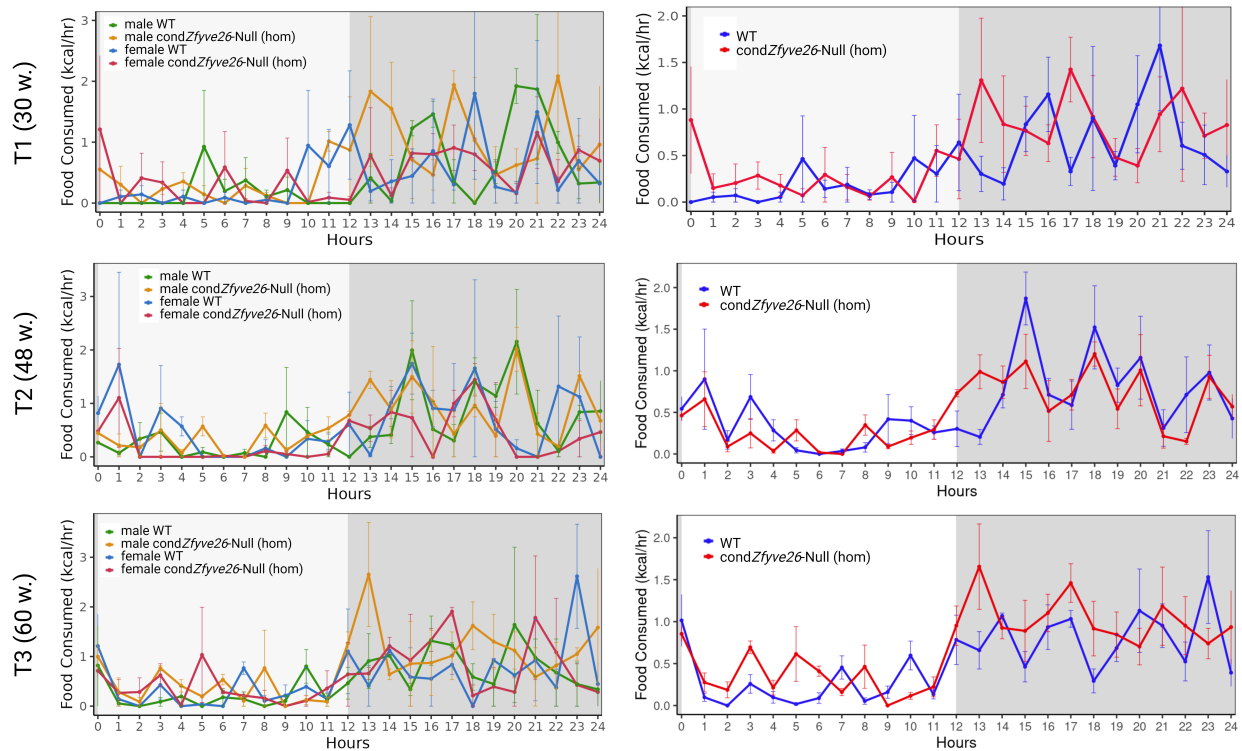


Figure 15. Indirect calorimetry: Food consumption. Mice were single housed and tested over time at three time points (T1–T3) at age 30, 48 and 60 weeks (w.). Food consumption was measured in kilocalories per hour (kcal/hr). *Left*: Four cohorts with wild-type (WT) male (N=2), homozygous (hom) *condZfyve26*-Null male (N=2), wild-type female (N=2) and homozygous *condZfyve26*-Null female (N=2). *Right*: Males and females grouped as wild-type (N=4) vs. homozygous *condZfyve26*-Null (N=4). Metabolic data versus time. 12 h light and 12 h dark photoperiods are indicated as white and grey backgrounds, respectively.

Water consumed per hour (ml/hr)

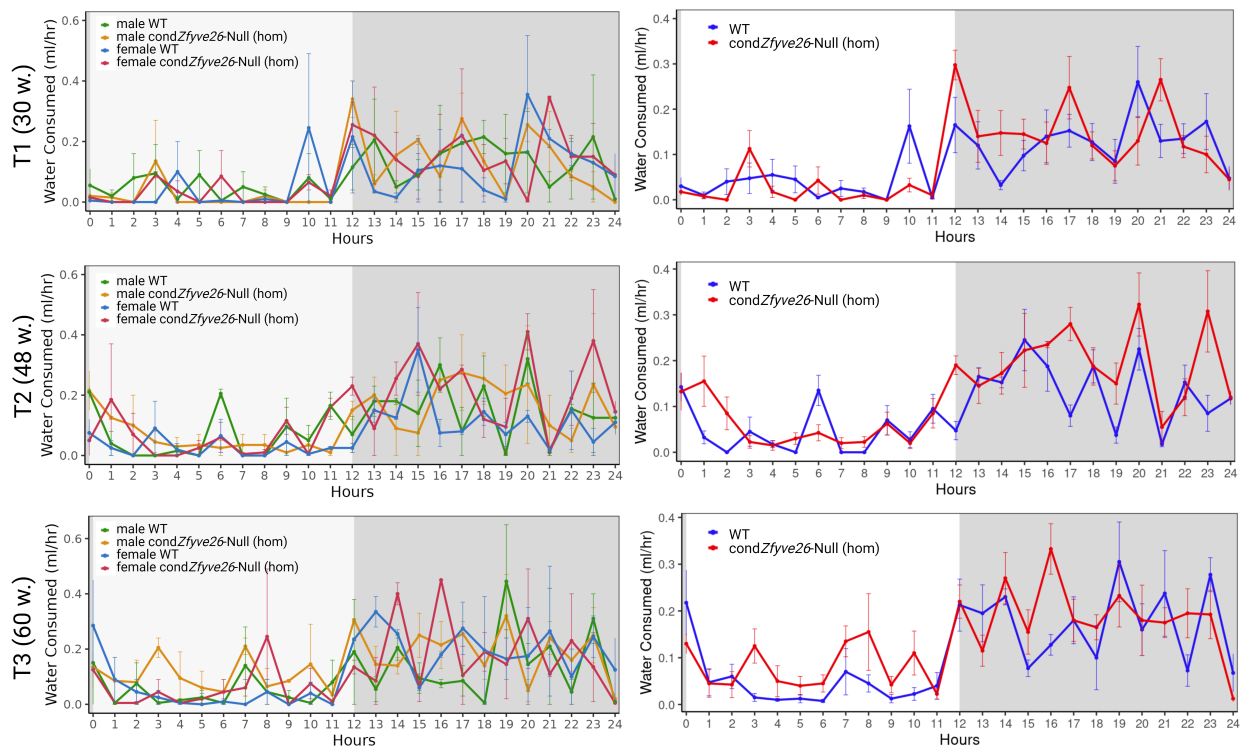


Figure 16. Indirect calorimetry: Water consumption. Mice were single housed and tested over time at three time points (T1–T3) at age 30, 48 and 60 weeks (w.). Water consumption was measured in millilitre per hour (ml/hr). *Left:* Four cohorts with wild-type (WT) male (N=2), homozygous (hom) condZfyve26-Null male (N=2), wild-type female (N=2) and homozygous condZfyve26-Null female (N=2). *Right:* Males and females grouped as wild-type (N=4) vs. homozygous condZfyve26-Null (N=4). Metabolic data versus time. 12 h light and 12 h dark photoperiods are indicated as white and grey backgrounds, respectively.

Locomotion and ambulation

Hourly assessment of locomotion and ambulation activity in beam breaks (beam breaks/hr) was higher during dark periods at all time points and in all groups. The data revealed a remarkably higher movement activity in 30 week old female wild-type animals during the dark period, which was temporally with 4000 beam breaks/hr twice as high as the other groups (Figure 17 and 18, each left). However, at 48 and 60 weeks of age locomotion and ambulation curves of homozygous *condZfyve26*-Null were mostly overlapping with those of wild-type mice, suggesting no clear differences in motor activity between the groups.

Locomotion activity (beam breaks/hr)

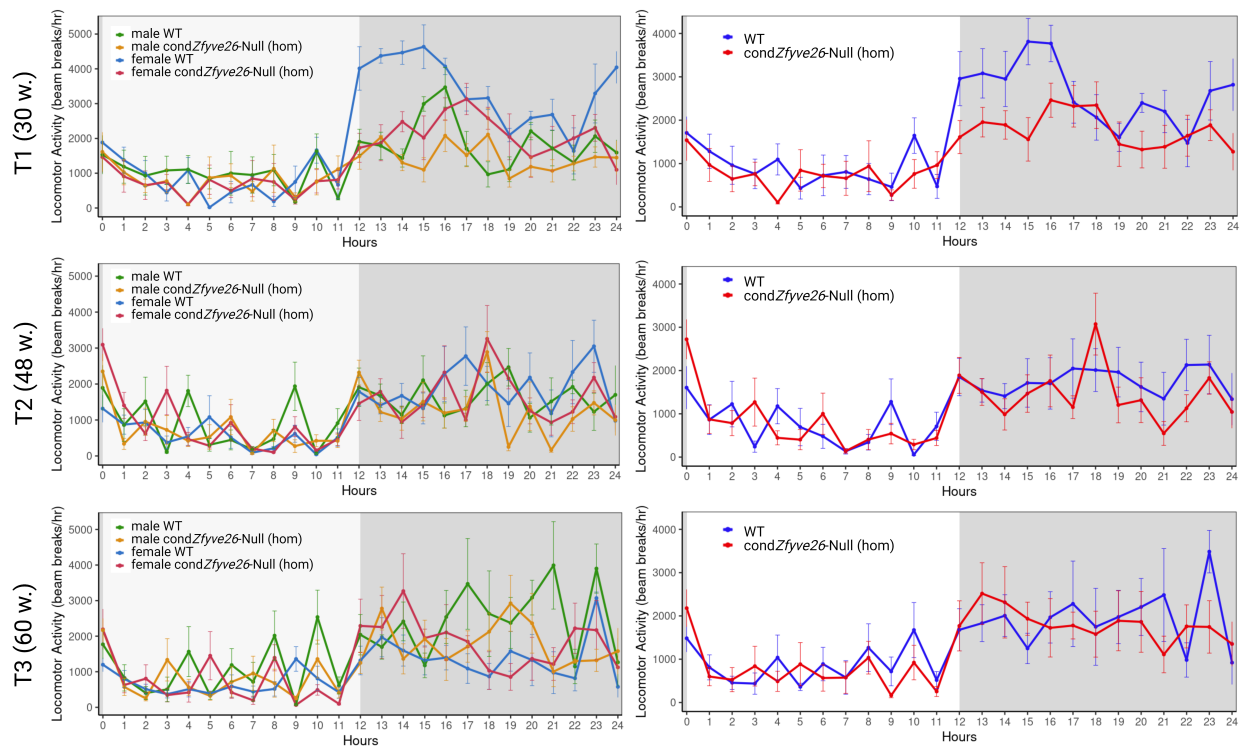


Figure 17. Indirect calorimetry: Locomotion activity. Mice were single housed and tested over time at three time points (T1–T3) at age 30, 48 and 60 weeks (w.). Horizontally directed movement (x- and y-dimension). *Left:* Four cohorts with wild-type (WT) male (N=2), homozygous (hom) *condZfyve26*-Null male (N=2), wild-type female (N=2) and homozygous *condZfyve26*-Null female (N=2). *Right:* Males and females grouped as wild-type (N=4) vs. homozygous *condZfyve26*-Null (N=4). Metabolic data versus time. 12 h light and 12 h dark photoperiods are indicated as white and grey backgrounds, respectively. hr: hour.

Ambulatory activity (beam breaks/hr)

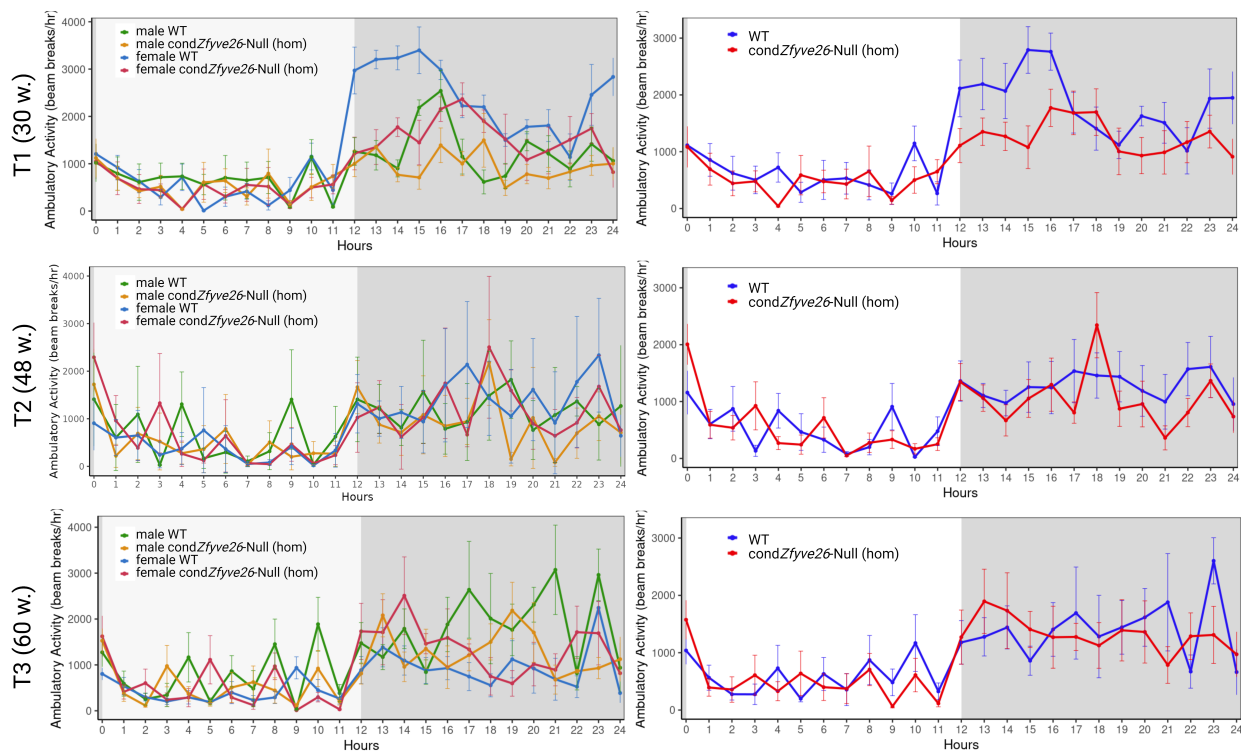


Figure 18. Indirect calorimetry: Ambulation activity. Mice were single housed and tested over time at three time points (T1–T3) at age 30, 48 and 60 weeks (w.). Vertically directed movement (z-dimension). *Left:* Four cohorts with wild-type (WT) male (N=2), homozygous (hom) *condZfyve26*-Null male (N=2), wild-type female (N=2) and homozygous *condZfyve26*-Null female (N=2). *Right:* Males and females grouped as wild-type (N=4) vs. homozygous *condZfyve26*-Null (N=4). Metabolic data versus time. 12 h light and 12 h dark photoperiods are indicated as white and grey backgrounds, respectively. hr: hour.

3.6 Disruption of *Zfyve26* gene caused neuronal loss.

To assess whether the brain is affected by neurodegeneration, both the cortex and the cerebellum were analyzed. Number of neurons (NeuN [antibody directed against a neuron specific nuclear protein] positive cells) in the cortex were reduced in homozygous *condZfyve26*-Null mice (mean number = 12.9) to 36.4% of wild-type levels (mean number = 35.4) (Figure 19). The simultaneous increase in GFAP (antibody directed against glial fibrillary acidic protein) positive cells in homozygous *condZfyve26*-Null brain sections is an indication of activation of astrogliosis along with neuronal loss.

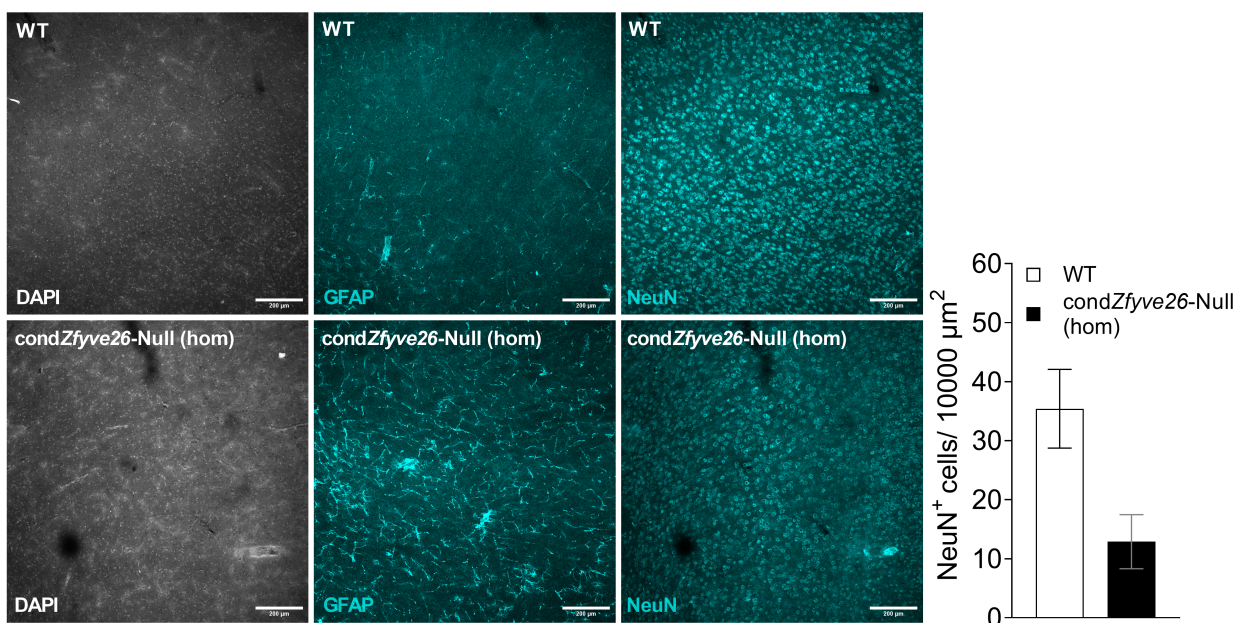


Figure 19. Quantification of neurons in the cortex. Staining of 10 μm thick brain sections with DAPI (nucleic acid staining), GFAP (astrocyte marker) and NeuN (neuronal marker). Compared to wild-type (WT) (N=1 with 1 male, 63 weeks old, n=10 ROIs analyzed), number of neurons in the cortex of homozygous (hom) *condZfyve26*-Null (N=1 with 1 male, 31 weeks old, n=10 ROIs analyzed) were decreased. Neuronal loss was accompanied by astrogliosis as the number of GFAP⁺ cells increased. Scale bar: 200 μm. Data shown as mean ± SD.

Number of Purkinje cells in the cerebellum was reduced in homozygous *condZfyve26*-Null mice (mean number = 18.3) by 23.7% compared to wild-type mice (mean number = 24) (Figure 20). Taken together, these data hinted at neurodegeneration processes in the brain of homozygous *condZfyve26*-Null mice upon *Zfyve26* gene disruption.

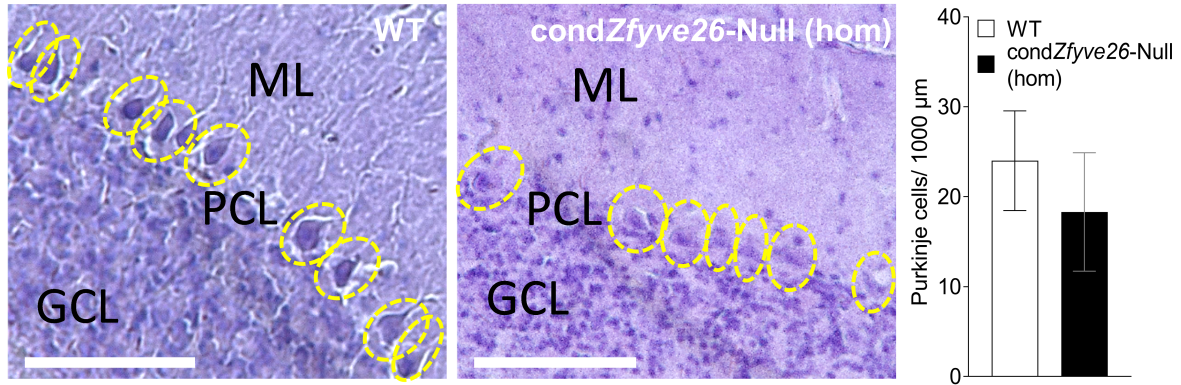


Figure 20. Quantification of Purkinje cells in the cerebellum. H&E staining of 10 μm thick brain sections. Compared to wild-type (WT) mice (N=3 with 1 male and 2 females, n=30 ROIs analyzed), Purkinje cells (yellow circles) in the cerebellum of homozygous (hom) *condZfyve26*-Null animals (N=4 with 2 males and 2 females, n=40 ROIs analyzed) were decreased. Average age: 61 weeks. ML molecular layer; PCL purkinke cell layer; GCL: granule cell layer. Scale bar: 100 μm . Data shown as mean \pm SEM.

3.7 Reduction of *Zfyve26* gene levels led to altered cell homeostasis.

Because of spastizin protein's role in the endolysosomal system, relevant sbucellular systems (e.g., lysosomes, endosomes, autophagosomes) were studied in mouse adult fibroblasts (MAF) isolated from wild-type and homozygous *condZfyve26*-Null mice (mice of both groups were 31 and 63 weeks old).

Stainings of MAFs with anti-Lamp1 revealed a decrease in the number of lysosomal vesicles (Lamp1⁺ puncta) in homozygous *condZfyve26*-Null compared to wild-type, while the size stayed unchanged (Figure 21 A). Both the number and size of early endosomes defined as EEA1 positive puncta did not differ (Figure 21 B). Vesicles labeled for LC3 were defined as autophagosomes. Quantification of LC3 positive puncta revealed an increase in the number and size of autophagosomes in homozygous *condZfyve26*-Null MAF compared to wild-type MAF (Figure 21 C). Together these findings hinted at an altered cellular homeostasis due to the reduction in *Zfyve26* gene levels, which might have affected the endolysosomal and autophagic pathway.

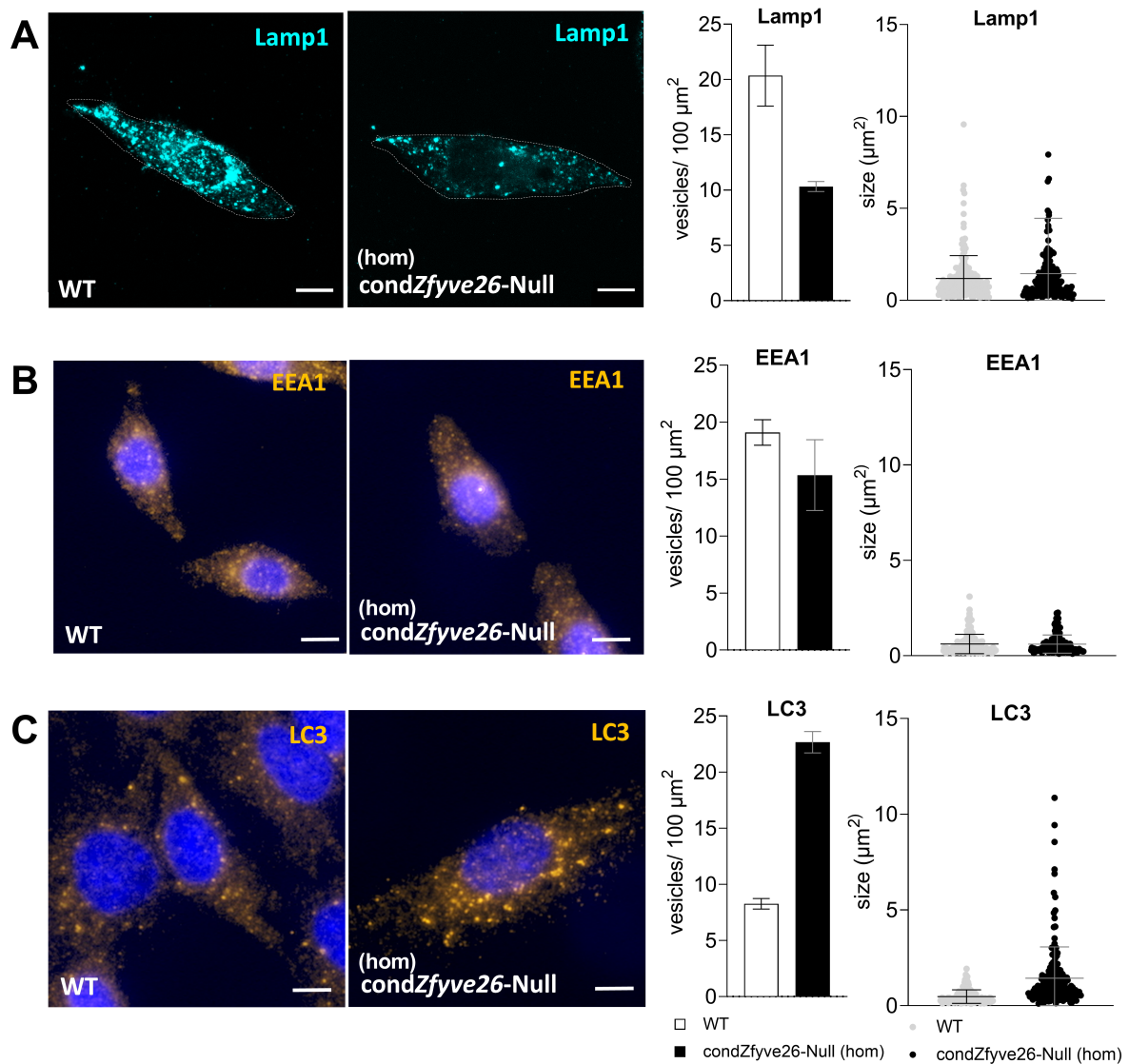


Figure 21. Characterization of relevant *Zfyve26* gene/Spastizin protein associated cell compartments in mouse adult fibroblasts (MAF). Representative primary MAF cells stained for (A) Lamp1 (turquoise), (B) EEA1 (yellow), (C) LC3 (yellow) and DAPI (blue, visualization of nuclear DNA). Quantification and sizing of lysosomes (Lamp1⁺), early endosomes (EEA1⁺) and autophagosomes (LC3⁺) in MAF derived from wild-type (WT, N=3 with 3 males, n=180 ROIs analyzed, 31 and 63 weeks old) and homozygous (hom) *condZfyve26*-Null (N=3 with 3 males, n=180 ROIs analyzed, 31 and 63 weeks old) animals. Scale bar: 10 μm . Data shown as mean \pm SEM.

Chapter 4

Discussion and Outlook

Until now there are no causative therapies available to treat Hereditary Spastic Paraplegia (HSP); treatments focus merely on symptoms [23, 24]. With respect to partly severe disease progressions, limited treatment options and the risk of inheritance of the gene defect it becomes clear that novel therapeutic approaches are necessary. The testing of such novel therapies requires valid disease models, such as murine HSP models. Therefore, this dissertation aimed to establish a new HSP type SPG15 mouse model, which should be functionally characterised and validated on various levels (phenotype, histology, cell biology). The novel *condZfyve26*-Null mouse model should serve as an experimental prerequisite to test and define the therapeutic potential of somatic gene repair in HSP type SPG15.

SPG15 is caused by bi-allelic loss-of-function mutations in the *Zfyve26* gene [81]. The conditional inactivation of *Zfyve26* gene function in mice by a floxed stop-cassette is expected to result in animals resembling a classical knockout. To confirm this hypothesis and hence validate the novel *condZfyve26*-Null mouse line as SPG15 disease model, a variety of functional analyses were applied. First, PCR and subsequent sequencing analyses of offspring genomic DNA confirmed the correct insertion of the stop-cassette into the murine *Zfyve26* gene. To test whether the modification of the genome of *condZfyve26*-Null mice had any effects on mouse viability and fertility, offspring were monitored on a weekly basis. In line with the Mendelian law of inheritance, reproduction results of 16 generations of *condZfyve26*-Null mice revealed the expected ratio between wild-type, heterozygous and homozygous offspring. Until the end of the study there were no differences in lifespan between the genotypes, neither homozygous nor heterozygous *condZfyve26*-Null mice exhibited higher mortality as all groups were characterized up to an age of 60 weeks. The stable inheritance of the floxed

stop-cassette over several generations, which did not have any observable off-target effects, speaks in favor of the applied *Zfyve26* gene targeting strategy, which holds the potential to downregulate *Zfyve26* gene activity.

Using the novel *condZfyve26*-Null mouse model, animals with sufficiently disrupted *Zfyve26* gene function were observed. It is the first murine model, in which *Zfyve26* was adequately inactivated using the stop-cassette system. In contrast to other classical constitutive HSP knockouts like the existing SPG15 mouse model (in which exon 15 was irreversibly deleted) [87], this novel mouse model bears the potential to reverse gene inhibition, allowing the controlled reactivation of the gene of interest at a defined time and in defined cells or tissue. Moreover, the novel *condZfyve26*-Null mouse line overcomes the limitation of studying postdevelopmental gene function, which is not possible in classical gene knockout systems [119, 120]. To restore *Zfyve26* gene expression, *condZfyve26*-Null mice with two floxed *Zfyve26* alleles will be crossed with animals carrying the Cre gene, which is driven by a ubiquitous or cell-specific promoter [111–113, 120]. With the help of the Cre-loxP system *Zfyve26* gene function can be studied at different stages of disease [119]. However, these experiments are content of future works. Here, the insertion of the floxed stop-cassette resulted in a reduction of *Zfyve26* transcripts by up to more than 90% compared to wild-type levels, which was more prominent in homozygous *condZfyve26*-Null offspring of the 2D3 embryonic stem cell (ESC) clone than the 1C5 ESC clone. These data hinted at a sufficient disruption in *Zfyve26* gene expression upon stop-cassette insertion, which is in line with findings obtained in the classical SPG15 KO mouse model [87]. Yet, the increase in sample size (*i.e.*, animal number) is necessary to confirm the data obtained and to perform statistical analyses. It is expected that the insertion of the stop-cassette into intron 2 of the murine *Zfyve26* gene caused a frame-shift leading to the generation of nonsense mRNA and its subsequent degradation [13, 81, 83, 87]. However, bi-allelic *Zfyve26* gene inactivation did not result in the total ablation of RNA transcripts. Reasons could be the presence of murine *Zfyve26* transcript isoforms [121, 122]. This issue can be avoided by using variant specific primers. A robust and sensitive method to detect and quantify alternative transcripts was described in [123]. Another reason could be of technical nature. Technical variation can be caused by intermediate working steps, including sample collection, RNA isolation, cDNA generation and finally qPCR. To facilitate the procedure and to reduce the risk of contamination, performing one-step RT-PCR (reverse transcription and qPCR taking place in a single tube) is

a possible option [124].

The validation of the novel *condZfyve26*-Null mouse line on the protein level could not be accomplished due to technical and methodological limitations. The expected absence of spastizin protein in homozygous *condZfyve26*-Null mice could not be confirmed, since its detection in wild-type brain protein lysates in western blotting was not possible. One crucial reason is that both spastizin antibodies, directed either against the N- or C-terminal epitope, turned out to have a low affinity towards spastizin resulting in unspecific protein bands in immunoblots. This restriction could have been reinforced by the low amount of available cytosolic spastizin, which is expressed at relatively low levels, with only 1,010 copies and a concentration of 0.84 nM in HeLa cells (compared with, e.g., 102,125 copies and 84.79 nM for HSP protein strumpellin) [125–127]. These problems were described before [87]. Solutions to the problem are the testing of other commercially available spastizin antibodies or conducting immunoprecipitation of spastizin after immunoblotting [99]. These approaches were not yet implemented due to time and resource restrictions, therefore are subject of future works.

Unlike existing mouse models of SPG15 [87] and SPG11 [128], the body weight of homozygous *condZfyve26*-Null animals was not obviously lower than those of wild-type littermates. The only observation fairly in line with literature [87, 128] was made in the second male cohort, where homozygous *condZfyve26*-Null males exhibited a weak reduction in body weight compared to wild-type males. Yet, in an SPG48 knockout (KO) mouse model [129] as well as a Null mouse model [113], in which the preproglucagon gene (pancreatic preproglucagon plays a role in glucose homeostasis [113]) was disrupted using the stop-cassette system, no reduced body weight was observed in KO and Null animals, respectively, supporting the novel *condZfyve26*-Null mouse model and hinting at a method specific consequence.

Regarding experimental cohort 1, body weights of wild-type males as well as of male and female homozygous *condZfyve26*-Null mice were abnormally high compared to standard C57BL/6N and C57BL/6J mouse strains and other mouse models, whose body weights reach maximal values around 30 g for males and 25 g for females [78, 87, 128, 130]. Moreover, homozygous *condZfyve26*-Null females of cohort 1 were clearly heavier than their wild-type littermates. This difference was not observed in any HSP mouse model before [78, 87, 128, 129], most notably because female animals were not included in any study. The observed body weight phenotype in cohort 1 could either be due to the gene targeting strategy itself or

due to the desired *Zfyve26* gene disruption. Nevertheless, this weight phenotype could not be replicated in the second experimental cohort. Body weights of animals in cohort 2 were within the normal range, hinting at a litter specific manifestation. Further assessment of the body weight with new experimental mouse cohorts are required to draw any conclusions.

Above all, the environmental conditions under which both cohorts grew up and were kept should not be neglected [131]. An exact replication of the housing conditions could not be realized and may have been "a source of systemic experimental variability" [132]. Animals of cohort 1 were kept in open cages with exposure to the ambient air. After the outbreak of a zoonotic pathogen in the animal facility and the subsequent culling of the entire first cohort (see official document in appendix), all future animals, including mice of cohort 2, were kept under sterile conditions in individually ventilated cages (IVC) with air filters preventing any exposure to the ambient air and additionally were kept at another animal facility. It is known that IVC housing imposes chronic stress on mice due to the constant noise and cold draught caused by the ventilation system, which can even alter experimental outcomes [132]. Despite the failure to replicate the noteworthy difference in the body weight of females, these observations have the potential to suggest a hitherto undescribed sexual dimorphism in HSP, pointing out the importance and urgency to include female animals into experimental studies [133, 134]. The complex interaction between nature (genotype) and nurture (environment) may had an important impact on the development of the phenotype of the animals [135].

To test whether the higher body weight observed in homozygous *condZfyve26*-Null 1C5 females of cohort 1 is correlated with alterations in metabolism, indirect calorimetry was carried out with a second experimental cohort (cohort 2) after the culling of cohort 1 because of the outbreak of a zoonotic pathogen in the animal facility (see official document in appendix). Recent studies revealed a link between spastizin [99] or spatacsin protein deficits [16] and defects in lipid metabolism in mice. Importantly, spastizin (associated with SPG15) and spatacsin (associated with SPG11) share common functions and pathways as they are interacting partners of the AP-5 protein complex, which plays a crucial role in membrane trafficking (see 1.2.3) [82, 100, 101]. Interestingly, the functional zinc finger domain of spastizin protein was described to be a key transcriptional regulator of adipogenesis, regulating adipocyte differentiation [88]. Furthermore, a higher obesity rate and damages in the hypothalamus were reported in SPG11 patients [136].

No clear differences were observed between wild-type and homozygous *condZfyve26*-Null

animals. Although the small sample size may compromise experimental interpretation due to large individual animal variation. Any equipment failure can be ruled out as calibration of the calorimeter was carried out prior to each experiment. To gain more insight into subcellular processes and to validate the findings, staining of cell cultures (e.g., primary cortical neurons, MAF, MEF) with the hydrophobic fluorescent probe Nile Red to label neutral lipids like cholesterol can be performed as done in [99]. Furthermore, it is important to look beyond the p value when interpreting results [115, 137, 138]. Since the detection of a true difference is dependent on the sample size of an experiment, "it would be unreasonable to discard (or fail to publish) results that are not statistically significant but show potentially biologically important effect sizes" [115]. Therefore, the issue of the sample size and the housing environment of experimental animals, as discussed above, needs to be addressed and adjusted in future studies. To this point, an alteration of the lipid metabolism in homozygous *condZfyve26*-Null females as the underlying pathology cannot be ruled out. The complex relationship between genotype and environment, paired with methodological and analytical issues make *in vivo* studies challenging.

Homozygous *condZfyve26*-Null mice, analyzed up to an age of 60 weeks, did not develop spastic paraplegia. This observation might argue against the use of the mouse to model HSP because of its limited axon length and limited age. However, existing KO mouse models for, e.g., SPG15 (48 weeks) [87] or SPG11 (52 weeks) [128] did develop late-onset HSP with a progressive movement disorder, ruling out any doubts about its suitability to model progressive axonopathies. For the novel *condZfyve26*-Null mouse model this could mean that gait impairments may start at over 60 weeks of age, which would be a very late disease onset. Thus, future characterization studies of the *condZfyve26*-Null mouse line should be conducted until natural death sets in (ca. 96 weeks of age). Notably, human SPG15 patients suffer from an early-onset spastic paraplegia [11, 81].

The crucial reason for the hitherto missing movement impairment could be the gene targeting strategy itself, which theoretically should cause *Zfyve26* gene mutation by a small insertion. Unlike the *condZfyve26*-Null mouse model, published SPG15 [87], SPG4 [139] or SPG31 [140] KO mouse models are constitutive knockouts, in which one or several exons were irreversibly deleted. In contrast to SPG15, SPG4 and SPG31 are autosomal dominant HSP forms [14, 139, 140], which may also impact the outcome of gene targeting. However, the previously mentioned SPG11 KO mouse model, which is also an autosomal recessive

HSP type, was generated by integrating a gene trap cassette into intron 1 of the associated *KIAA1840* gene [128], proving that in general mutations in HSP genes, which are autosomal recessively inherited, caused by insertions are possible.

A further factor to consider is that the existing SPG15 KO mouse model [87] was generated using the widely used inbred strain C57BL/6J, while *condZfyve26*-Null mice were generated using the C57BL/6N mouse strain. Interestingly, differences in motor behavior (e.g., grip strength, rotarod) and a range of other phenotypic parameters (e.g., immune response, metabolism, fear response, effect of anesthetics) [141] can exist between both strains, "that have the potential to impact upon penetrance and expressivity of mutational effects in these strains" [142]. Nevertheless, the confirmation of the correct insertion and stable inheritance of the floxed stop-cassette without having any effects on mouse viability and fertility, the sufficient *Zfyve26* gene inactivation as well as the cell biological and histological data support the gene targeting strategy applied. This hypothesis was supported by the trend towards a poorer performance in homozygous *condZfyve26*-Null animals compared to their wild-type littermates revealed by the gait analysis. This was evidenced by 1) the slightly smaller foot base angle of homozygous *condZfyve26*-Null mice; 2) their higher score of mistakes in the ladder climbing test; 3) their weaker neuromuscular function (grip strength) and 4) their poorer performance in the rotarod test, which may hint at a looming gait dysfunction. Still, these assumptions need to be treated critically especially those with subtle differences between the groups. Methodological and analytical limitations may have contributed to the results obtained. Examples are the FBA determination, which allowed a certain degree of leeway or the free definition of mistakes in the ladder climbing test, whose parameters are not established yet. Furthermore, the decreased latency to fall observed in homozygous *condZfyve26*-Null females may have correlated with their higher body weights making them less agile on the rotating beam [143]. Moreover, testings were not carried out around the same daytime and were always conducted against the circadian rhythm of nocturnal mice during their sleeping phase, which very likely had an impact on the outcome of behavioural parameters [144–146]. Overall, the outcome of the tests were sensitive to environmental conditions and to methodological constraints. Furthermore, the standard measures used in this study may not have been suitable or sufficient to detect subtle changes in motor behavior of homozygous *condZfyve26*-Null mice. Taken together, the difference in the gene targeting strategy as well as the difference in genetic background/strain between

the novel cond*Zfyve26*-Null mouse model and existing HSP mouse models [87, 128, 139, 140] may have contributed to the difference in gait impairment onset and progress.

Loss of *Zfyve26* gene activity in homozygous cond*Zfyve26*-Null mice led to brain neurodegeneration with loss of neurons in the cortex and loss of Purkinje cells in the cerebellum. These observations are in line with those made in previously published SPG15 [87] and SPG11 [128] mouse models as well as in human SPG15 patients who displayed cortical and cerebellar atrophy [81, 83, 147]. However, neuronal populations affected and individual cortical layers were not further specified here due to time constraints. To detect motor neurons in deep cortical layers V and VI, anti-ctip2 antibody, which labels layer V neurons, can be used in future experiments as done in [128]. Furthermore, neuronal loss in the cortex was accompanied by activation of astrogliosis, a sign of central nervous system (CNS) damage [148]. In case of a damage astrocytes express high levels of GFAP (glial fibrillary acidic protein), which is an intermediate filament protein expressed in several CNS cell types [149] and served as a marker here. Astrogliosis is characterized among others by alterations in reactive astrocytes as "a defense mechanism to minimize and repair the initial damage after CNS injuries" [148]. As Purkinje cells and cortical (motor) neurons are crucial for motor coordination as well as the control and execution of motor behaviours [150, 151], their loss is expected to result in ataxia and movement dysfunction. Hence, it is a matter of time until the phenotypic correlate would manifest in homozygous cond*Zfyve26*-Null mice.

The histopathological hallmark of HSP is axon degeneration in the CNS. In the existing SPG15 KO mouse model, axon degeneration within the corticospinal tract was observed even before mice developed a progressive gait dysfunction [87]. In homozygous cond*Zfyve26*-Null, the examination of the spinal cord was not possible due to technical constraints, *i.e.*, the absence of appropriate devices and expertise, hence need to be addressed in future studies. Taken together, the clear signs of neurodegeneration on the anatomical level together with the trend towards a poorer performance in the gait analysis hint at an incipient gait dysfunction in homozygous cond*Zfyve26*-Null mice and support the gene targeting strategy.

What is the cellular pathology behind neurodegeneration? Analysis of mouse adult fibroblasts (MAF) of homozygous cond*Zfyve26*-Null mice revealed defects in the endolysosomal trafficking pathway in the absence of *Zfyve26* gene. The decrease in free lysosomes (Lamp1⁺ puncta) and the accumulation of autophagosomes (LC3⁺ puncta) in homozygous

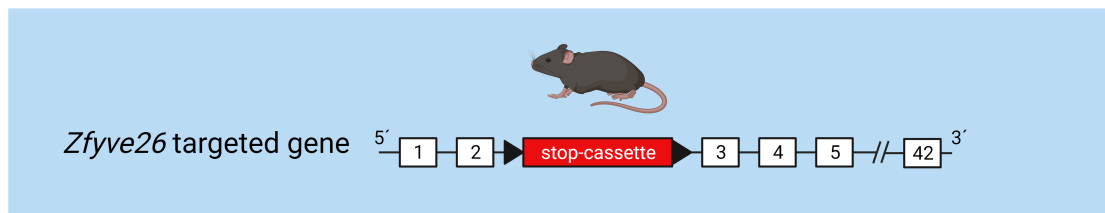
cond*Zfyve26*-Null MAFs suggest defects in autophagic lysosome reformation (ALR), a recycling pathway that generates new lysosomes from autolysosomes [86, 97]. The lack of free lysosomes results in the increase in mature autophagosomes unable to fuse with lysosomes to form autolysosomes, which terminate autophagy [86, 98]. Similar results were obtained in fibroblasts derived from SPG15 and SPG11 patients [86] as well as in Purkinje cells and mouse embryonic fibroblasts of SPG15 KO and SPG11 KO mice [78, 128, 152, 153], demonstrating a crucial role of *Zfyve26* associated protein, spastizin, in ALR. However, the size of Lamp1⁺ organelles was not enlarged as observed in SPG15 and SPG11 patient fibroblasts and SPG15 studies with HeLa cells [86, 152]. Enlargement of lysosomes is induced by short term starvation, but fails to restore baseline size upon spastizin protein depletion [86]. The size differences of Lamp1⁺ organelles between the current and previously published studies could be due to technical limitations, e.g., correct identification of organelles, definition of appropriate thresholds during data analysis and interpretation of data. However, this is unlikely as the data for the other cell organelles analyzed are in accordance with literature. Furthermore, levels of endosomes (EEA1⁺ puncta) were unchanged, which is in line with literature [87]. The increased size of autophagosomes in homozygous cond*Zfyve26*-Null MAFs may have been caused by the accumulation of autophagic material destined for degradation, e.g., lipids [16, 78], suggesting clearance failure upon *Zfyve26* disruption. Defects in ALR due to fusion defects of free lysosomes with autophagosomes cannot be excluded since the analysis of autolysosomes (Lamp1⁺ and LC3⁺ puncta) was not included in the study as double stainings with the antibody combinations available were not possible, but should be subject of further experiments as performed in [78]. Taken together the *ex vivo* data are consistent with previous reports and support a disruption of ALR upon *Zfyve26* gene inactivation in the novel cond*Zfyve26*-Null mouse model.

In summary, the data of this study support previous findings and confirm defects in the autophagic as well as lysosomal system as the underlying pathomechanism of *Zfyve26* associated HSP type SPG15. In future studies, homozygous cond*Zfyve26*-Null mice will be crossed with mice that express Cre recombinase in specific cells or tissue to assess the effect of *Zfyve26* reactivation and thus expression of spastizin protein (Figure 22). This will allow first conclusions about the potential of somatic gene repair in mice as well as the definition of conditions required for such approaches.

In brief, the overarching goals behind the generation of the novel *condZfyve26*-Null mouse line are defined as follows (Figure 22):

1. *Functional characterization and validation of the novel condZfyve26-Null mouse model.*
2. *Definition of the therapeutic potential of somatic gene repair in murine HSP type SPG15.*

1. Functional characterization and validation of the novel *condZfyve26*-Null mouse model.



2. Definition of the therapeutic potential of somatic gene repair in murine HSP type SPG15.

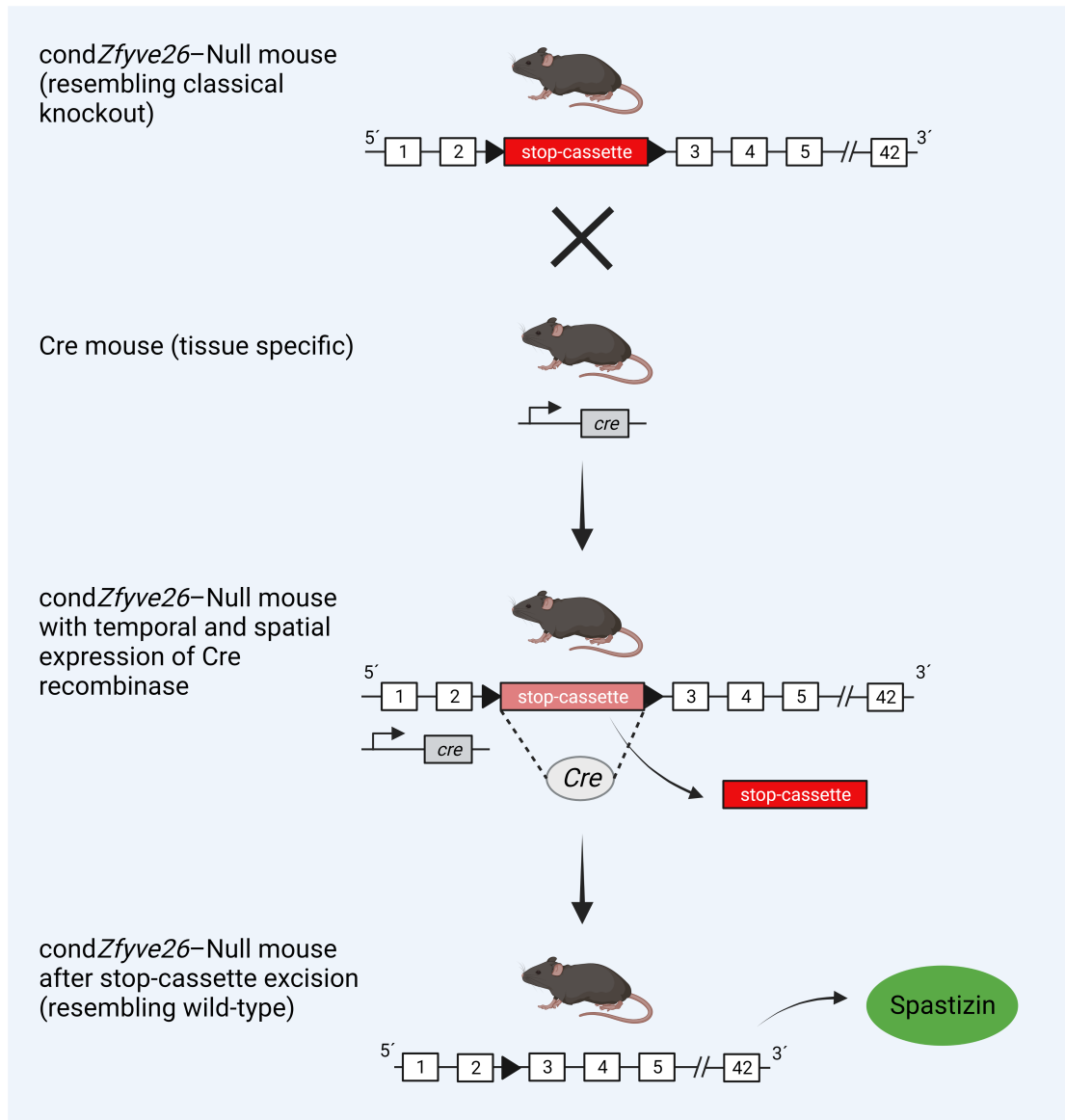


Figure 22. A novel *condZfyve26*-Null mouse model. Goals behind the generation of the novel *condZfyve26*-Null mouse model are: 1. Functional characterization and validation of the novel *condZfyve26*-Null mouse model (subject of this doctoral thesis). 2. Definition of the therapeutic potential of somatic gene repair in murine HSP type SPG15 (subject of future studies). (1) *condZfyve26*-Null mice were generated using the stop-cassette system. Insertion of the loxP-flanked stop-cassette into intron 2 of the murine *Zfyve26* gene results in animals resembling a classical knockout mouse. (2) Crossing of *condZfyve26*-Null animals having two floxed alleles with mice carrying the Cre gene driven by a ubiquitous or cell-specific promoter. Controlled induction of Cre expression in progeny leads to the excision of the floxed loci in a time and tissue specific manner. Reactivation of *Zfyve26* gene expression leads to the expression of spastizin protein. "Rescued" mouse resembles a wild-type condition.

Chapter 5

Conclusion

This study aimed at the functional characterization and validation of a novel *condZfyve26*-Null mouse model as a prerequisite for testing and defining the therapeutic potential of somatic gene repair in HSP.

Despite the obstacles encountered during this doctorate (e.g., Covid-19 pandemic, outbreak of zoonotic pathogen and subsequent culling of experimental cohort 1) the set goals and milestones were reached. Characterization of general parameters (e.g., viability, fertility and body weight) and movement of the novel *condZfyve26*-Null mouse model as well as its characterization on the molecular, cell biological and histological level revealed findings that are in line with previous studies. Follow-up experiments that confirm the absence of spastizin protein in homozygous *condZfyve26*-Null upon *Zfyve26* gene disruption and the analysis of spinal cord sections to confirm axon degeneration of motor neurons are required to validate its relevance as a novel SPG15 disease model. It would also be advisable to replicate the functional characterization with mice derived from the *condZfyve26*-Null 2D3 embryonic stem cell line as the gene expression data hinted at a more powerful *Zfyve26* gene inhibition in 2D3 than 1C5; the 2D3 line is currently subject to *in vitro* fertilization for breeding purposes. Overall, sample sizes of experimental cohorts have to be increased to perform statistical analyses, which will allow to draw clear conclusions.

Taken together the novel *condZfyve26*-Null mouse line can be used as a sophisticated tool to control *Zfyve26* gene expression *in vivo* both in time and space. Therewith, the *condZfyve26*-Null line provides the experimental basis for defining the therapeutic potential of somatic gene repair in murine HSP type SPG15, which would be an attempt in the direction of a causal therapy.

Bibliography

1. Blackstone, C. Cellular pathways of hereditary spastic paraplegia. *Annual review of neuroscience* **35**, 25–47 (2012).
2. Fink, J. K. Hereditary spastic paraplegia. *Current neurology and neuroscience reports* **6**, 65–76 (2006).
3. Depienne, C., Stevanin, G., Brice, A. & Durr, A. Hereditary spastic paraplegias: an update. *Current opinion in neurology* **20**, 674–680 (2007).
4. Salinas, S., Proukakis, C., Crosby, A. & Warner, T. T. Hereditary spastic paraplegia: clinical features and pathogenetic mechanisms. *The Lancet Neurology* **7**, 1127–1138 (2008).
5. Dion, P. A., Daoud, H. & Rouleau, G. A. Genetics of motor neuron disorders: new insights into pathogenic mechanisms. *Nature Reviews Genetics* **10**, 769–782 (2009).
6. Reid, E. Science in motion: common molecular pathological themes emerge in the hereditary spastic paraplegias. *Journal of medical genetics* **40**, 81–86 (2003).
7. Blackstone, C., O’kane, C. J. & Reid, E. Hereditary spastic paraplegias: membrane traffic and the motor pathway. *Nature Reviews Neuroscience* **12**, 31–42 (2011).
8. DeLuca, G. C., Ebers, G. & Esiri, M. The extent of axonal loss in the long tracts in hereditary spastic paraplegia. *Neuropathology and applied neurobiology* **30**, 576–584 (2004).
9. Lang, N., Optenhoefel, T., Deuschl, G. & Klebe, S. Axonal integrity of corticospinal projections to the upper limbs in patients with pure hereditary spastic paraplegia. *Clinical neurophysiology* **122**, 1417–1420 (2011).

10. Harding, A. E. Friedreich's ataxia: a clinical and genetic study of 90 families with an analysis of early diagnostic criteria and intrafamilial clustering of clinical features. *Brain: a journal of neurology* **104**, 589–620 (1981).
11. Ebrahimi-Fakhari, D., Alecu, J. E. & Blackstone, C. Spastic paraplegia 15. *GeneReviews* (2021).
12. Vander Stichele, G., Durr, A., Yoon, G., Schüle, R., Blackstone, C., Esposito, G., Buffel, C., Oliveira, I., Freitag, C. & van Rooijen, S. An integrated modelling methodology for estimating global incidence and prevalence of hereditary spastic paraplegia subtypes SPG4, SPG7, SPG11, and SPG15. *BMC neurology* **22**, 115 (2022).
13. Schüle, R. & Schöls, L. Genetics of hereditary spastic paraplegias. **31**, 484–493 (2011).
14. Blackstone, C. *Hereditary spastic paraplegia* 633–652 (Elsevier, 2018).
15. Giudice, T. L., Lombardi, F., Santorelli, F. M., Kawarai, T. & Orlandi, A. Hereditary spastic paraplegia: clinical-genetic characteristics and evolving molecular mechanisms. *Experimental neurology* **261**, 518–539 (2014).
16. Boutry, M., Pierga, A., Matusiak, R., Branchu, J., Houllegatte, M., Ibrahim, Y., Balse, E., El Hachimi, K.-H., Brice, A. & Stevanin, G. Loss of spatacsin impairs cholesterol trafficking and calcium homeostasis. *Communications Biology* **2**, 380 (2019).
17. Solowska, J. M. & Baas, P. W. Hereditary spastic paraplegia SPG4: what is known and not known about the disease. *Brain* **138**, 2471–2484 (2015).
18. Mohan, N., Qiang, L., Morfini, G. & Baas, P. W. Therapeutic Strategies for Mutant SPAST-Based Hereditary Spastic Paraplegia. *Brain Sciences* **11**, 1081 (2021).
19. Qiang, L., Piermarini, E., Muralidharan, H., Yu, W., Leo, L., Hennessy, L. E., Fernandes, S., Connors, T., Yates, P. L. & Swift, M. Hereditary spastic paraplegia: gain-of-function mechanisms revealed by new transgenic mouse. *Human Molecular Genetics* **28**, 1136–1152 (2019).
20. Piermarini, E., Akarsu, S., Connors, T., Kneussel, M., Lane, M. A., Morfini, G., Karabay, A., Baas, P. W. & Qiang, L. Modeling gain-of-function and loss-of-function components of SPAST-based hereditary spastic paraplegia using transgenic mice. *Human Molecular Genetics* **31**, 1844–1859 (2022).

21. Zhao, J., Matthies, D. S., Botzolakis, E. J., Macdonald, R. L., Blakely, R. D. & Heder, P. Hereditary spastic paraplegia-associated mutations in the NIPA1 gene and its *Caenorhabditis elegans* homolog trigger neural degeneration in vitro and in vivo through a gain-of-function mechanism. *Journal of Neuroscience* **28**, 13938–13951 (2008).
22. Jahic, A., Khundadze, M., Jaenisch, N., Schüle, R., Klimpe, S., Klebe, S., Frahm, C., Kassubek, J., Stevanin, G. & Schöls, L. The spectrum of KIAA0196 variants, and characterization of a murine knockout: implications for the mutational mechanism in hereditary spastic paraplegia type SPG8. *Orphanet Journal of Rare Diseases* **10**, 1–10 (2015).
23. Soderblom, C. & Blackstone, C. Traffic accidents: molecular genetic insights into the pathogenesis of the hereditary spastic paraplegias. *Pharmacology & therapeutics* **109**, 42–56 (2006).
24. Fink, J. K. Hereditary spastic paraplegia: clinical principles and genetic advances. **34**, 293–305 (2014).
25. Bellofatto, M., De Michele, G., Iovino, A., Filla, A. & Santorelli, F. M. Management of hereditary spastic paraplegia: a systematic review of the literature. *Frontiers in neurology* **10**, 3 (2019).
26. Riccardo, M., Angela, L., Angela, D., Vita, P., Giulio, L., Pietroq, F., Giancarlo, I. & Marisa, M. Combined treatment Fkt-botulinum toxin type A (Btx-A) in patients with Strumpell-Lorrain disease. *Current Pharmaceutical Design* **22**, 758–763 (2016).
27. Hecht, M. J., Stolze, H., Auf Dem Brinke, M., Giess, R., Treig, T., Winterholler, M., Wissel, J. & Group, G. S. E. Botulinum neurotoxin type A injections reduce spasticity in mild to moderate hereditary spastic paraplegia—Report of 19 cases. *Movement disorders* **23**, 228–233 (2008).
28. Niet, M. d., de Bot, S. T., van de Warrenburg, B. P., Weerdesteijn, V. & Geurts, A. Functional effects of botulinum toxin type-A treatment and subsequent stretching of spastic calf muscles: a study in patients with hereditary spastic paraplegia (2015).
29. Sills, G. J. The mechanisms of action of gabapentin and pregabalin. *Current opinion in pharmacology* **6**, 108–113 (2006).

30. Scheuer, K., Svenstrup, K., Jennum, P., á Rogvi-Hansen, B., Werdelin, L., Fenger, K. & Nielsen, J. Double-blind crossover trial of gabapentin in SPG4-linked hereditary spastic paraplegia. *European journal of neurology* **14**, 663–666 (2007).
31. Mondrup, K. & Pedersen, E. The clinical effect of the GABA-agonist, progabide, on spasticity. *Acta neurologica scandinavica* **69**, 200–206 (1984).
32. Guidubaldi, A., Piano, C., Santorelli, F. M., Silvestri, G., Petracca, M., Tessa, A. & Bentivoglio, A. R. Novel mutations in SPG11 cause hereditary spastic paraplegia associated with early-onset levodopa-responsive Parkinsonism. *Movement Disorders* **26**, 553–556 (2011).
33. Vanderver, A., Tonduti, D., Auerbach, S., Schmidt, J. L., Parikh, S., Gowans, G. C., Jackson, K. E., Brock, P. L., Patterson, M. & Nehrebecky, M. Neurotransmitter abnormalities and response to supplementation in SPG11. *Molecular genetics and metabolism* **107**, 229–233 (2012).
34. Wijemanne, S. & Jankovic, J. Dopa-responsive dystonia—clinical and genetic heterogeneity. *Nature reviews neurology* **11**, 414–424 (2015).
35. Mignarri, A., Malandrini, A., Del Puppo, M., Magni, A., Monti, L., Ginanneschi, F., Tessa, A., Santorelli, F. M., Federico, A. & Dotti, M. T. Treatment of SPG5 with cholesterol-lowering drugs. *Journal of neurology* **262**, 2783–2785 (2015).
36. Schöls, L., Rattay, T. W., Martus, P., Meisner, C., Baets, J., Fischer, I., Jäggle, C., Fraidakis, M. J., Martinuzzi, A. & Saute, J. A. Hereditary spastic paraplegia type 5: natural history, biomarkers and a randomized controlled trial. *Brain* **140**, 3112–3127 (2017).
37. Pease, W. S. THERAPEUTIC ELECTRICAL STIMULATION FOR SPASTICITY: Quantitative Gait Analysis: 1. *American journal of physical medicine & rehabilitation* **77**, 351–355 (1998).
38. Bertolucci, F., Di Martino, S., Orsucci, D., Ienco, E. C., Siciliano, G., Rossi, B., Mancuso, M. & Chisari, C. Robotic gait training improves motor skills and quality of life in hereditary spastic paraplegia. *NeuroRehabilitation* **36**, 93–99 (2015).
39. Seo, H. G., Oh, B.-M. & Kim, K. Robot-assisted gait training in a patient with hereditary spastic paraplegia. *PM&R* **7**, 210–213 (2015).

40. Murala, S., Nagarajan, E. & Bollu, P. C. Hereditary spastic paraplegia. *Neurological Sciences* **42**, 883–894 (2021).
41. Asir, J. S., Vencita, P. A., Trapthi, K. & Pokhrel, M. Physical therapy interventions for the patient with Hereditary Spastic Paraparesis - An exploratory case reports. *International Journal of Physiotherapy and Research* (2013).
42. Margetis, K., Korfiatis, S., Boutos, N., Gatzonis, S., Themistocleous, M., Siatouni, A., Dalivigka, Z., Flaskas, T., Stranjalis, G. & Boviatsis, E. Intrathecal baclofen therapy for the symptomatic treatment of hereditary spastic paraplegia. *Clinical neurology and neurosurgery* **123**, 142–145 (2014).
43. Dan, B. & Chéron, G. Intrathecal baclofen normalizes motor strategy for squatting in familial spastic paraplegia: a case study. *Neurophysiologie Clinique/Clinical Neurophysiology* **30**, 43–48 (2000).
44. Heetla, H. W., Halbertsma, J. P., Dekker, R., Staal, M. J. & van Laar, T. Improved gait performance in a patient with hereditary spastic paraplegia after a continuous intrathecal baclofen test infusion and subsequent pump implantation: a case report. *Archives of physical medicine and rehabilitation* **96**, 1166–1169 (2015).
45. Sharma, J., Bonfield, C. & Steinbok, P. Selective dorsal rhizotomy for hereditary spastic paraparesis in children. *Child's Nervous System* **32**, 1489–1494 (2016).
46. Kai, M., Yongjie, L. & Ping, Z. Long-term results of selective dorsal rhizotomy for hereditary spastic paraparesis. *Journal of Clinical Neuroscience* **21**, 116–120 (2014).
47. Waldrop, M. A., Karingada, C., Storey, M. A., Powers, B., Iammarino, M. A., Miller, N. F., Alfano, L. N., Noritz, G., Rossman, I. & Ginsberg, M. Gene therapy for spinal muscular atrophy: safety and early outcomes. *Pediatrics* **146** (2020).
48. Pena, S. A., Iyengar, R., Eshraghi, R. S., Bencie, N., Mittal, J., Aljohani, A., Mittal, R. & Eshraghi, A. A. Gene therapy for neurological disorders: challenges and recent advancements. *Journal of drug targeting* **28**, 111–128 (2020).
49. Shribman, S., Reid, E., Crosby, A. H., Houlden, H. & Warner, T. T. Hereditary spastic paraplegia: from diagnosis to emerging therapeutic approaches. *The Lancet Neurology* **18**, 1136–1146 (2019).

50. Lallemand-Dudek, P., Darios, F. & Durr, A. Recent advances in understanding hereditary spastic paraplegias and emerging therapies. *Faculty Reviews* **10** (2021).
51. Spuch, C., Saida, O. & Navarro, C. Advances in the treatment of neurodegenerative disorders employing nanoparticles. *Recent patents on drug delivery & formulation* **6**, 2–18 (2012).
52. Kondiah, P. J., Choonara, Y. E., Kondiah, P. P., Marimuthu, T., Kumar, P., Du Toit, L. C. & Pillay, V. A review of injectable polymeric hydrogel systems for application in bone tissue engineering. *Molecules* **21**, 1580 (2016).
53. Sampson, T. R. & Weiss, D. S. CRISPR-Cas systems: new players in gene regulation and bacterial physiology. *Frontiers in cellular and infection microbiology* **4**, 37 (2014).
54. Kruminis-Kaszkiel, E., Juranek, J., Maksymowicz, W. & Wojtkiewicz, J. CRISPR/Cas9 technology as an emerging tool for targeting amyotrophic lateral sclerosis (ALS). *International journal of molecular sciences* **19**, 906 (2018).
55. Aubourg, P. *Gene therapy for disorders of the central nervous system 1859–1866* (Elsevier, 2013).
56. Yang, S., Ma, S.-q., Wan, X., He, H., Pei, H., Zhao, M.-j., Chen, C., Wang, D.-w., Dong, X.-y. & Yuan, J.-j. Long-term outcomes of gene therapy for the treatment of Leber’s hereditary optic neuropathy. *EBioMedicine* **10**, 258–268 (2016).
57. Piguet, F., Alves, S. & Cartier, N. Clinical gene therapy for neurodegenerative diseases: past, present, and future. *Human gene therapy* **28**, 988–1003 (2017).
58. Rubinstein, A. L. Zebrafish: from disease modeling to drug discovery. *Current Opinion in Drug Discovery and Development* **6**, 218–223 (2003).
59. Giardoglou, P. & Beis, D. On zebrafish disease models and matters of the heart. *Biomedicines* **7**, 15 (2019).
60. Cabezas-Sáinz, P., Pensado-López, A., Sáinz Jr, B. & Sánchez, L. Modeling cancer using zebrafish xenografts: drawbacks for mimicking the human microenvironment. *Cells* **9**, 1978 (2020).

61. Boutry, M., Branchu, J., Lustremant, C., Pujol, C., Pernelle, J., Matusiak, R., Seyer, A., Poirel, M., Chu-Van, E. & Pierga, A. Inhibition of lysosome membrane recycling causes accumulation of gangliosides that contribute to neurodegeneration. *Cell reports* **23**, 3813–3826 (2018).
62. Maris, I. F. S. Testing Miglustat Administration in Subjects With Spastic Paraplegia 11.
63. Lin, P., Li, J., Liu, Q., Mao, F., Li, J., Qiu, R., Hu, H., Song, Y., Yang, Y. & Gao, G. A missense mutation in SLC33A1, which encodes the acetyl-CoA transporter, causes autosomal-dominant spastic paraplegia (SPG42). *The American Journal of Human Genetics* **83**, 752–759 (2008).
64. Zivony-Elboum, Y., Westbroek, W., Kfir, N., Savitzki, D., Shoval, Y., Bloom, A., Rod, R., Khayat, M., Gross, B. & Samri, W. A founder mutation in Vps37A causes autosomal recessive complex hereditary spastic paraparesis. *Journal of medical genetics* **49**, 462–472 (2012).
65. Roberts, D. B. *Drosophila melanogaster*: the model organism. *Entomologia experimentalis et applicata* **121**, 93–103 (2006).
66. Benzer, S. Behavioral mutants of *Drosophila* isolated by countercurrent distribution. *Proceedings of the National Academy of Sciences* **58**, 1112–1119 (1967).
67. Jeibmann, A. & Paulus, W. *Drosophila melanogaster* as a model organism of brain diseases. *International journal of molecular sciences* **10**, 407–440 (2009).
68. Orso, G., Martinuzzi, A., Rossetto, M. G., Sartori, E., Feany, M. & Daga, A. Disease-related phenotypes in a *Drosophila* model of hereditary spastic paraplegia are ameliorated by treatment with vinblastine. *The Journal of clinical investigation* **115**, 3026–3034 (2005).
69. Prüßing, K., Voigt, A. & Schulz, J. B. *Drosophila melanogaster* as a model organism for Alzheimer’s disease. *Molecular neurodegeneration* **8**, 1–12 (2013).
70. Nishikawa, S.-i., Goldstein, R. A. & Nierras, C. R. The promise of human induced pluripotent stem cells for research and therapy. *Nature reviews Molecular cell biology* **9**, 725–729 (2008).

71. Park, I.-H., Lerou, P. H., Zhao, R., Huo, H. & Daley, G. Q. Generation of human-induced pluripotent stem cells. *Nature protocols* **3**, 1180–1186 (2008).
72. Saha, K. & Jaenisch, R. Technical challenges in using human induced pluripotent stem cells to model disease. *Cell stem cell* **5**, 584–595 (2009).
73. Zhu, P.-P., Denton, K. R., Pierson, T. M., Li, X.-J. & Blackstone, C. Pharmacologic rescue of axon growth defects in a human iPSC model of hereditary spastic paraplegia SPG3A. *Human molecular genetics* **23**, 5638–5648 (2014).
74. Havlicek, S., Kohl, Z., Mishra, H. K., Prots, I., Eberhardt, E., Denguir, N., Wend, H., Plötz, S., Boyer, L. & Marchetto, M. C. Gene dosage-dependent rescue of HSP neurite defects in SPG4 patients' neurons. *Human molecular genetics* **23**, 2527–2541 (2014).
75. Vandamme, T. F. Use of rodents as models of human diseases. *Journal of pharmacy & bioallied sciences* **6**, 2 (2014).
76. Fisher, E. M. & Bannerman, D. M. Mouse models of neurodegeneration: Know your question, know your mouse. *Science Translational Medicine* **11**, eaaq1818 (2019).
77. Deutch, A. Y., Hedera, P. & Colbran, R. J. REEPing the benefits of an animal model of hereditary spastic paraplegia. *The Journal of Clinical Investigation* **123**, 4134–4136 (2013).
78. Khundadze, M., Ribaud, F., Hussain, A., Stahlberg, H., Brocke-Ahmadinejad, N., Franzka, P., Varga, R.-E., Zarkovic, M., Pungsrinont, T. & Kokal, M. Mouse models for hereditary spastic paraplegia uncover a role of PI4K2A in autophagic lysosome reformation. *Autophagy* **17**, 3690–3706 (2021).
79. Hauser, S., Poenisch, M., Schelling, Y., Höflinger, P., Schuster, S., Teegler, A., Betten, R., Gustafsson, J.-Å., Hübener-Schmid, J. & Schlake, T. mRNA as a novel treatment strategy for hereditary spastic paraplegia type 5. *Molecular Therapy-Methods & Clinical Development* **15**, 359–370 (2019).
80. Pirozzi, M., Quattrini, A., Andolfi, G., Dina, G., Malaguti, M. C., Auricchio, A. & Rugarli, E. I. Intramuscular viral delivery of paraplegin rescues peripheral axonopathy in a model of hereditary spastic paraplegia. *The Journal of clinical investigation* **116**, 202–208 (2006).

81. Hanein, S., Martin, E., Boukhris, A., Byrne, P., Goizet, C., Hamri, A., Benomar, A., Lossos, A., Denora, P. & Fernandez, J. Identification of the SPG15 gene, encoding spastizin, as a frequent cause of complicated autosomal-recessive spastic paraplegia, including Kjellin syndrome. *The American Journal of Human Genetics* **82**, 992–1002 (2008).
82. Hirst, J., Borner, G. H., Edgar, J., Hein, M. Y., Mann, M., Buchholz, F., Antrobus, R. & Robinson, M. S. Interaction between AP-5 and the hereditary spastic paraplegia proteins SPG11 and SPG15. *Molecular biology of the cell* **24**, 2558–2569 (2013).
83. Schüle, R., Schlipf, N., Synofzik, M., Klebe, S., Klimpe, S., Hehr, U., Winner, B., Lindig, T., Dotzer, A. & Rieß, O. Frequency and phenotype of SPG11 and SPG15 in complicated hereditary spastic paraplegia. *Journal of Neurology, Neurosurgery & Psychiatry* **80**, 1402–1404 (2009).
84. National Center for Biotechnology Information https://www.ncbi.nlm.nih.gov/nuccore/NM_015346. Accessed: 2023-02-12.
85. Kutateladze, T. & Overduin, M. Structural mechanism of endosome docking by the FYVE domain. *Science* **291**, 1793–1796 (2001).
86. Chang, J., Lee, S. & Blackstone, C. Spastic paraplegia proteins spastizin and spatacsin mediate autophagic lysosome reformation. *The Journal of clinical investigation* **124**, 5249–5262 (2014).
87. Khundadze, M., Kollmann, K., Koch, N., Biskup, C., Nietzsche, S., Zimmer, G., Hennings, J. C., Huebner, A. K., Symmank, J. & Jahic, A. A hereditary spastic paraplegia mouse model supports a role of ZFYVE26/SPASTIZIN for the endolysosomal system. *PLoS genetics* **9**, e1003988 (2013).
88. Cassandri, M., Smirnov, A., Novelli, F., Pitolli, C., Agostini, M., Malewicz, M., Melino, G. & Raschellà, G. Zinc-finger proteins in health and disease. *Cell death discovery* **3**, 1–12 (2017).
89. Gibson, T. J., Postma, J. P., Brown, R. S. & Argos, P. A model for the tertiary structure of the 28 residue DNA-binding motif ('zinc finger') common to many eukaryotic transcriptional regulatory proteins. *Protein Engineering, Design and Selection* **2**, 209–218 (1988).

90. O'Shea, E. K., Rutkowski, R. & Kim, P. S. Evidence that the leucine zipper is a coiled coil. *Science* **243**, 538–542 (1989).
91. in. *Cell Biology (Third Edition)* (eds Pollard, T. D., Earnshaw, W. C., Lippincott-Schwartz, J. & Johnson, G. T.) Third Edition, 165–187 (Elsevier, 2017). ISBN: 978-0-323-34126-4.
92. Landschulz, W. H., Johnson, P. F. & McKnight, S. L. The leucine zipper: a hypothetical structure common to a new class of DNA binding proteins. *Science* **240**, 1759–1764 (1988).
93. Liang, C., E, X. & Jung, J. U. Downregulation of autophagy by herpesvirus Bcl-2 homologs. *Autophagy* **4**, 268–272 (2008).
94. Thoresen, S. B., Pedersen, N. M., Liestøl, K. & Stenmark, H. A phosphatidylinositol 3-kinase class III sub-complex containing VPS15, VPS34, Beclin 1, UVRAG and BIF-1 regulates cytokinesis and degradative endocytic traffic. *Experimental cell research* **316**, 3368–3378 (2010).
95. Sagona, A. P., Nezis, I. P., Bache, K. G., Haglund, K., Bakken, A. C., Skotheim, R. I. & Stenmark, H. A tumor-associated mutation of FYVE-CENT prevents its interaction with Beclin 1 and interferes with cytokinesis. *PLoS one* **6**, e17086 (2011).
96. McKnight, N. C., Zhong, Y., Wold, M. S., Gong, S., Phillips, G. R., Dou, Z., Zhao, Y., Heintz, N., Zong, W.-X. & Yue, Z. Beclin 1 is required for neuron viability and regulates endosome pathways via the UVRAG-VPS34 complex. *PLoS genetics* **10**, e1004626 (2014).
97. Vantaggiato, C., Crimella, C., Airoidi, G., Polishchuk, R., Bonato, S., Brighina, E., Scarlato, M., Musumeci, O., Toscano, A. & Martinuzzi, A. Defective autophagy in spastizin mutated patients with hereditary spastic paraparesis type 15. *Brain* **136**, 3119–3139 (2013).
98. Vantaggiato, C., Crimella, C., Airoidi, G., Polishchuk, R., Bonato, S., Brighina, E., Scarlato, M., Musumeci, O., Toscano, A. & Martinuzzi, A. Defective autophagy in spastizin mutated patients with hereditary spastic paraparesis type 15. *Brain* **136**, 3119–3139 (2013).

99. Marrone, L., Marchi, P. M., Webster, C. P., Marroccella, R., Coldicott, I., Reynolds, S., Alves-Cruzeiro, J., Yang, Z.-L., Higginbottom, A. & Khundadze, M. SPG15 protein deficits are at the crossroads between lysosomal abnormalities, altered lipid metabolism and synaptic dysfunction. *Human Molecular Genetics* **31**, 2693–2710 (2022).
100. Hirst, J., Edgar, J. R., Esteves, T., Darios, F., Madeo, M., Chang, J., Roda, R. H., Dürr, A., Anheim, M. & Gellera, C. Loss of AP-5 results in accumulation of aberrant endolysosomes: defining a new type of lysosomal storage disease. *Human molecular genetics* **24**, 4984–4996 (2015).
101. Hirst, J., Itzhak, D. N., Antrobus, R., Borner, G. H. & Robinson, M. S. Role of the AP-5 adaptor protein complex in late endosome-to-Golgi retrieval. *PLoS biology* **16**, e2004411 (2018).
102. Breza, M., Hirst, J., Chelban, V., Banneau, G., Tissier, L., Kol, B., Bourinaris, T., Said, S. A., Péréon, Y. & Heinzmann, A. Expanding the Spectrum of AP5Z1-Related Hereditary Spastic Paraplegia (HSP-SPG48): A Multicenter Study on a Rare Disease. *Movement Disorders* **36**, 1034–1038 (2021).
103. Pfisterer, S. G., Peränen, J. & Ikonen, E. LDL-cholesterol transport to the endoplasmic reticulum: current concepts. *Current opinion in lipidology* **27**, 282 (2016).
104. Béreau, M., Anheim, M., Chanson, J.-B., Tio, G., Echaniz-Laguna, A., Depienne, C., Collongues, N. & de Sèze, J. Dalfampridine in hereditary spastic paraplegia: a prospective, open study. *Journal of Neurology* **262**, 1285–1288 (2015).
105. Judge, S. I. & Bever Jr, C. T. Potassium channel blockers in multiple sclerosis: neuronal Kv channels and effects of symptomatic treatment. *Pharmacology & therapeutics* **111**, 224–259 (2006).
106. Blight, A. R. Effect of 4-aminopyridine on axonal conduction-block in chronic spinal cord injury. *Brain research bulletin* **22**, 47–52 (1989).
107. Preiningerova, J. L., Baumhackl, U., Csepány, T., Czaplinski, A., Deisenhammer, F., Derfuss, T., Fabjan, T. H., Fazekas, F., Fuchs, S. & Havrdova, E. Recommendations for the Use of Prolonged-Release Fampridine in Patients with Multiple Sclerosis (MS). *CNS neuroscience & therapeutics* **19**, 302–306 (2013).

108. Uygunoglu, U., Gunduz, A., Tutuncu, M., Akalin, M. A., Saip, S. & Siva, A. The effects of dalfampridine on hereditary spastic paraparesis. *European Neurology* **76**, 152–153 (2016).
109. Martin, E., Yanicostas, C., Rastetter, A., Naini, S. M. A., Maouedj, A., Kabashi, E., Rivaud-Péchoux, S., Brice, A., Stevanin, G. & Soussi-Yanicostas, N. Spatacsin and spastizin act in the same pathway required for proper spinal motor neuron axon outgrowth in zebrafish. *Neurobiology of disease* **48**, 299–308 (2012).
110. Denton, K., Mou, Y., Xu, C.-C., Shah, D., Chang, J., Blackstone, C. & Li, X.-J. Impaired mitochondrial dynamics underlie axonal defects in hereditary spastic paraplegias. *Human molecular genetics* **27**, 2517–2530 (2018).
111. Sternberg, N. & Hamilton, D. Bacteriophage P1 site-specific recombination: I. Recombination between loxP sites. *Journal of molecular biology* **150**, 467–486 (1981).
112. Ray, M. K., Fagan, S. P. & Brunicardi, F. C. The Cre-loxP system: A versatile tool for targeting genes in a cell-and stage-specific manner. *Cell transplantation* **9**, 805–815 (2000).
113. Chambers, A. P., Sorrell, J. E., Haller, A., Roelofs, K., Hutch, C. R., Kim, K.-S., Gutierrez-Aguilar, R., Li, B., Drucker, D. J. & D'Alessio, D. A. The role of pancreatic preproglucagon in glucose homeostasis in mice. *Cell metabolism* **25**, 927–934 (2017).
114. Pfaffl, M. W. A new mathematical model for relative quantification in real-time RT-PCR. *Nucleic acids research* **29**, e45–e45 (2001).
115. Mina, A. I., LeClair, R. A., LeClair, K. B., Cohen, D. E., Lantier, L. & Banks, A. S. CalR: a web-based analysis tool for indirect calorimetry experiments. *Cell metabolism* **28**, 656–666 (2018).
116. Trummer, B., Haubenberger, D. & Blackstone, C. Clinical trial designs and measures in hereditary spastic paraplegias. *Frontiers in Neurology* **9**, 1017 (2018).
117. Studholme, K. M., Gompf, H. S. & Morin, L. P. Brief light stimulation during the mouse nocturnal activity phase simultaneously induces a decline in core temperature and locomotor activity followed by EEG-determined sleep. *American Journal of Physiology-Regulatory, Integrative and Comparative Physiology* **304**, R459–R471 (2013).

118. Schmidt-Nielsen, K. *Animal physiology: adaptation and environment* (Cambridge university press, 1997).
119. Elefteriou, F. & Couasnay, G. Advantages and limitations of Cre mouse lines used in skeletal research. *Skeletal Development and Repair: Methods and Protocols*, 39–59 (2021).
120. McLellan, M. A., Rosenthal, N. A. & Pinto, A. R. Cre-loxP-mediated recombination: general principles and experimental considerations. *Current protocols in mouse biology* **7**, 1–12 (2017).
121. NCBI *Zfyve26 isoforms* <https://www.ncbi.nlm.nih.gov/gene/211978>. Accessed: 2023-02-21.
122. NCBI *Zfyve26 isoforms* https://www.ncbi.nlm.nih.gov/datasets/tables/genes/?table_type=transcripts&key=8df3e061533806393fe8ec3965c1933e. Accessed: 2023-02-21.
123. Camacho Londoño, J. & Philipp, S. E. A reliable method for quantification of splice variants using RT-qPCR. *BMC molecular biology* **17**, 1–12 (2016).
124. Wacker, M. J. & Godard, M. P. Analysis of one-step and two-step real-time RT-PCR using SuperScript III. *Journal of biomolecular techniques: JBT* **16**, 266 (2005).
125. Hein, M. Y., Hubner, N. C., Poser, I., Cox, J., Nagaraj, N., Toyoda, Y., Gak, I. A., Weisswange, I., Mansfeld, J. & Buchholz, F. A human interactome in three quantitative dimensions organized by stoichiometries and abundances. *Cell* **163**, 712–723 (2015).
126. Itzhak, D. N., Tyanova, S., Cox, J. & Borner, G. H. Global, quantitative and dynamic mapping of protein subcellular localization. *elife* **5**, e16950 (2016).
127. *The HeLa Spatial Proteome* <http://mapofthecell.biochem.mpg.de/>. Accessed: 2023-02-03.
128. Varga, R.-E., Khundadze, M., Damme, M., Nietzsche, S., Hoffmann, B., Stauber, T., Koch, N., Hennings, J. C., Franzka, P. & Huebner, A. K. In vivo evidence for lysosome depletion and impaired autophagic clearance in hereditary spastic paraplegia type SPG11. *PLoS genetics* **11**, e1005454 (2015).

129. Khundadze, M., Ribaud, F., Hussain, A., Rosentreter, J., Nietzsche, S., Thelen, M., Winter, D., Hoffmann, B., Afzal, M. A. & Hermann, T. A mouse model for SPG48 reveals a block of autophagic flux upon disruption of adaptor protein complex five. *Neurobiology of disease* **127**, 419–431 (2019).
130. *The Jackson Laboratory C57BL/6N mouse strain* <https://www.jax.org/jax-mice-and-services/strain-data-sheet-pages/body-weight-chart-005304>. Accessed: 2023-02-21.
131. Kafkafi, N., Agassi, J., Chesler, E. J., Crabbe, J. C., Crusio, W. E., Eilam, D., Gerlai, R., Golani, I., Gomez-Marin, A. & Heller, R. Reproducibility and replicability of rodent phenotyping in preclinical studies. *Neuroscience & Biobehavioral Reviews* **87**, 218–232 (2018).
132. David, J. M., Knowles, S., Lamkin, D. M. & Stout, D. B. Individually ventilated cages impose cold stress on laboratory mice: a source of systemic experimental variability. *Journal of the American Association for Laboratory Animal Science* **52**, 738–744 (2013).
133. Mazure, C. M. & Jones, D. P. Twenty years and still counting: including women as participants and studying sex and gender in biomedical research. *BMC women's health* **15**, 1–16 (2015).
134. Buch, T., Moos, K., Ferreira, F. M., Fröhlich, H., Gebhard, C. & Tresch, A. Benefits of a factorial design focusing on inclusion of female and male animals in one experiment. *Journal of molecular medicine* **97**, 871–877 (2019).
135. Wachs, T. D. *The nature of nurture* (Sage publications, 1992).
136. De Carvalho Cardozo-Hernández, A. L., Rezende, T. J. R. & França Jr, M. C. Hereditary spastic paraplegia type 11 (SPG11) is associated with obesity and hypothalamic damage. *Journal of the Neurological Sciences* **416**, 116982 (2020).
137. Kaiyala, K. J. What does indirect calorimetry really tell us? *Molecular metabolism* **3**, 340 (2014).
138. Gelman, A. & Stern, H. The difference between “significant” and “not significant” is not itself statistically significant. *The American Statistician* **60**, 328–331 (2006).

139. Tarrade, A., Fassier, C., Courageot, S., Charvin, D., Vitte, J., Peris, L., Thorel, A., Mouisel, E., Fonknechten, N. & Roblot, N. A mutation of spastin is responsible for swellings and impairment of transport in a region of axon characterized by changes in microtubule composition. *Human molecular genetics* **15**, 3544–3558 (2006).
140. Beetz, C., Koch, N., Khundadze, M., Zimmer, G., Nietzsche, S., Hertel, N., Huebner, A.-K., Mumtaz, R., Schweizer, M. & Dirren, E. A spastic paraplegia mouse model reveals REEP1-dependent ER shaping. *The Journal of clinical investigation* **123**, 4273–4282 (2013).
141. *The Jackson Laboratory C57BL/6N and C57BL/6N mouse strains* <https://www.jax.org/news-and-insights/2013/April/a-tool-for-telling-apart-c57bl-6j-versus-c57bl-6n-substrains>. Accessed: 2023-02-22.
142. Simon, M. M., Greenaway, S., White, J. K., Fuchs, H., Gailus-Durner, V., Wells, S., Sorg, T., Wong, K., Bedu, E. & Cartwright, E. J. A comparative phenotypic and genomic analysis of C57BL/6J and C57BL/6N mouse strains. *Genome biology* **14**, 1–22 (2013).
143. McDonald, A. A., Hebert, S. L., Kunz, M. D., Ralles, S. J. & McLoon, L. K. Disease course in mdx: utrophin+/- mice: comparison of three mouse models of Duchenne muscular dystrophy. *Physiological reports* **3**, e12391 (2015).
144. Eckel-Mahan, K. & Sassone-Corsi, P. Phenotyping circadian rhythms in mice. *Current protocols in mouse biology* **5**, 271–281 (2015).
145. Pernold, K., Rullman, E. & Ulfhake, B. Major oscillations in spontaneous home-cage activity in C57BL/6 mice housed under constant conditions. *Scientific Reports* **11**, 4961 (2021).
146. Metzger, J., Wicht, H., Korf, H.-W. & Pfeffer, M. Seasonal variations of locomotor activity rhythms in melatonin-proficient and-deficient mice under seminatural outdoor conditions. *Journal of Biological Rhythms* **35**, 58–71 (2020).
147. Boukhris, A., Feki, I., Denis, E., Miladi, M. I., Brice, A., Mhiri, C. & Stevanin, G. Spastic paraplegia 15: linkage and clinical description of three Tunisian families. *Movement disorders: official journal of the Movement Disorder Society* **23**, 429–433 (2008).
148. Sharma, K., Zhang, G. & Li, S. *Astrogliosis and axonal regeneration* 181–196 (Elsevier, 2015).

149. Kang, W., Balordi, F., Su, N., Chen, L., Fishell, G. & Hébert, J. M. Astrocyte activation is suppressed in both normal and injured brain by FGF signaling. *Proceedings of the National Academy of Sciences* **111**, E2987–E2995 (2014).
150. Paul, M. S. & Limaiem, F. in *Histology, Purkinje Cells* (StatPearls Publishing, 2021).
151. Song, J., Ampatzis, K., Björnfors, E. R. & El Manira, A. Motor neurons control locomotor circuit function retrogradely via gap junctions. *Nature* **529**, 399–402 (2016).
152. Renvoisé, B., Chang, J., Singh, R., Yonekawa, S., FitzGibbon, E. J., Mankodi, A., Vanderver, A., Schindler, A. B., Toro, C. & Gahl, W. A. Lysosomal abnormalities in hereditary spastic paraplegia types SPG 15 and SPG 11. *Annals of clinical and translational neurology* **1**, 379–389 (2014).
153. Branchu, J., Boutry, M., Sourd, L., Depp, M., Leone, C., Corriger, A., Vallucci, M., Esteves, T., Matusiak, R. & Dumont, M. Loss of spatascin function alters lysosomal lipid clearance leading to upper and lower motor neuron degeneration. *Neurobiology of disease* **102**, 21–37 (2017).

Appendix

Official letter on mouse stock infection with a zoonotic pathogen in the laboratory animal facility at Charité.

Charité | Campus Mitte | 10098 Berlin

An die Wissenschaftler:innen
der Charité - Universitätsmedizin Berlin
Campus Virchow-Klinikum

Bestandsinfektion mit einem Zoonoseerreger in der Versuchstierhaltung

Sehr geehrte Wissenschaftlerinnen und Wissenschaftler,
liebe Kolleginnen und Kollegen,

wie Sie wissen, ist es in der zentralen Versuchstierhaltung auf dem Campus Virchow-Klinikum Ende Juli 2021 zu einer Bestandsinfektion im Großtierhaltungsbereich mit einem Zoonoseerreger gekommen. Seitdem ist der Forschungsbetrieb in dieser Anlage beeinträchtigt und es ist noch nicht eindeutig festzulegen, wann die Anlage wieder uneingeschränkt in Betrieb gehen kann. Wir rechnen damit jedoch noch in diesem Monat.

Von diesen Betriebsbeeinträchtigungen war die gesamte Anlage betroffen, also auch angrenzende Kleintierhaltungsbereiche sowie mikrochirurgische Eingriffsräume und Großtier-OPs, sodass die meisten der dort aktiven Forschungsprojekte in dieser Zeit nicht wie geplant durchgeführt werden konnten.

Aufgrund wiederholter, erregerspezifischer Nachweise in der Haltung der Kleintiere, konnte der dortige Tierbestand aus arbeitsschutzrechtlichen Gründen nicht weiter für die Forschung verwendet werden. Es ist davon auszugehen, dass für betroffene Projekte Beeinträchtigungen auch noch für eine bestimmte Zeit in die Zukunft nachwirken, bis entsprechende Tierbestände nachgezüchtet und Ersatzversuchsgruppen neu aufgebaut werden können.

Bei Bedarf nutzen Sie bitte dieses Anschreiben und auch die offizielle Pressemitteilung der Charité vom 17.12.2021 (siehe Anlage und Link), um bei betroffenen Projekten etwaige Verzögerungen in der Bearbeitung von Forschungsinhalten gegenüber Ihren Drittmittelgebern anzuzeigen.

(https://www.charite.de/service/pressemitteilung/artikel/detail/charite_setzt_umfaengreiche_vorsorgemaassnahmen_im_tiersuchslabor_um/)

Mit freundlichen Grüßen


Prof. Dr. Christian Hagemeyer
Prodekan für Forschung


Dr. Stefan Nagel-Riedasch
Leiter der FEM

CHARITÉ
UNIVERSITÄTSMEDIZIN
BERLIN

Körperschaft des öffentlichen Rechts
Gliedkörperschaft der
Freien Universität Berlin und der
Humboldt-Universität zu Berlin

Charitéplatz 1 | 10117 Berlin
Telefon +49 30 450 50
www.charite.de

Berlin, 14. Januar 2022

DER PRODEKAN FÜR
FORSCHUNG
mit präklinischem Schwerpunkt

Prof. Dr. Christian Hagemeyer

Bearbeiterin:
Kerstin Dlab
Referentin der Fakultätsleitung
Prodekanat für Forschung

Campus Charité Mitte
Charitéplatz 1 | 10117 Berlin

Interne Geländeadresse:
Friedrich Althoff-Haus

Telefon +49 30 450 576 067
Fax +49 30 450 7576 067
kerstin.dlab@charite.de
www.charite.de

Pressemitteilung

Charité setzt umfangreiche Vorsorgemaßnahmen im Tierversuchslabor um

Berlin, 17.12.2021

Zum Schutz der Mitarbeiterinnen und Mitarbeiter wird die Charité – Universitätsmedizin Berlin das Tierversuchslabor am Campus Virchow-Klinikum umfangreich dekontaminieren. Hintergrund sind positive Befunde von Coxiellen innerhalb eines eng begrenzten Bereichs.

Coxiellose ist eine bakterielle Erkrankung, die bei Tieren meist asymptomatisch verläuft, bei Menschen unter anderem zu grippeartigen Symptomen führen kann und Q-Fieber genannt wird. Tiere und Menschen in der näheren Umgebung eines infizierten Tieres können sich durch Einatmen von Staub und Tröpfchen anstecken. Da der Erreger die Fähigkeit besitzt, Dauerformen zu bilden und eine hohe Abwehrkraft gegenüber Austrocknung hat, kann er anhaltend in Staub, auf Heu oder in Wolle überleben. Eine Übertragung von Mensch zu Mensch ist nicht möglich.

Die von der Charité nun beschlossenen Maßnahmen sehen eine grundlegende Desinfektion des eng begrenzten Bereichs vor. Zudem ist die Tötung von einzelnen Versuchstierbeständen unumgänglich. Es handelt sich um rund 1.200 kleine Nagetiere, in deren unmittelbarer Haltung wiederholt positive Befunde erhoben wurden.

Die Charité nimmt ihre Verantwortung für den Schutz der Beschäftigten sehr ernst. Daher bleibt der gesamte Bereich für die Forschung bis zum Abschluss der vollständigen Dekontamination gesperrt.

Die notwendigen Vorsorgemaßnahmen erfolgen nach vorherigem Austausch mit dem Landesamt für Gesundheit und Soziales und dem Landesamt für Arbeitsschutz, Gesundheitsschutz und technische Sicherheit. Dabei wurden neben der Fürsorgesorgepflicht gegenüber Mitarbeiterinnen und Mitarbeitern auch tierschutzrechtliche Aspekte intensiv besprochen.

Die Charité bedauert die notwendig gewordene Tötung der Versuchstiere. Sie engagiert sich intensiv für eine verstärkte Umsetzung des 3R-Prinzips in Forschung und Lehre und hat dafür vor einigen Jahren Charité 3R gegründet. Der Name Charité 3R bezieht sich auf die Begriffe Replace, Reduce und Refine. Ziel dieses Prinzips ist es, Tierversuche zu ersetzen, die Anzahl der Versuchstiere zu reduzieren und die Belastung für Versuchstiere zu mindern. In der biomedizinischen Forschung spielen Tierversuche nach wie vor eine wichtige Rolle. Charité 3R will den Tierschutz in diesem Forschungsumfeld verstärkt vorantreiben und nicht ersetzbare Tierversuche verbessern. Außerdem suchen die Wissenschaftlerinnen und Wissenschaftler dort nach neuen Möglichkeiten, um Tierversuche durch Alternativmethoden zu ersetzen.

Kontakt:

Manuela Zingl

Unternehmenssprecherin

Charité – Universitätsmedizin Berlin

t: +49 30 450 570 400

Weitere Pressemitteilungen

© 2021 Charité – Universitätsmedizin Berlin

Über **diesen Verweis** können Sie einen Link zum Bearbeiten und Löschen Ihrer Newsletter-Daten anfordern.

Unser Newsletter wird automatisiert verschickt.

Kritik, Probleme oder Anregungen schicken Sie bitte an  presse@charite.de

Statutory Declaration

“I, Thanh Tuyen Pham, by personally signing this document in lieu of an oath, hereby affirm that I prepared the submitted dissertation on the topic

*Characterization of a novel condZfyve26–Null mouse model:
A prerequisite for defining the therapeutic potential of somatic gene repair
in Hereditary Spastic Paraplegia Type SPG15*

*Charakterisierung des condZfyve26–Null Mausmodells
als Tool für die Bestimmung des therapeutischen Potenzials
somatischer Genreparatur bei HSP Typ SPG15*

independently and without the support of third parties, and that I used no other sources and aids than those stated. All parts which are based on the publications or presentations of other authors, either in letter or in spirit, are specified as such in accordance with the citing guidelines. The sections on methodology (in particular regarding practical work, laboratory regulations, statistical processing) and results (in particular regarding figures, charts and tables) are exclusively my responsibility.

Furthermore, I declare that I have correctly marked all of the data, the analyses, and the conclusions generated from data obtained in collaboration with other persons, and that I have correctly marked my own contribution and the contributions of other persons (cf. declaration of contribution). I have correctly marked all texts or parts of texts that were generated in collaboration with other persons.

My contributions to any publications to this dissertation correspond to those stated in the below joint declaration made together with the supervisor. All publications created within the scope of the dissertation comply with the guidelines of the ICMJE (International Committee of Medical Journal Editors; <http://www.icmje.org>) on authorship. In addition, I declare that I shall comply with the regulations of Charité – Universitätsmedizin Berlin on ensuring good scientific practice.

I declare that I have not yet submitted this dissertation in identical or similar form to another Faculty.

The significance of this statutory declaration and the consequences of a false statutory declaration under criminal law (Sections 156, 161 of the German Criminal Code) are known to me.”

Date

Signature

Curriculum Vitae

Mein Lebenslauf wird aus datenschutzrechtlichen Gründen in der elektronischen Version meiner Arbeit nicht veröffentlicht.

Publication list

Sancer, G., Kind, E., Uhlhorn, J., Volkmann, J., Hammacher, J., **Pham, T.**, Plazaola-Sasieta, H. and Wernet, M.F., 2020. Cellular and synaptic adaptations of neural circuits processing skylight polarization in the fly. *Journal of Comparative Physiology A*, 206, pp.233-246.

Sancer, G., Kind, E., Plazaola-Sasieta, H., Balke, J., **Pham, T.**, Hasan, A., Münch, L.O., Courgeon, M., Mathejczyk, T.F. and Wernet, M.F., 2019. Modality-specific circuits for skylight orientation in the fly visual system. *Current Biology*, 29(17), pp.2812-2825.

Acknowledgments

I would like to express my deepest gratitude to my supervisor, PD Dr. Dr. Amir Jahić, for his trust and support. I also could not have undertaken this journey without Prof. Mathias Wernet, Prof. Hendrik Fuchs and Dr. Jens Dervedde, who generously provided knowledge and expertise. Additionally, this endeavor would not have been possible without the financial support from the Deutsche Gesellschaft für Klinische Chemie und Laboratoriumsmedizin, the Maddi Foundation, the Tom Wahlig Stiftung and the Sonnenfeld-Stiftung.

I am also grateful to my colleagues, especially my office mates, for their help, feedback sessions, and moral support. Thanks should also go to Ulli and other members of the Biofluid Mechanics Laboratory, who were always there for a fun dancing and drinking session.

Lastly, words cannot express my gratitude to my family. Their belief in me has kept my spirits and motivation high during this process. *Nam Mo A Di Da Phat *



Name, Vorname: Pham, Thanh Tuyen
Emailadresse: thanh-tuyen.pham@charite.de
Matrikelnummer: 228617
PromotionsbetreuerIn: Amir Jahic
Promotionsinstitution / Klinik: CC05 Institut für Laboratoriumsmedizin, Klinische Chemie und Pathobiochemie

Bescheinigung

Hiermit bescheinige ich, dass Frau Thanh Tuyen Pham innerhalb der Service Unit Biometrie des Instituts für Biometrie und klinische Epidemiologie (iBikE) bei mir eine statistische Beratung zu einem Promotionsvorhaben wahrgenommen hat. Folgende Beratungstermine wurden wahrgenommen:

- Termin 1: 05.02.21
- Termin 2: 09.02.23

Folgende wesentliche Ratschläge hinsichtlich einer sinnvollen Auswertung und Interpretation der Daten wurden während der Beratung erteilt:

- Aufgrund der kleinen Fallzahl Fokus auf deskriptive Analysen legen
- Tests auf statistische Signifikanz nur in ausgewählten Fällen verwenden (wenn es die Fallzahl zulässt und es Sinn macht)
- Bitte auf explorativen Charakter der p-Werte verweisen und darauf, dass nicht für multiples Testen adjustiert wird.
- Interpretation vor allem im Hinblick auf die klinische Relevanz und nicht auf statistische Signifikanz.

Diese Bescheinigung garantiert nicht die richtige Umsetzung der in der Beratung gemachten Vorschläge, die korrekte Durchführung der empfohlenen statistischen Verfahren und die richtige Darstellung und Interpretation der Ergebnisse. Die Verantwortung hierfür obliegt allein dem Promovierenden. Das Institut für Biometrie und klinische Epidemiologie übernimmt hierfür keine Haftung.

Datum:

Anna
Poehlmann

Unterschrift BeraterIn, Institutsstempel

Name des Beraters\ der Beraterin: